

DEVELOPMENT OF BIODEGRADABLE COATING BY
USING BIOPOLYMER ANTI CORROSIVE REAGENT

ILING AEMA WONNIE MA

FACULTY OF SCIENCE
UNIVERSITY OF MALAYA
KUALA LUMPUR

2017

**DEVELOPMENT OF BIODEGRADABLE COATING BY
USING A BIOPOLYMER ANTI CORROSIVE REAGENT**

ILING AEMA WONNIE MA

**THESIS SUBMITTED IN FULFILMENT OF THE
REQUIREMENTS FOR THE DEGREE OF MASTER OF
SCIENCE**

**DEPARTMENT OF PHYSICS
FACULTY OF SCIENCE
UNIVERSITY OF MALAYA
KUALA LUMPUR**

2017

UNIVERSITY OF MALAYA
ORIGINAL LITERARY WORK DECLARATION

Name of Candidate: **ILING AEMA WONNIE MA** ████████████████████

Matric No: **SGR150027**

Name of Degree: **MASTER OF SCIENCE**

Title of Project Paper/Research Report/Dissertation/Thesis (“this Work”):

DEVELOPMENT OF BIODEGRADABLE COATING BY USING A BIOPOLYMER ANTI CORROSIVE REAGENT

Field of Study: **EXPERIMENTAL PHYSICS**

I do solemnly and sincerely declare that:

- (1) I am the sole author/writer of this Work;
- (2) This Work is original;
- (3) Any use of any work in which copyright exists was done by way of fair dealing and for permitted purposes and any excerpt or extract from, or reference to or reproduction of any copyright work has been disclosed expressly and sufficiently and the title of the Work and its authorship have been acknowledged in this Work;
- (4) I do not have any actual knowledge nor do I ought reasonably to know that the making of this work constitutes an infringement of any copyright work;
- (5) I hereby assign all and every rights in the copyright to this Work to the University of Malaya (“UM”), who henceforth shall be owner of the copyright in this Work and that any reproduction or use in any form or by any means whatsoever is prohibited without the written consent of UM having been first had and obtained;
- (6) I am fully aware that if in the course of making this Work I have infringed any copyright whether intentionally or otherwise, I may be subject to legal action or any other action as may be determined by UM.

Candidate’s Signature

Date:

Subscribed and solemnly declared before,

Witness’s Signature

Date:

Name:

Designation:

ABSTRACT

Biopolymer nanofiller is an approachable reinforcement agent of emerging interest to protect metals against corrosion due to its ability as a renewable, biodegradable and biocompatible polymer resource in the earth. In this study, a series of nanocomposites based on nanocellulose (NC) and nanochitosan (NCH) with an undiluted clear difunctional bisphenol A/epichlorohydrin derived liquid epoxy resin (EP) were prepared and applied on mild steel under room temperature. Furthermore, the composition was cured with isophorone diamine with a constant ratio of 70:30 for all systems. Each system consists of neat epoxy with 1.0 wt.%, 1.5 wt.% and 2.0 wt.% of epoxy/nanocellulose (ENC) nanocomposites and 0.5 wt.%, 1.0 wt.% and 2.0 wt.% of epoxy/nanochitosan (ECH) nanocomposites. The thickness of the dry film was measured by using coating thickness gauge and found to be about $60 \pm 5 \mu\text{m}$ for all systems. Nanofiller and nanocomposite samples were characterized by X-ray diffraction (XRD), Field Emission Scanning Electron Microscope (FESEM) and Fourier transform infrared (FTIR). The thermophysical properties of the nanocomposites were determined using differential scanning calorimetry (DSC) and thermogravimetric analysis (TGA). Moreover, the transparency of the nanocomposite specimens was examined by UV-vis spectroscopy at a range of 300 - 800 nm. Corrosion protection properties of coated mild steel substrate in 3.5 wt.% NaCl solution was comparatively studied by Electrochemical impedance spectroscopy (EIS) for 30 days. The anticorrosion performance of nanocomposite contains with 1.0 wt.% of NC and 0.5 wt.% of NCH contents revealed the most pronounced anticorrosion performance and also influenced the degradation, thermal stability and transparency of coating film. In accordance with that, all the results showed that the nanocomposite coatings with nanofiller noticeably influenced the epoxy-diamine liquid pre-polymer, both physically and chemically.

ABSTRAK

Pengisi biopolimer bersaiz nano adalah sebuah agen pengukuhan yang mewujudkan kepentingan kepada saduran pelindung terhadap pengaratan berdasarkan kepada kelebihanannya sebagai sumber polimer yang boleh diperbaharui, terbiodegradasikan dan terbioserasikan di muka bumi. Dalam kajian ini, satu siri komposit nano berasaskan nanoselulosa dan nanokitosan berserta dengan cecairan resin epoksi yang diubahsuaikan dengan bisphenol A/epiklorohidrin telah disediakan dan disadurkan ke atas keluli lembut di bawah suhu bilik. Formulasi ini dikukuhkan dengan menggunakan isoforon diamina dalam nisbah 70:30 bagi semua sistem saduran. Setiap sistem terdiri daripada epoksi berserta 1.0wt.%, 1.5wt.% dan 2.0 wt.% bagi nanokomposit epoksi/nanoselulosa juga 0.5 wt.%, 1.0 wt.% dan 2.0 wt.% bagi nanokomposit epoksi/nanokitosan. Ketebalan filem saduran bagi semua spesimen diukur menggunakan alat ukur ialah dalam anggaran 60 ± 5 μm . Pencirian pengisi nano dan nanokomposit adalah dengan menggunakan XRD, FESEM dan FTIR. Sifat-sifat termofizikal bagi nanokomposit telah dikenalpasti dengan menggunakan DSC dan TGA. Ketelusan spesimen nanokomposit telah diuji menggunakan spektroskopi UV-vis dalam julat 300 - 800 nm. Sifat-sifat pelindung pengaratan ke atas substrat keluli lembut yang telah disadurkan telah dikaji dengan menggunakan EIS selama 30 hari di dalam larutan 3.5 wt.%. Prestasi anti kakisan nanokomposit yang mengandungi 1.0 wt.% daripada NC dan 0.5 wt.% daripada NCH telah mendedahkan hasil yang memberangsangkan terhadap sifat anti kakisan dan juga mempengaruhi degradasi, keseimbangan haba dan ketelusan lapisan. Dengan itu, hasil kajian telah membuktikan bahawa penambahan pengisi nano biopolimer ini telah mempengaruhi sifat epoksi secara fizikal mahupun tindakbalas kimia.

ACKNOWLEDGEMENTS

Doing a research study is the first to complete a scientific project independently with critical thinking, from which I have learned a lot including the operation of all kinds of equipment and instruments. This project would not have been done without the help of many people. Here, I would like to express my heartfelt thanks for all your guidance, help and advice.

Foremost, I would like to express my sincere gratitude to my supervisors Associate Professor Dr. Ramesh Kasi and Professor Dr. Ramesh T. Subramaniam for providing me continuous support, enthusiasm and motivation along with my study. I would like to thank Ammar Shafaamri for his continuous collaboration and immense knowledge, especially with the corrosion electrochemical experiments. I would also like to thank Dr. Vengadaesvaran Balakrishnan for supervising me during this project and helpful discussions in the progress meetings.

I would also like to thank Farah Nadia Zaini for guiding and helping me in the experiments and discussing the results with me. I would also like to express my thanks to the people of the groups I had the pleasure to work in, namely Centre For Ionics University of Malaya, Advanced Material Science Laboratory and INFRA.

I would like to thank everyone who has given me help and support when I feel confused. It was a pleasure to work with you all!

Last but not the least, I would like to thank my family for supporting me spiritually and financially throughout my life.

TABLE OF CONTENTS

ABSTRACT	iii
ABSTRAK.....	iv
ACKNOWLEDGEMENTS.....	v
LIST OF FIGURES	x
LIST OF TABLES.....	xiv
LIST OF SYMBOLS AND ABBREVIATIONS.....	xv
LIST OF APPENDICES.....	xvi
CHAPTER 1: INTRODUCTION	1
1.1 Background.....	1
1.2 Advantages.....	4
1.3 Objectives of the study.....	5
1.3 Outline of the thesis.....	6
CHAPTER 2: LITERATURE REVIEW.....	7
2.1 Introduction.....	7
2.2 Corrosion.....	8
2.3 Corrosion Protection	11
2.3.1 Cathodic Protection	11
2.3.2 Corrosion Inhibitor	12
2.3.3 Protective Coating	13
2.3.4 Metal Surface and Environment Protection.....	15
2.4 Metallic Surface - Mild Steel	16
2.5 Cellulose and Chitosan as Pigment.....	17
2.5.1 Cellulose	18

2.5.2 Chitosan	20
2.6 Epoxy as Binder	22
2.7 Nanocomposite Coating	26
CHAPTER 3: METHODOLOGY	28
3.1 Introduction	28
3.2 Materials	29
3.3 Method of Preparations	32
3.3.1 Preparation of nanocellulose	32
3.3.2 Preparation of epoxy/nanocellulose nanocomposite coatings	33
3.3.3 Preparation of nanochitosan	34
3.3.4 Preparation of epoxy/nanochitosan nanocomposite coating	35
3.4 Characterization	36
3.4.1 Surface morphology and structural characterization	36
3.4.1.1 Field Emission Scanning Electron Microscopy (FESEM)	36
3.4.1.2 X-Ray Diffraction (XRD)	38
3.4.1.3 Fourier Transform Infrared Spectroscopy (FTIR)	40
3.4.2 Ultraviolet-Visible (UV-Visible) analysis of nanocomposite films	41
3.4.3 Thermal properties analyses of nanocomposite films	42
3.4.3.1 Thermogravimetric Analysis (TGA)	42
3.4.3.2 Differential Scanning Calorimetry (DSC)	43
3.4.4 Electrochemical Impedance Spectroscopy (EIS)	44
CHAPTER 4: RESULTS AND DISCUSSION OF EPOXY/NANOCELLULOSE NANOCOMPOSITE COATING SYSTEMS	46
4.1 Introduction	46
4.2 Field Emission Scanning Electron Microscope (FESEM) Analysis	47

4.2.1 Preparation of nanocellulose from raw microcellulose	47
4.2.2 Epoxy/nanocellulose nanocomposite coating systems	49
4.3 Structural Analysis	52
4.3.1 X-ray Diffraction (XRD)	52
4.3.2 Fourier Transform Infrared (FTIR)	54
4.4 UV-Visible Spectroscopy.....	57
4.5 Thermal Analysis	59
4.5.1 Thermogravimetric Analysis (TGA)	59
4.5.2 Differential Scanning Calorimetry (DSC)	62
4.6 Electrochemical Impedance Spectroscopy (EIS).....	66
 CHAPTER 5: RESULTS AND DISCUSSION OF EPOXY/NANOCHITOSAN	
NANOCOMPOSITE COATING SYSTEMS.....	72
5.1 Introduction	72
5.2 Field Emission Scanning Electron Microscope (FESEM) Analysis.....	73
5.2.2 Epoxy/nanochitosan nanocomposite coating systems	73
5.2.2 Epoxy/nanochitosan nanocomposite coating systems	76
5.3 Structural Analysis	78
5.3.1 X-ray Diffraction (XRD)	78
5.3.2 Fourier Transform Infrared (FTIR) Spectroscopy.....	79
5.4 UV-Visible Spectroscopy.....	81
5.5 Thermal Analysis	82
5.5.1 Thermogravimetric Analysis (TGA)	82
5.5.2 Differential Scanning Calorimetry (DSC)	85
5.6 Electrochemical Impedance Spectroscopy (EIS).....	88

CHAPTER 6: DISCUSSION	95
CHAPTER 7: CONCLUSION AND RECOMMENDATION	98
REFERENCES	102
LIST OF PUBLICATIONS AND PAPERS PRESENTED	109
APPENDIX A	110
APPENDIX B	111

University of Malaya

LIST OF FIGURES

Figure 2.1	: Anode and Cathode reactions on metal surface.....	10
Figure 2.2	: General structure of cellulose.....	18
Figure 2.3	: General structure of chitosan	21
Figure 2.2	: General structure of DGEBA Source	22
Figure 2.3	: Molecular reaction of epoxide group and primary amine	23
Figure 2.4	: Molecular reaction of epoxide group and secondary amine.....	25
Figure 2.5	: Molecular reaction of epoxide group and tertiary amine.....	24
Figure 2.6	: General structure of isophorone diamine (IPDA).....	25
Figure 2.7(a)	: Nanocomposite coating formed by nanoparticles.	26
Figure 2.7(b)	: Nanocomposite coating formed by nanotubes.	26
Figure 2.7(c)	: Nanocomposite coating formed by nanolayer.	26
Figure 3.1	: Flow chart of nanocomposite coating systems	28
Figure 3.2	: Preparation of nanocellulose.....	32
Figure 3.3	: Preparation of nanochitosan.....	34
Figure 3.4	: Field emission scanning electron microscopy	36
Figure 3.5	: X-ray diffraction.....	38
Figure 3.6	: Fourier transform infrared spectroscopy	40
Figure 3.7	: Ultraviolet-visible spectroscopy	41
Figure 3.8	: Thermogravimetric analysis	42
Figure 3.9	: Differential scanning calorimetry.....	43
Figure 3.10	: Set of an electrochemical cell	44
Figure 3.10	: Schematic diagram of the experimental setup for EIS.....	45
Figure 4.1(a)	: FESEM images of MCC at scale 10, 000 of magnification	47
Figure 4.1(b)	: FESEM images of MCC at scale 50, 000 and of magnification	47
Figure 4.1(c)	: FESEM images of MCC at scale 100, 000 of magnification.....	47

Figure 4.2(a) : FESEM images of NC at scale 10, 000 of magnification.....	48
Figure 4.2(b) : FESEM images of NC at scale 50, 000 of magnification.....	48
Figure 4.2(c) : FESEM images of NC at scale 100, 000 of magnification.....	48
Figure 4.3(a) : FESEM images of ENC at scale 20, 000 of magnification neat epoxy	49
Figure 4.3(b) : FESEM images of ENC at scale 20, 000 of magnification 1.0 wt.% of NCs.....	49
Figure 4.3(c) : FESEM images of ENC at scale 20, 000 of magnification 1.5 wt.% NCs.....	49
Figure 4.3(d) : FESEM images of ENC at scale 20, 000 of magnification 2.0 wt.% NCs	49
Figure 4.4(a) : FESEM images of ENC at scale 30, 000 of magnification neat epoxy	50
Figure 4.4(b) : FESEM images of ENC at scale 30, 000 of magnification 1.0 wt.% NCs	50
Figure 4.4(c) : FESEM images of ENC at scale 30, 000 of magnification 1.5 wt.% NCs.....	50
Figure 4.4(d) : FESEM images of ENC at scale 30, 000 of magnification 2.0 wt.% NCs	50
Figure 4.5 : XRD spectra of MCC, NC and ENC nanocomposite coating systems.....	53
Figure 4.6 : FTIR of the MCC, NC and ENC nanocomposite coating systems.....	56
Figure 4.7 : UV-Vis spectra for the ENC nanocomposite specimens	58
Figure 4.8(a) : TGA thermograms of the neat epoxy (ENC0).....	60
Figure 4.8(b) : TGA thermograms of the ENC nanocomposite coating systems ENC1.0	61
Figure 4.8(c) : TGA thermograms of the ENC nanocomposite coating systems ENC1.5	61
Figure 4.8(d) : TGA thermograms of the ENC nanocomposite coating systems ENC2.0	62
Figure 4.9(a) : DSC thermograms of the neat epoxy (ENC0).....	64
Figure 4.9(b) : DSC thermograms of the ENC nanocomposite coatings ENC1.0.....	64
Figure 4.9(c) : DSC thermograms of the ENC nanocomposite coatings ENC1.5	65
Figure 4.9 : DSC thermograms of the ENC nanocomposite coatings ENC2.0.....	65
Figure 4.10(a): Representative Bode plots in terms of impedance of the neat epoxy (ENC0) and ENC nanocomposite coating systems after 1 day of immersion.....	67
Figure 4.10(b): Representative Bode plots in terms of phase angle of the neat epoxy (ENC0) and ENC nanocomposite coating systems after 1 day of immersion.....	67

Figure 4.11(a): Representative Bode plots in terms of impedance of the neat epoxy (ENC0) and ENC nanocomposite coating systems after 30 days of immersion.....	68
Figure 4.11(b): Representative Bode plots in terms of phase angle of the neat epoxy (ENC0) and ENC nanocomposite coating systems after 30 days of immersion.....	68
Figure 4.12 : The equivalent circuits used for fitting the EIS Bode plots	70
Figure 5.1(a) : FESEM images of CHI at scale 10, 000 of magnification	73
Figure 5.1(b) : FESEM images of CHI at scale 50, 000 of magnification	73
Figure 5.1(c) : FESEM images of CHI at scale 100, 000 of magnification	73
Figure 5.2(a) : FESEM images of NCH at scale 50, 000 of magnification.....	74
Figure 5.2(b) : FESEM images of NCH at scale 100, 000 of magnification.....	74
Figure 5.2(c) : FESEM images of NCH at scale 150, 000 of magnification	74
Figure 5.3(a) : FESEM images of ECH at scale 20, 000 of magnification neat epoxy	76
Figure 5.3(b) : FESEM images of ECH at scale 20, 000 of magnification 0.5 wt.% NCHs	76
Figure 5.3(c) : FESEM images of ECH at scale 20, 000 of magnification 1.0 wt.% NCHs.....	76
Figure 5.3(d) : FESEM images of ECH at scale 20, 000 of magnification 1.5 wt.% NCHs	76
Figure 5.4(a) : FESEM images of ECH at scale 50, 000 of magnification neat epoxy	77
Figure 5.4(b) : FESEM images of ECH at scale 50, 000 of magnification 0.5 wt.% NCHs.	77
Figure 5.4(c) : FESEM images of ECH at scale 50, 000 of magnification 1.0 wt.% NCHs.....	77
Figure 5.4(d) : FESEM images of ECH at scale 50, 000 of magnification 1.5 wt.% NCHs.	77
Figure 5.5 : XRD spectra of CHI, NCH and ECH nanocomposite coating systems.....	78
Figure 5.6 : FTIR of the CHI, NCH, neat epoxy and ECH nanocomposite coating systems..	80
Figure 5.7 : UV-Vis spectra for the ECH nanocomposite specimens	81
Figure 5.8(a) : TGA thermograms of the neat epoxy (ECH0).....	83
Figure 5.8(b) : TGA thermograms of the ECH nanocomposite coating systems ECH0.5	84
Figure 5.8(c) : TGA thermograms of the ECH nanocomposite coating systems ECH1.0	84
Figure 5.8(d) : TGA thermograms of the ECH nanocomposite coating systems ECH1.5	85

Figure 5.9(a) : DSC thermograms of the neat epoxy (ECH0).....	87
Figure 5.9(b) : DSC thermograms of the and ECH nanocomposite coatings ECH0.5	87
Figure 5.9(c) : DSC thermograms of the and ECH nanocomposite coatings ECH1.0.....	88
Figure 5.9(d) : DSC thermograms of the and ECH nanocomposite coatings ECH1.5	88
Figure 5.10(a): Representative Bode plots in terms of impedance of the neat epoxy (ECH0) and NCH nanocomposite coating systems after 1 day of immersion	90
Figure 5.10(b): Representative Bode plots in terms of phase angle of the neat epoxy (ECH0) and NCH nanocomposite coating systems after 1 day of immersion	90
Figure 5.11(a): Representative Bode plots in terms of impedance of the neat epoxy (ECH0) and NCH nanocomposite coating systems after 30 days of immersion	91
Figure 5.10(b): Representative Bode plots in terms of phase angle of the neat epoxy (ECH0) and NCH nanocomposite coating systems after 30 days of immersion	91
Figure 5.12 : The equivalent circuits of used for fitting the EIS Bode plots.....	92

LIST OF TABLES

Table 3.1 : Chemical properties of Microcrystalline Cellulose	29
Table 3.2 : Chemical properties of High Molecular Chitosan	29
Table 3.3 : Properties of Epoxy Resin.....	30
Table 3.4 : Properties of curing agent Isophorone Diamine.....	30
Table 3.5 : Epoxy/nanocellulose nanocomposite coating systems	33
Table 3.6 : Epoxy/nanochitosan nanocomposite coating systems	35
Table 4.1 : Fitted parameter values of the equivalent circuit elements along with the utilised model for ENC nanocomposite coatings after 1 days of immersion.	71
Table 4.2 : Fitted parameter values of the equivalent circuit elements along with the utilised model for ENC nanocomposite coatings after 30 days of immersion	71
Table 5.1 : Fitted parameter values of the equivalent circuit elements along with the utilised model for ECH nanocomposite coatings after 1 days of immersion	93
Table 5.3 : Fitted parameter values of the equivalent circuit elements along with the utilised model for ECH nanocomposite coatings after 30 days of immersion	93

LIST OF SYMBOLS AND ABBREVIATIONS

θ	:	Bragg's Angle
λ	:	Incident Wavelength
$\beta_{1/2}$:	Full Width at the Half Maximum
d	:	Spacing between the planes in the atomic lattice
I	:	Current
I_{200}	:	Intensity of the (2 0 0) peak
I_{200}	:	Amorphous Minimum Region
K	:	Scherrer Constant
R	:	Resistance
V	:	Voltage
CI	:	Crystallinity Index
CS	:	Crystallite Size
CE	:	Counter Electrode
CHI	:	Chitosan
DSC	:	Differential scanning calorimetry
ECH	:	Epoxy/Nanochitosan Nanocomposite
EIS	:	Electrochemical impedance spectroscopy
ENC	:	Epoxy/Nanocellulose Nanocomposite
FESEM	:	Field Emission Scanning Electron Microscopy
FTIR	:	Fourier transform infrared spectroscopy
MCC	:	Microcrystalline Cellulose
NC	:	Nanocellulose
NCH	:	Nanochitosan
RE	:	Reference Electrode
TGA	:	Thermogravimetric Analysis
TPP	:	Sodium Triopolyphosphate
UV	:	Ultra Violet
WE	:	Working Electrode
XRD	:	X-ray diffraction

LIST OF APPENDICES

APPENDIX A	110
APPENDIX B	111

University of Malaya

CHAPTER 1: INTRODUCTION

1.1 Background

Corrosion leads to profound consequences to our society such as industrial resources, health and safety, economics and technologies. It is well known that environment plays the key role that affects the corrosion rate on many types of materials. When metallic materials such as iron are exposed to a natural atmosphere, corrosive agents such as oxygen or water interact with iron atoms and form an iron oxide with brownish layer appeared on the surface. We usually called this brownish forming as rust but phenomenon knew it as corrosion. Moreover, a corrosion reaction can be defined as the destruction of the material due to interaction with the environment. Many actions have been taken to reduce corrosion rate such as monitoring the environment, controlling the use of reactive materials and inventing protective layer on the material surface.

Generally, protective coatings are applied onto the material surface to prevent the detrimental effects of corrosive species. With consists of binders, pigments and additives are all required for blending a protective coating. In this study, a new formulation of protective coating against corrosion was developed in which nanocellulose (NC) and nanochitosan (NCH) were chosen to be the pigments or as an inhibitor used in an epoxy/diamine pre-polymer solution.

Along with the development of organic coatings, nanocellulose and nanochitosan are believed to intensify the performance of protective coatings. With the various processes for generating biopolymer nanofiller, it is possible that it can enhance epoxy elastomer and act as a good reinforcement for transparent composite coatings.

The inclusion of nanocellulose in epoxy remarkably improves the thermal and mechanical behaviour of the composite films, as well as its transparency (Cross et al., 2013; James et al., 2012). Because of the hydrophilic surface of NC, conversion of the

congeniality and curtailing the hygroscopicity must be performed. Because of the reactive surface of the OH side groups, grafting of chemical species can be done to functionalize the NC surface. Herein, NC was obtained from MCC via acid hydrolysis method using sulfuric acid. Generally, the nanocellulose particles resulting from sulfuric acid treatment are easily dispersible in water due to the presence of negatively charged sulphate half-ester groups that result from a reaction of sulfuric acid with the –OH groups on the cellulose surfaces (Wang et al., 2007). Under the controlled condition, NC can be obtained by this treatment purposely to remove high amorphous region and release single form of NCs.

Moreover, chitosan nanoparticle can be used as an inhibitor for corrosion protection on cold-rolled mild steel. With the capability of more polar function in chitosan molecules such as N and O, it was believed that this organic biopolymer is efficient for corrosion protection. For instance, El-Haddad and Fekry and Mohamed have reported chitosan as an effective corrosion inhibitor for copper and mild steel substrates in acidic medium (El-Haddad, 2013; Fekry & Mohamed, 2010). The inhibition efficiency increased with increasing the concentration of chitosan. Freky et al., 2012 have studied the stability and corrosion inhibition of chitosan on mild steel in medium sulphuric acid concentration, resulting in better corrosion protection as well as enhanced inhibition efficiency in acid.

On the other hand, Zheludkevich et al., 2011 have reported a type of corrosion protective self-healing coating which was constituted by a chitosan-based pre-layer coating onto a metal surface. The corrosion protection properties were studied using electrochemical impedance spectroscopy and resulted in good corrosion protection coating with the presence of inhibitor-doped chitosan.

Epoxy/diamine pre-polymer are extensively used as a coating in many industrial applications especially onto the metal surface. When applied this mixture to the metal surface, a chemical bond between epoxy/amine with metal oxide and hydroxide will be

formed. This phenomenon creates an interphase between the coating and metal surface which is practically increased the adhesion of the coating layer. Roche et al., 2002 have investigated the formation of epoxy/diamine with metal interphase. Ionised metal atom diffused within epoxy/diamine prepolymer solution and reacts with the amine group of the diamine monomer which then forming organometallic complexes by coordination.

The investigations describe some parts of the properties of protective coating that may guide to the development of anticorrosion performance with the presence of biopolymer enhancement agent. The development of new corrosion non-toxic inhibitor can be a promising environmental friendly reagent for coating protection which does not contain harmful substances such as chromate or nitrate based that widely used as a corrosion inhibitor. Applying biopolymer inhibitor as nanofiller in an organic coating system can also be another enhancing product due to their superior potency and structural versatility leading biodegradable compound (John et al., 2015; Truong et al., 2000). The application of polymer as a protective coating for metal is commonly found in manufacturing industries. To improve the interaction of this coating material with the metal substrate, there will be a need of obtaining suitable inhibitor agent to be incorporated into the polymer.

1.2 Advantages

Protecting metal surfaces with an anti-corrosive agent incorporates with the organic coating is an alternative way to enhance the mechanical properties of the metal and prevent it from eroding quickly. By introducing natural resources as a basis for biopolymer coating can reduce erosion corrosion activity and more durable. As an instance, cellulose and chitosan are renewable biopolymers abundantly found in the world, have attracted much attention such as an interesting structure which is allowing optimisation on their physicochemical properties. Moreover, their promising characteristics including hydrophilic, chirality, biodegradability and the ability to form semi-crystalline morphological fiber have attracted significant increase and promoted interdisciplinary research worldwide on biopolymer and its products over the past few decades. With a modified binder system as an additional source of biopolymers for corrosion protection has increased the performance of surface protection layer when there is damage. Also, increase the adhesion layer on the steel substrate to prevent delamination of the defect and the complexion of iron or oxygen.

Hence, to reduce the corrosion rate with the use of biological and environmentally friendly anticorrosive layer at the interface between the metal, it is crucial to use the excess supply of renewable natural biopolymers and biomass-based economy of assorted sizes around the world. This is because it also has a lower density, lower cost and save energy consumption. It has a high specific strength, modulus and reactive surface that can be used to graft a certain group in the future.

1.3 Objectives of the study

To achieve a good protective coating against corrosive environment on a metal surface, this study aims to develop a new formulation of the organic coating by using an enhancing agent from biopolymer resources. In that regard, nanocellulose and nanochitosan were prepared from their raw sources which later be blended with epoxy/diamine pre-polymer solution. The composite coating systems were then characterised and evaluated.

The aims of the study are summarised as follows;

- a. To develop the biopolymer anti-corrosive agent to be used in the organic coating.
- b. To study the method of preparation and characterization of biopolymer anti-corrosive agents.
- c. To evaluate the physical and thermal properties of the developed coating against corrosion.
- d. To examine the corrosion protection performance of the developed coating using electrochemical impedance spectroscopy.

1.3 Outline of the thesis

This part summarises the outline of the thesis:

- **Chapter 1** consists the background that briefly introduced the purpose of this work and the advantages of the study. This section also describes the aims of this work.
- **Chapter 2** summarised the literature study including the common knowledge of coating types and corrosion, synthesize methods of nanocellulose and nanochitosan and the review of nanocomposite coatings. Previous works that have been established in this study area also have been discussed. The methodology of two types of filler preparations and coating designations will be discussed in **Chapter 3**. This section also describes the materials and explains the equipment used for characterization and anticorrosion performance.
- **Chapter 4** presents the results and discussion of the nanocomposite coating by using nanocellulose as an enhancing agent. This section consists of the analyses on morphology and chemical bonding, thermal analyses and transparency testing. Foremost, the evaluation of anticorrosion performance has also been discussed in this section. In the other hand, the developed coating by using prepared nanochitosan will be discussed in **Chapter 5** with same analysed results in Chapter 4.
- **Chapter 6** compiles overall discussion of all results obtained in this project. The conclusion for the results obtained and further suggestions on this work were discussed in **Chapter 7**.

CHAPTER 2: LITERATURE REVIEW

2.1 Introduction

This chapter covers the effects of corrosion protective methods and the recent developments in coating technology. The performance of organic inhibitors is associated with the chemical structure and physical or mechanical properties of the coating systems. Corrosion inhibition may be due to the adsorption of molecules or ions on the anodic/cathodic sites, increase in the cathodic/anodic overvoltage and forming a protective barrier film. Some of the factors that contribute to inhibitor action is a long chain, molecular size, bonding, aromatic/conjugated, bond strength to the substrate, the ability to cross, solubility in the environment (Rani & Basu, 2012).

Organic coating is important as proper surface treatment, a simple mode coating and cost effective of corrosion protection for metal objects and low structure must be emphasised. The outer surface of metal rust like iron and aluminium alloys need to be protected from their environment with coating systems. The coating system is one of the oldest histories of the layer to be performed, so the problem of understanding how and why a layer of corrosion control is a key issue for environment control.

Herein, general studies and reviews that have been done were summarised intensively to propose the development of this work. Information was extracted from various literatures and resources as the references before beginning the actual work.

2.2 Corrosion

Corrosion can be defined as the deterioration of a metallic surface because of interaction with their surrounding environment. Material such as metal reacts chemically with the external environment and as time elapsed the structure will deteriorate slowly until can cause damage to itself. Metal surface will undergo oxidation reaction usually with oxygen in the atmosphere whenever exposed to the external environment (Davis, 2000). The basis of the corrosion process on the metal surface can be explained by electrochemical reaction.

There are three essential constituents for corrosion process:

i. An anode

The anode is the site at which the metal atoms lose electrons and the part where metal is corroded. When metal is corroded (anode) the metal is oxidized, forming metal ions and free electrons.

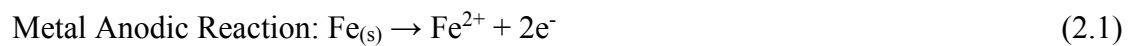
ii. A cathode

The cathode is the site where reduction takes place and electrons are transferred to the reduced part. At this point, the free electrons can reduce the oxygen and most of the times forming hydroxide.

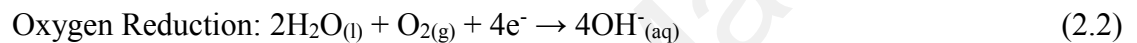
iii. An electrolyte

The electrolyte is the corrosive medium such as water, salt water, or any conducting medium. Hence the corrosion current between the anode and the cathode consists of electrons flowing within the metal and ions flowing within the electrolyte (Zhang et al., 2010).

The anodic reaction is where oxidation occurs, meaning electrons are removed from the anode site. In corrosion process, metal atoms are ionised to an electrolyte as positively charged ions, releasing electrons to oxygens molecules and form metal ions (Levy, 1995; McCafferty, 2010; Uhlig, 2008).



The produced electrons are used up in the cathodic reaction. At the cathodic site, the hydrogen ions reduced to their atomic form which then reacts with electrons and forms hydrogen gas.



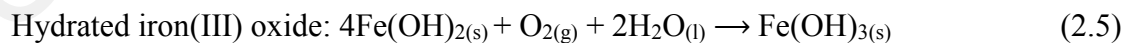
or



Hydration reaction usually occurs in acidic medium within pH value range 6 - 8. Besides, oxidation reduction is the most important reaction.



Normally, iron(II) hydroxide is greenish since it oxidised partially in the air and produced by corrosion in the first place.



Eventually, the reddish or brownish rust formed from the further oxidation or hydration reactions. This rust usually seen on the material surface attributed to the corrosion attacked the surface.

The electrochemical reaction can be illustrated as shown in Figure 2.1 below.

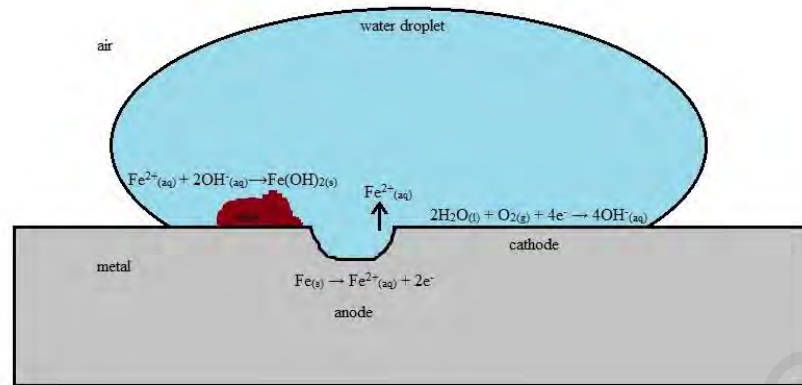


Figure 2.1: Anode and Cathode reactions on metal surface.

Most metallic materials are prone to corrosion. Generally, uniform attack corrosion is the most common corrosion occurred on the metal surface. It causes an electrochemical reaction that results in damage to the material surface or deterioration of the entire surface that exposed to the environment or anticorrosive species (Cornell & Schwertmann, 2003; Jones, 1993). Nevertheless, there are many types of corrosion such as galvanic corrosion, intergranular corrosion and localised corrosion. Also, many proper ways to slow the rate of corrosion depending on the circumstances and the environment of the metal being corroded.

As an instance, a protective coating method, where damage is prevented by mechanically isolating the package contents from aggressive caustic by using a protective film, layer, paint or coating. Since this method is known as a passive corrosion protection, it does not alter the aggressiveness of corrosive species. Corrosion may occur instantaneously if the protective layer or film is destroyed. The protective coating isolates the metal surface from aggressive media.

2.3 Corrosion Protection

2.3.1 Cathodic Protection:

Cathodic protection (CP) is a technique used to control the corrosion rate of a metal surface by converting the anodic sites to the cathodic site in an electrochemical cell (Ashworth, 2010; Bahadori, 2014). Two methods can be performed in this technique;

i. Sacrificial Anode - This method sacrifices another metal to act as anode and can be introduced to the electrolyte then corrodes to protect the metal surface on the cathode. The metal ions move from the anode to the cathode where the anode will corrode fast. Because of that, the anode or sacrificial metals can be replaced regularly. Sacrificial metals or anodes are generally made of reactive metal such as aluminium, zinc or magnesium. These metals have the most negative electro-potential of metal.

ii. Impressed Current - this method requires an impressed current which is applied in an alternate direction to invalidate the corrosion current and convert the corroding anode to the cathode. Usually, an alternative source of direct current is used to the electrolyte, the metal is connected to the negative terminal, while an auxiliary anode is attached to the positive terminal. However, the auxiliary anode would not sacrifice as in sacrificial anode system.

Cathodic protection techniques usually applied on pipelines, ships and boats, steel in concrete, marine, etc. It mostly protects the metallic structure from galvanic corrosion in the various environment, especially in seawater. This galvanic corrosion occurs when two different metal submerged in a corrosive electrolyte or in close proximity on moist soils and often attacks oil and gas pipelines and offshore rigs (Ahmad, 2006).

2.3.2 Corrosion Inhibitor:

Corrosion inhibitors are chemical compound that reacts with the corrosion species or with the metal's surface, thereby, decreased the rate of corrosion on the metal's surface. The chemical compound is so-called inhibitors which absorbing onto the metal's surface and acts as a protective coating or a barrier (Granath, 2010; Saji, 2010).

However, rate of corrosion could be slow down by the following process of the inhibitor;

- i. Decreasing the diffusion of corrosive species to the metal's surface.
- ii. Changing the polarisation behaviour at the cathodic or anodic site.
- iii. Increasing the resistance or impedance of the metal's surface.

The advantage of using corrosion inhibitor technique is that it can be simply applied directly to metals or in-situ method and form as a passivation layer (Aliofkhazraei, 2014; Lamaka et al., 2007). This technique is applied most in oil and gas exploration, petroleum refining or in chemical production.

Nevertheless, polymer coatings are vastly applied for metal surface protection against corrosion. They can form a barrier against the corrosive species which are providing the passive protection. Simultaneously, they also serve as a polymeric matrix for the interaction of anticorrosive agents, which are responsible for an active anticorrosive action to embed within the matrix and crosslinked.

2.3.3 Protective Coating:

Protective coatings are covering layer that applied on the material surface to protect from the corrosive environment (Stratmann et al., 1994). Paint, tar and varnish are commonly used for protective coating. However, organic coatings are very prominent protective paints to protect the material from the degradation effect of corrosive environment.

The binder of the coating can be in many forms such as solvent-based or water-based anticorrosion resins. Solvent-based is a very high-quality protective coating but have a long drying process which may take a week for fully cured film. In contrary, water-based systems have short curing time but highly temperature dependent (Elmore et al., 2002). Another type of protective coating is dipping waxes and oils without solvent. They are relatively complex and inadequate quality of coating, however, can achieve a good quality of coating with the addition of the inhibitor.

The composition of organic coating depends on the formulation of materials component (Bierwagen, 1996; Zorll, 1985). These components have specific functions due to the use.

The four important components in an organic coating are:

- i. Pigment

The main function of pigment is to provide colour in organic coatings and not only that, it also works beneath of the layer to protect the surface within. Moreover, pigment helps to hold together the paint system together. The amount of pigments content embedded into the paint system might change the physical and mechanical properties of the paint.

ii. Binder

Binders are usually the major component of a paint system. They are sometimes called the backbone of coating component which leads to stick together and hold the pigment to the surface of the substrate. Generally, they are polymeric substances such as polyurethane, epoxy resin and alkyd resin. They can be dissolved by certain solvents.

iii. Additives

Additives are chemicals that must be chosen to be dried quickly and capable of dissolving the binder but would not polymerize. Additives, however, able to modify the properties of the paint system, as an instance, the drying or curing period of the resin.

iv. Solvents

In coating formulation, solvents are used to dissolve or disperse any additional components such as pigments. By adding solvent in the coating system, it helps to achieve the desired consistency such as the viscosity of the solution. Once the coating is applied on the material surface, the solvent evaporates and allowing the coating layer to dry.

These four components are cooperating where pigments are essentially dispersed in binder medium or resin. The proportion of pigments in the resin can change the properties of the medium physically and chemically due to the nature behaviour of the present pigments (Galliano & Landolt, 2002). Also, be advantageous of the solitary function of the solvent in the medium helps to control the viscosity of the coating system for ease of the subsequent applications.

2.3.4 Metal Surface and Environment Protection:

No metal is resistant to corrosion in most of the environments, hence, by changing the type of metal and through monitoring the environment can lead to control the corrosion rate significantly (Pots & Hendriksen, 2000; Uhlig, 2008).

More understandings are needed in making material selection especially on the composition and the specification of the components. As an implementation, the development of new type of alloys are designed to protect the surface of the material against the corrosion in certain environmental but are still under control due to the expenses and the contribution to the friendly environment scales (Presuel-Moreno, Jakab, Tailleart, Goldman, & Scully, 2008). Monitoring the environmental condition also helps to limit the contact with corrosive species and avoid the high exposure of sulphur, oxygen or chloride content (Zhang et al., 2010).

Moreover, the deterioration of surface can also be caused by the result of manufacture production. As an instance, crevices and cracks on the surface may come from the operational process (McMurray & Williams, 2010). Surface failures can cause corrosion to occur beneath the painted substrate due to the presence of corrosive species within the process. Therefore, proper monitoring is what manufacturing really needs to eliminate vulnerable surface on materials and prevention the use of reactive metal in the operational compositions.

2.4 Metallic Surface - Mild Steel

Mild steel is used mostly in the manufacturing industry especially for mounting equipment applications like machine parts, cook wares, vehicles and all-purpose engineering materials. This type of steel is often used because of the ease handled metal such as annealing and forming due to low carbon contains which making it become very durable, weldable and malleable (Li & Wang, 2011). In order to be good in structural integrity, mild steel also inherent with good its conductivity properties where electricity can flow easily through without impacting its structure. In contrary, high carbon steel is extremely hard, it requires heat treatment or high stress for structuring the shape and special operational in welding.

Ideally, the chemical composition of mild steel consists 0.16 - 0.18 % of carbon, 0.40 % of silicon at the maximum amount, 0.70 - 0.90 % of manganese, 0.40 % of sulphur and phosphorus at maximum amount to meet the grade type. In cold drawn condition will determine the mechanical properties. They consist of 400-560 n/mm^2 of maximum stress, 300-440 n/mm^2 min of yield stress, 280-420 n/mm^2 min of 0.2 % proof stress and 10 - 14 % min of elongation. These mechanical progressions are all dependent on the ruling section.

Unfortunately, with its good tensile strength, mild steel, however, is poor corrosion resistance and it must be sealed or painted with a protective coating such as grease or oil. Protective coatings might help the metal surface from exposure to the wet environment and prevent from rusting (Dehri & Erbil, 2000; Tan & Blackwood, 2003). Since, most daily products made from mild steel materials and least expensive types of metal available, they become a most popular choice in the wide market. Protect it from degradation, rust and damage becomes the main priority to keep their quality and prolonged to use.

2.5 Cellulose and Chitosan as Pigment

The addition of nano-material to the coatings is believed to help to enhance the properties of the neat coatings and improving functional coating due to their small size of the particle. This study proposes two different types of the nanofiller act as a pigment into epoxy/diamine prepolymer systems.

Now, we can ask about the factors that make cellulose and chitosan such an important substance. The appeal of cellulose and chitosan arises from its specific structure. Its macromolecules are composed of repeating glucose units that produce surprising specificity and impressively diverse function, structure and reactivity. They also have been regarded as a biomaterial in the fields of biomedicine and biotechnology due to biocompatibility, biodegradability and biological activity.

Some important parameters make cellulose a unique material, that are, the reaction and properties of cellulose are determined by the isolation process used, the number of inter- and intra-molecular hydrogen bonds, chain length, chain length distribution, the degree of crystallinity and distribution of functional groups along the polymer and the polymer chain.

On the other hand, the reasons for the versatility or difficult-to-decompose properties of chitosan as hard crystal structure with the presence of acetamide or primary amino group residue, which is important for forming conformance features via internal or intermolecular hydrogen bonds. These properties make chitosan become another special kind material.

2.5.1 Cellulose

The suitability of using biopolymer materials, such as polysaccharides, proteins and lipids, in film production has been intensively studied recently to produce biodegradable packaging materials. The development of biomaterials holds great promise to alleviate many sustainability problems and offers the potential of renewability, biodegradability and a path away from harmful additives. Compared with other materials, cellulose is the most abundant natural carbohydrate biopolymer on earth that is renewable, biodegradable and non-toxic. It is a hydrophilic polymer composed of repeating β -1,4-linked-D-glucopyranose units and consists of three hydroxyl groups per anhydroglucose unit (AGU), which allows the cellulose molecule to establish strong hydrogen bonds (Zugenmaier, 2008).

Knowledge of the molecular structure of cellulose is crucial, as it explains the characteristic properties of cellulose, such as hydrophilicity, chirality, biodegradability and high functionality. The morphology and the properties of the cellulose nanocrystals are influenced by its preparation and the dissolution methods used (Chang & Zhang, 2011; Chang et al., 2010; El-Wakil and Hassan, 2008). As a renewable material, cellulose and its derivatives have been comprehensively studied, with a focus on their biological, chemical and mechanical properties.

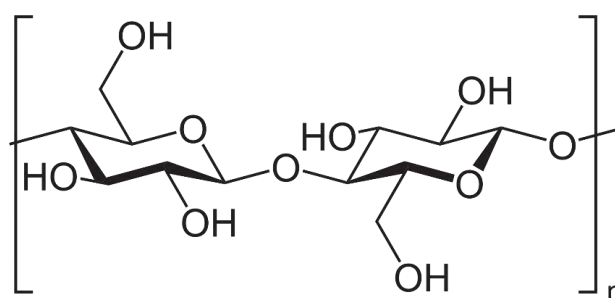


Figure 2.2: General structure of cellulose.

Studies of cellulose in nano size and their application as reinforcing components in polymer composites have received considerable attention. As the size of bulk wood cells to nanofibrils decreases, the elastic modulus of the cellulose increases to about 10 to 70 GPa or more and the mechanical properties of the cellulose nanofibril reinforced polymer composite are markedly improved.

Nanocellulose (NC) has been generated from microcrystalline cellulose (MCC) via acid hydrolysis to improve the physical, mechanical and gas barrier properties of biopolymer films because of its attractive features, such as high aspect ratio and light weight (Peng et al., 2011). These remarkable physicochemical properties and wide application prospects have attracted significant interest from both researchers and industrialists.

Along with the development of organic coatings, cellulose nanocrystals are believed to intensify the performance of protective coatings. Thus, the preparation of NC from MCC is important and needs to be considered. Poaty et al., 2014 implemented the modification of cellulose nanocrystals with various acryloyl chlorides as reinforcement derivatives for wood coatings, which resulted in an enhanced abrasion resistance of the coatings. Satyamurthy and Vigneshwaran (2013) studied the novel process of preparing spherical NC using anaerobic microbial hydrolysis with MCC and found that the bimodal particle formed by NC has potential in commercial applications. Shankar and Rhim (2016) prepared NC from MCC using an alkaline dissolution method, followed by the regeneration of cellulose, neutralisation and ultrasonication, which decreased the nano level as a result.

Thus, the biodegradability, low density, worldwide availability, low cost and alterable surface properties of these novel materials offer the opportunity to develop new generation materials based on cellulose fibers.

2.5.2 Chitosan

Chitosan is a naturally abundant organic polymer and a kind of polysaccharide composed of N-Acetylglucosamine and glucosamine units, with many special characteristics such as biocompatibility, biodegradability, nontoxicity and chemical reaction. Because of these outstanding properties, chitosan can be selected as a useful and effective polymer matrix in composite materials. Due to the presence of hydroxyl and amino groups, the reaction of chitosan much more versatile than cellulose and probably beneficial for the homogeneous phases in the chemical cross-linking network (Dash et al., 2011).

Chitosan is a weak base and is insoluble in water and organic solvents. However, it is soluble in dilute aqueous acidic medium (pH <6.5). It precipitates in an alkaline solution or in a polyanion and forms a gel at low pH. Almost all are soluble in diluted acids but insoluble in sulfuric acid and water.

Many studies had investigated that the chemical reactions of chitosan in an aqueous solution of acids, N-acylation and N-alkylidinations. Under of acidic condition, chitosan will be hydrolysed and dissolved in water due to the unstable reaction. This because of the presence of glycosidic unit in chitosan is hemiacetal which caused it not stable in acid. Dutta et al., 2004 discovered that N-acylation of chitosan with acyl halides introduced amido groups at the chitosan nitrogen while N-alkylidination with aldehydes produced N-alkyl chitosan upon hydrogenation (Dutta et al., 2004; Lim & Hudson, 2004; Rinaudo, 2006), resulting in decreased molecular weight and viscosity of chitosan. Henceforth, the increased in degree of degradation caused increase in crystallinity index and decomposition temperature, also decrease in molecular weight of chitosan and the water absorption (Yuan et al., 2011)

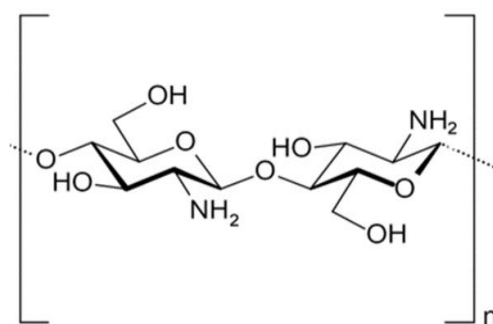


Figure 2.3: General structure of chitosan.

In a recent study, the nanoparticle of chitosan has been discovered by many studies as an attracted attention for their broad applications due to their ability such as degradability, biocompatibility and nontoxicity. Many methods have been studied to prepare chitosan nanoparticles and its characterization (Dudhani & Kosaraju, 2010). Huang et al., 2009 has degraded chitosan into lower-weight-chitosan using different concentrations of phosphoric acid and then prepared nanochitosan with concentrations of sodium tripolyphosphate, resulting in the lower potential surface of optimal crosslinked ratio of low molecular weight chitosan and sodium tripolyphosphate. Sudha et al., 2014 used ionic gelation method for ionically cross-linked chitosan with sodium tripolyphosphate in dilute solution to synthesise nanoparticle. The ionotropic gelation method is an ionic interaction between the negatively charged groups of sodium tripolyphosphate (TPP) and the positively charged primary -NH₂ of chitosan. TPP is a polyanion used as an ion crosslinking agent due to its multivalent properties. It helps the cross-linking process to avoid possible toxicity of chemical or biological reagent and prevent from any other undesirable effects (Fan et al., 2012; Tsai et al., 2011; Vijayalakshmi et al., 2014).

2.6 Epoxy as Binder

Since epoxy resin was introduced in the paint industry in the late 1940's, epoxy resin occupied a prominent position among paint chemists' available materials. This is because these resins are very versatile and it is possible to formulate a wide variety of coating systems. These epoxy coatings are widely used for industrial baking finishes that demonstrate maximum performance in solvent resistance and chemical resistance to maintenance systems for corrosive environments.

Epoxy polymer or resin are characterized by the presence of epoxide groups which is a three-membered oxide ring. This resin contains more than one epoxide group per molecule and can be polymerised with the crosslinking agent (Materne et al., 2012; Zhang et al., 2000). The crosslinking agent also known as curing agent or hardener will react with the epoxide or hydroxyl groups to form a three-dimensional network. Generally, epoxy resin is the forming reaction of diglycidyl ether of bis-phenol A (DGEBA) or the product of the reaction between epichlorohydrin and of bisphenol A (BPA) in sodium hydroxide (NaOH). It has the general structure as illustrated in Figure 2.2.

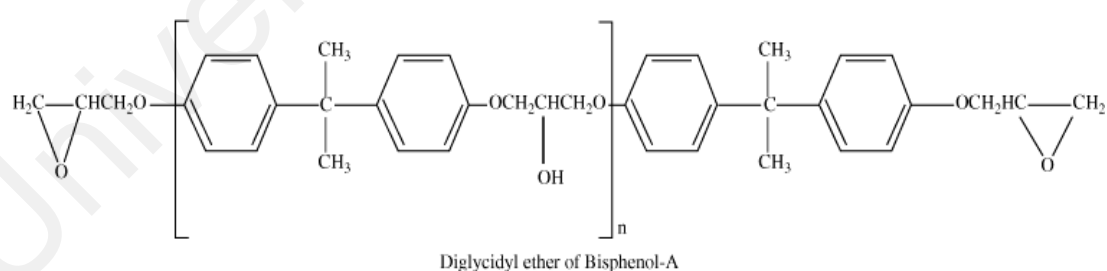


Figure 2.2: General structure of DGEBA Source (Sales & Brunelli, 2005).

The chemical characterization of epoxy can be determined analytically with curing agents as the starting material and followed with the crosslinking process. Finally, the determination of the cured product properties such as forming of the network chain and chemical bonding.

The most common type of curing agent or hardener for the epoxy resin is an amine. It can be primary, secondary or tertiary amines, they react with the epoxy ring through the ether linkages from the active sites of the curatives (Fraga et al., 2008).

Primary amines - It has two active hydrogens that react with an epoxide group. Network chain is developed when more than one primary amine per molecule are used in this curative. The reaction of epoxide group and primary amine is illustrated in Figure 2.3

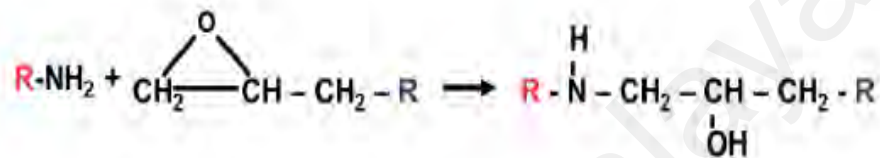


Figure 2.3: Molecular reaction of epoxide group and primary amine.

Secondary amines - It reacts with only another one epoxide group and the rate of reaction is much slower compared to the primary amine curing agents. The reaction of secondary amine with epoxy group can be illustrated as in Figure 2.4

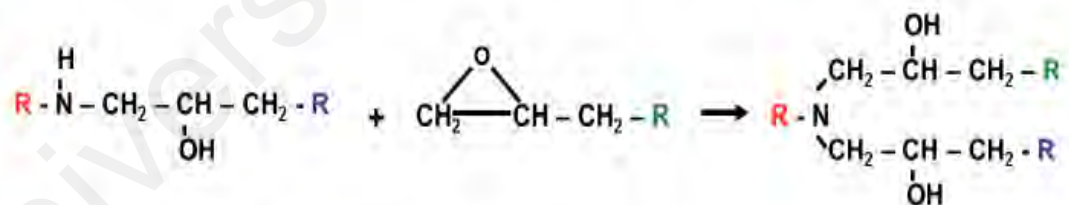


Figure 2.4: Molecular reaction of epoxide group and secondary amine.

Tertiary amines - this type of curative have no active hydrogens and not react with epoxy resins. However, it can cure epoxy resins in homopolymerization by the catalytic system and helps to accelerate the curing rate of between epoxy resins and primary and secondary amines. Figure 2.5 illustrates the reaction of a tertiary amine with an epoxy group.

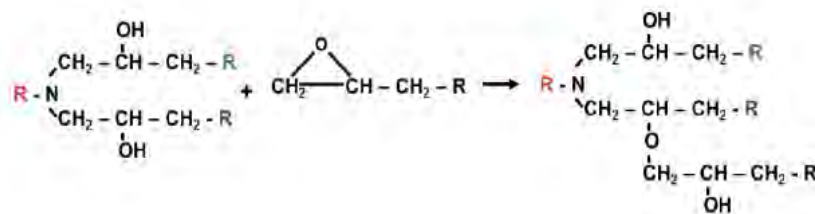


Figure 2.5: Molecular reaction of epoxide group and tertiary amine.

Figures above represent the reaction curing of epoxy resin with glycidyl amine. However, there are many reactivities can be occurred in epoxy matrices due to the dictation of curing agents. Therefore, the selection of curative or curing agents is depending on the desired properties or processing methods. In most cases, the ratio of epoxy-curative must be considered stoichiometrically. This because it may affect the properties of the cured resins such as kinetic and mechanical properties.

Achilias et al., 2006 have studied the cured kinetic of epoxy systems by using diamine curative, isophorone diamine based. They claimed that the reactions on curing process of epoxy resins can be varied, either sequentially or simultaneously and reactivity rate due to temperature or reactants. The reaction may take place at the epoxide ring, end of the epoxy chains with amine groups and the etherification of the oxirane ring with a hydroxyl group (Karayannidou et al., 2006).

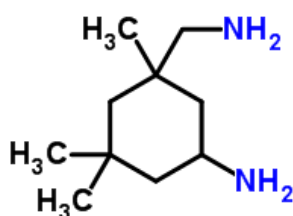


Figure 2.6: General structure of isophorone diamine (IPDA).

Also, Roche et al., 2002 have investigated the interphase formation between epoxy-diamine and the metal surface. The interaction between diamine and metal surface chemically formed and practically increase the adhesion of the cured epoxy-diamine prepolymer. Moreover, they claimed that chemical bonding of diamine-metal parallel orientated on the metal surface which leads to improving the chemical and physical properties epoxy-diamine as good primary layer on the metal surface (Roche, Bouchet, & Bentadjine, 2002).

Moreover, polymer-clay nanocomposite coatings have been studied using epoxy-diamine prepolymer in which isophorone diamine (Figure 2.6) as a curative (Zaarei et al., 2010). Incorporation of nanolayer clay which has plate-like shape into epoxy-diamine prepolymer decreased the corrosion receptivity of coating attribute good corrosion protection performance.

2.7 Nanocomposite Coating

A nanocomposite coating can be defined as a coating composed of two or more non-miscible phases which means one of the components is restricted to the nano size dimension. The nanoscale component is known as filler in nano size, so called, nanofiller. Hence, to form a nanocomposite coating, this nanofiller must fill or disperse into a monomer matrix (Lince, 1991).

The properties may vary depends on the chemical and physical nature of each component in the composition. For an instance, the type and size of the filler can enhance the adhesion of pre-polymer solution. This filler can be a nanoparticle and it is highly affirmed to investigate the structure, morphology and the size of the nanoparticle and they can be nanotube or nanofiber.

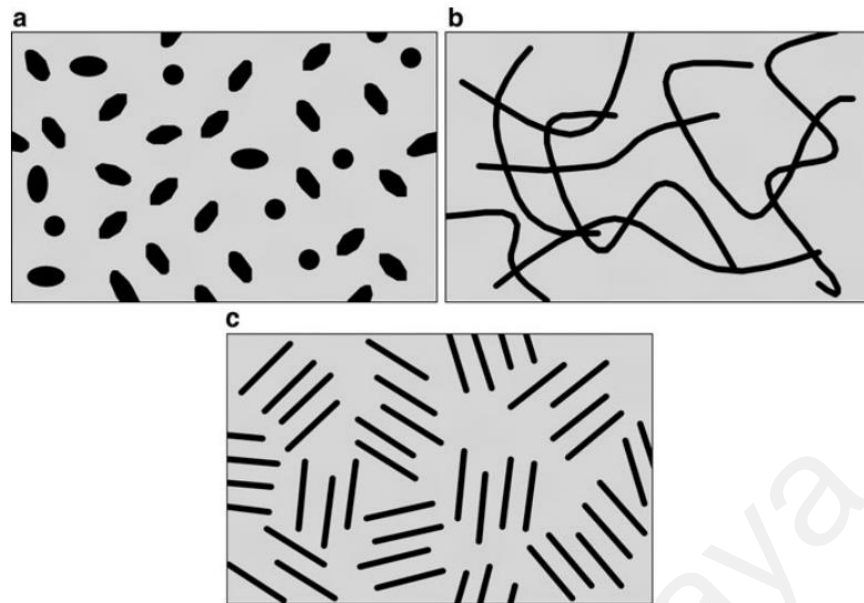


Figure 2.7: Nanocomposite coating formed by (a) nanoparticles, (b) nanotubes and (c) nanolayer (Wang & Chung, 1991).

Moreover, incorporation of nanofiller in polymer matrix lead to advantageous of application in coating industry such as self-healing and antifouling coatings. Swati Gaur and Khanna (2015) have investigated the functional coating created through incorporation with nanoparticles. In the first place, a hydrophobic surface was created with fluorosilane and then different nanoparticles were added in according to application mechanisms. Zinc oxide nanoparticles and nanosilica were used for self-cleaning and anti-fouling coatings, respectively (Gaur & Khanna, 2015).

According to Musil (2000) in order to protect the most material from unsafe environment, the significant formation of hard and superhard coating single layer of nanocomposite coating become a new attention in which a strong correlation was developed between hardness and nanocomposite coatings. He also suggested that nanocomposite of MeN/a-nitride and MeN/metal are two types superhard film. As a result, a superhard film composed of two cases, first is composed of two hard phases and second is a composition of one hard phase and another is a soft phase (Musil, 2000).

Notably, introducing nanofiller into polymers promising to improve the physicochemical properties such heat resistance, adherence, tensile strength and mechanical properties (Bagherzadeh & Mahdavi, 2007; Lin et al., 2014; Yeh et al., 2006). Due to their small size and large specific surface area, nanofiller tend to occupy empty pore in pre-polymer molecules and thus acts as a bridge to connect intermolecularly. Apart from that, incorporating of nanofiller in nanocomposite coating enhance the corrosion protection performance (Ammar et al., 2016; Palimi et al., 2014; Shi et al., 2009).

University of Malaya

CHAPTER 3: METHODOLOGY

3.1 Introduction

This chapter explains the preparation of nanofillers, namely, nanocellulose and nanochitosan, which later used for nanocomposite coating prepared with epoxy/diamine pre-polymer. As it has been notified, the purpose of this study is to develop epoxy based nanocomposite coating systems. This part also explains briefly the analytical methods that have been used in this study to measure the physical, chemical and structure properties of the coating systems. Moreover, several techniques also have been used to evaluate the thermal stability and corrosion performance of each coating system. The overall nanocomposite coating systems and its characterizations are illustrated as in Figure 3.1.

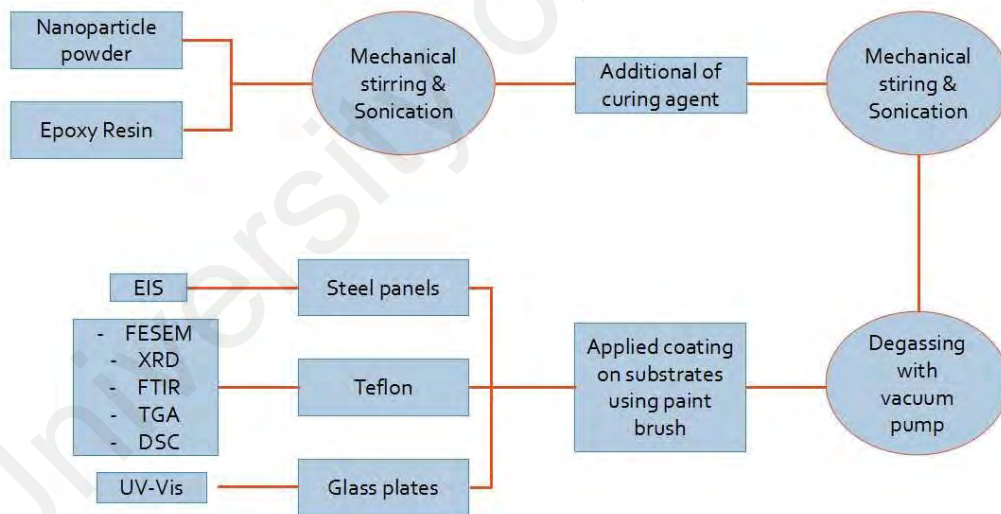


Figure 3.1: Flow chart of nanocomposite coating systems.

3.2 Materials

The following raw chemicals were used for the preparation of nanofiller.

- The raw microcrystalline cellulose (MCC) extracted from softwood pulp was purchased from R&M Chemicals (Essex, U.K.) with 50 μm of particles size.

Table 3.1: Chemical properties of Microcrystalline Cellulose.

Molecular Formula	$(\text{C}_6\text{H}_{10}\text{O}_5)_n$
Appearance	White lap sheet
Thermal Decomposition ($^{\circ}\text{C}$)	260 – 270 (500 $^{\circ}\text{F}$ – 518 $^{\circ}\text{F}$)
Solubility	Insoluble in water

- High molecular chitosan (CHI) extracted from shrimps in form of coarse ground flakes and powder without further purification was purchased from Aldrich Chemistry (USA).

Table 3.2: Chemical properties of High Molecular Chitosan.

Molecular Formula	$\text{C}_{12}\text{H}_{24}\text{N}_2\text{O}_9$
Appearance	Off-White to beige
Molecular weight (Da)	310000-375000
Solubility	Insoluble in water

The following resins were used as binder and additives for coating systems.

- The medium-viscosity liquid epoxy was produced from bisphenol A and epichlorohydrin with an unsaturation concentration of approximately 5260 to 5420 mmol/kg and a molar mass of 184 to 190 weight per equivalent was supplied by ASAChemicals (Selangor, Malaysia) and used as received without any further modification.

Table 3.3: Properties of Epoxy Resin.

Viscosity at 25 °C (Pa.s)	12.0 - 14.0
Density at 25 °C (kg/l)	1.16
Diluents	No
Colour (Pt-Co)	100 max

- The ASAChemicals also supplied the isophorone diamine (IPDA) curing agent, which was 3-aminomethyl-3,5,5-trimethylcyclohexylamine, 99.7 wt.% solute content in water solution with a molar mass of 170.30 g/mol and a pH value of 11.6.

Table 3.4: Properties of curing agent Isophorone Diamine.

Viscosity at 20 °C (mPa.S)	18
Density at 20 °C (g/cm³)	0.92
Odour	Amine-like
Colour	Colourless to yellow

The lists of solvents used in preparation of nanofillers;

- i. Sulfuric acid (H_2SO_4) (98 wt.%) was purchased from Fisher Scientific (Selangor, Malaysia).
- ii. Sodium hydroxide (NaOH) (0.5 w/v%) was purchased from Bendosen Laboratory Chemicals (Selangor, Malaysia).
- iii. Ultra-pure water ($18 \text{ M}\Omega\cdot\text{cm}$, $25 \text{ }^\circ\text{C}$) was provided by INFRA Analytical Laboratory (Kuala Lumpur, Malaysia).
- iv. 99 % acetic acid (CH_3COOH) from Shikmayu's Pure Chemical (Selangor, Malaysia).
- v. 99.6 % absolute ethanol (EtOH) was purchased from Fisher Scientific (Selangor, Malaysia).
- vi. 85 % phosphoric acid (H_3PO_4) was purchased from Friendemann Schmidt (Selangor, Malaysia).
- vii. Sodium Tripolyphosphate ($\text{Na}_5\text{P}_3\text{O}_{10}$) was purchased from Sigma Aldrich (Selangor, Malaysia).

3.3 Method of Preparations

3.3.1 Preparation of nanocellulose

Firstly, the microcrystalline celluloses (MCCs) powder was dried in a vacuum at 70 °C for 24 hours. Nanocellulose (NC) were prepared according to a modified method of Johar et al., 2012 and Shankar and Rhim (2016). For this, three gram of the MCC has then added to a 40 wt.% H₂SO₄ solution and the solution was vigorously stirred at 60 °C for 1 h. Then, the suspension was quenched with type-1 ultra-pure water, which was removed by successive centrifugation at 6000 rpm for 10 min. The treated MCC was collected and washed 4 to 6 times with 50 w/v% NaOH and EtOH, followed by centrifugation to remove any remnants of NaOH. After washing, the treated MCC was suspended with EtOH until the suspension reached a pH value of 8 to 10. The suspension was stirred at 400 rpm for 30 min and sonicated for 2 min using a 2 mm probe at 60 % amplitude. The dispersed NC was dried overnight and desiccated until further use.

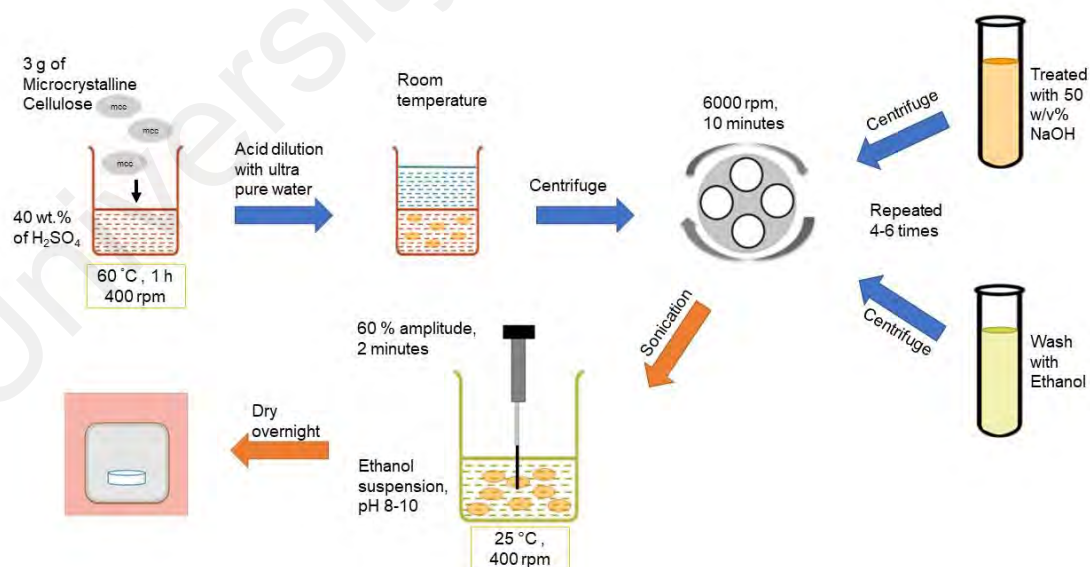


Figure 3.2: Preparation of nanocellulose.

3.3.2 Preparation of epoxy/nanocellulose nanocomposite coatings

The epoxy paint was formulated by directly adding various amounts of dried NC powder (1.0 wt.%, 1.5 wt.% and 2.0 wt.%) to the epoxy/diamine pre-polymer solution. The mixtures were stirred mechanically with a glass rod for 2 mins and then sonicated for 30 s at 60% amplitude for dispersion. The blended solution was not held in the sonication probe longer than 30 s to prevent overheating; thus, stirring and sonicating were alternately repeated 3 to 4 times. The diamine curing agent was then added to the mixture with an epoxy/hardener ratio of 4:1 at close to vacuum. The mixture was then coated onto mild steel via brushing. The steel panels were abraded with a sand blaster, followed by acetone degreasing. They were kept in a desiccator until use. Furthermore, the free films of the coating were cast on a Teflon® Petri dish for analytical measurements and the coated mild steel samples were then dried and cured for seven days at room temperature, which lead to the formation of uniform protection coating for the anticorrosion test. Moreover, the thickness of the film was measured by using coating thickness gauge (elcometer® 456, Manchester, England) and purposely to be about an average of $60 \pm 5 \mu\text{m}$ for further characterization measurement. The designation of the nanocomposite coating systems is tabulated in Table 3.5.

Table 3.5: Epoxy/nanocellulose nanocomposite coating systems.

Epoxy (wt.%)	IPDA (wt.%)	Nanocellulose (wt.%)	Designation
80	20	-	ENC0
80	20	1.0	ENC1.0
80	20	1.5	ENC1.5
80	20	2.0	ENC2.0

3.3.3 Preparation of nanochitosan

Chitosan (CHI) was hydrolyzed by a method based on Huang et al., 2009 and followed by the preparation of nanochitosan with acetic acid and sodium tripolyphosphate (TPP). A 5 g of chitosan was added into 100 g of 85 % phosphoric acid. The solution was stirred up at 60 °C for 4 hours and was precipitated in excess ethanol at 600 rpm for 24 hours. The solution was then decanted to remove the unreacted phosphoric acid. 1 % triethylamine was added to remove salt from hydrolysed chitosan. Mixtures were centrifuged with ethanol for several times and then were washed with 1 litre of ultrapure water at room temperature for 48 hours. For the complete removal of phosphate ions, an aqueous NaOH was added until reached pH 10 - 11 range and then were further washed with ultra-pure water. Collected chitosans were dried overnight in vacuum. For the preparation of nanochitosan (NCH), 0.5 g of collected chitosan was dissolved in 0.2 wt.% acetic acid and stirred for 30 min at 400 rpm. Then, 100 ml of the solution was added to 40 ml of TPP 0.2 g/L, stirred for 2 hours at ambient temperature and then centrifuged at high speed. The isolated nanochitosan was rinsed with distilled water, dried and analysed.

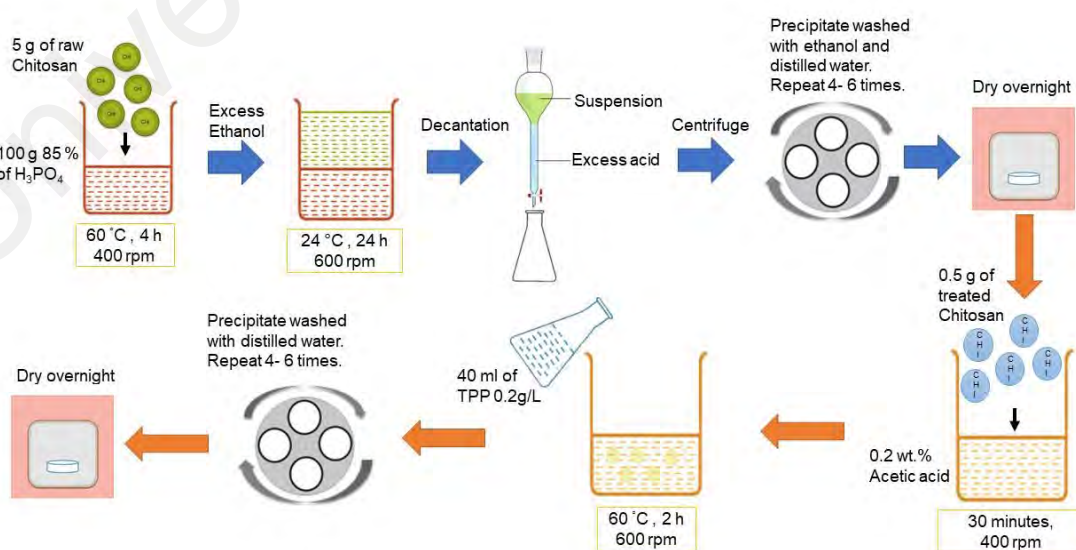


Figure 3.3: Preparation of nanochitosan.

3.3.4 Preparation of epoxy/nanochitosan nanocomposite coating

The epoxy paint was formulated by addition of dried NCH powder (0.5, 1.0 and 1.5) wt.% to the solution of epoxy/diamine pre-polymer solution. The mixtures were stirred mechanically by using glass rod for 2 mins and were sonicated for 30 seconds at 60 % amplitude for dispersion. The blended solution cannot be held longer in the sonication probe to prevent overheating, thus, stirring and sonicating are repeated 3 - 4 times alternately. The diamine curing agent was then added to the mixture with an epoxy/hardener ratio of 4:1 and close to vacuum before coated on mild steel by brushing method. The steel panels were abraded with sand blaster followed by acetone degreasing and kept in a desiccator for further used. The free films and coated samples of the coating were cast on a Teflon® Petri dish and evaporated at room temperature for seven days to obtain a uniform coating. Moreover, the thickness of the film was measured by using coating thickness gauge (elcometer® 456, Manchester, England) and purposely to be about an average of $60 \pm 5 \mu\text{m}$ coated of mild steel for further characterization measurements. Samples were labelled as EP for controller and ECH0.5 followed with 1.0 and 1.5 correspond with particular amount the of nanofiller. The designation of the nanocomposite coating systems is tabulated in Table 3.6.

Table 3.6: Epoxy/nanochitosan nanocomposite coating systems.

Epoxy (wt.%)	IPDA (wt.%)	Nanochitosan (wt.%)	Designation
80	20	-	ECH0
80	20	0.5	ECH1.0
80	20	1.0	ECH1.5
80	20	1.5	ECH2.0

3.4 Characterization

3.4.1 Surface morphology and structural characterization

3.4.1.1 Field Emission Scanning Electron Microscopy (FESEM)

The surface morphology and the behaviour of the treated filler products and nanocomposite film samples were examined by field-emission scanning electron microscopy (FESEM) (Quanta FEG 450, EDX-OXFORD, Eindhoven, Netherland) after being coated with gold by using gold sputter coater (Bio-Rad, Watford, England). FESEM is a microscope that operates using a high-energy electron beam irradiated to a sample (powder or film) and forms an interaction between incident electrons and constituent atoms in the sample to generate various output signals.

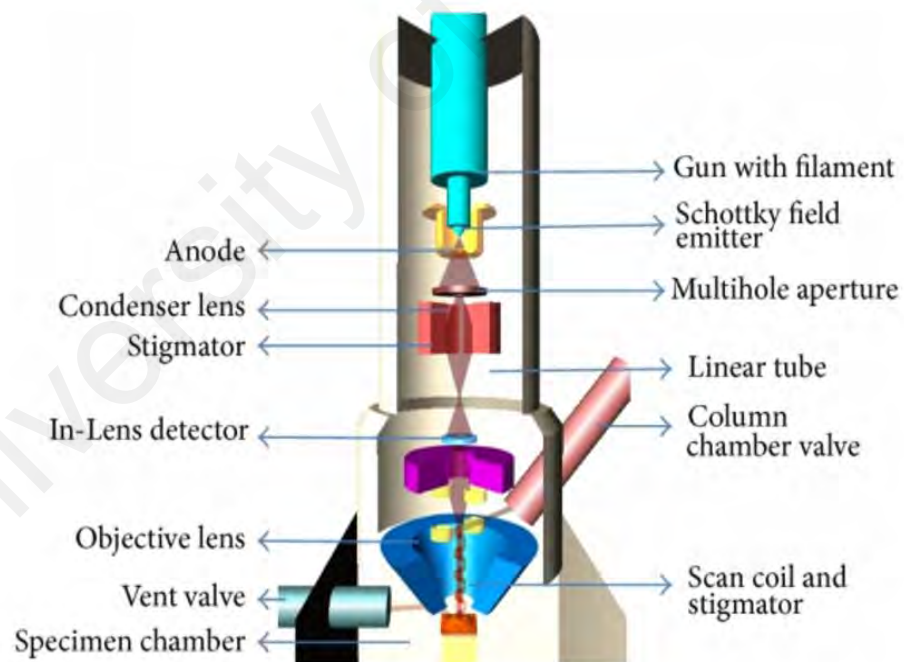


Figure 3.4: Field emission scanning electron microscopy (Jusman et al., 2014).

The electrons are released from the field emission source and accelerated with a high electric field gradient. In the high vacuum tower, these so-called primary electrons are focused and deflected by an electron lens which produces a narrow scanning beam impinging on the object.

As a result, secondary electrons are emitted from each spot on the object. The angle and velocity of these secondary electrons are related to the surface structure of the object. The detector captures the secondary electrons and generates an electronic signal. This signal is amplified, converted to a video scanned image on the monitor or in the digital image and can be further saved and processed.

The primary electron beam interacts with the sample in several key ways;

- i. Primary electrons generate low energy secondary electrons, which are related to the topographical nature of the sample.
- ii. Primary electrons can be backscattered and if there is a contrast between atomic number, an advanced image can be obtained.
- iii. Ionised atoms can be relaxed by shell-to-shell transitions of electrons leading to either X-ray radiation or Auger electron emission. The emitted X-rays are characteristic of elements of several micrometres at the top of the sample

3.4.1.2 X-Ray Diffraction (XRD)

The crystalline nature of the treated filler product and the crystalline phases present in the nanocomposite film samples were determined by X-ray diffraction (XRD) (EMPYREAN, PANalytical, EA Almelo, Netherland) at room temperature. XRD is a non-destructive and rapid analytical technique that provides detailed information such as unit not only the chemical composition but also about the crystallographic structure or unit cell dimensions of the materials. Figure 3.5 illustrated the powder X-Ray Diffraction spectroscopy.

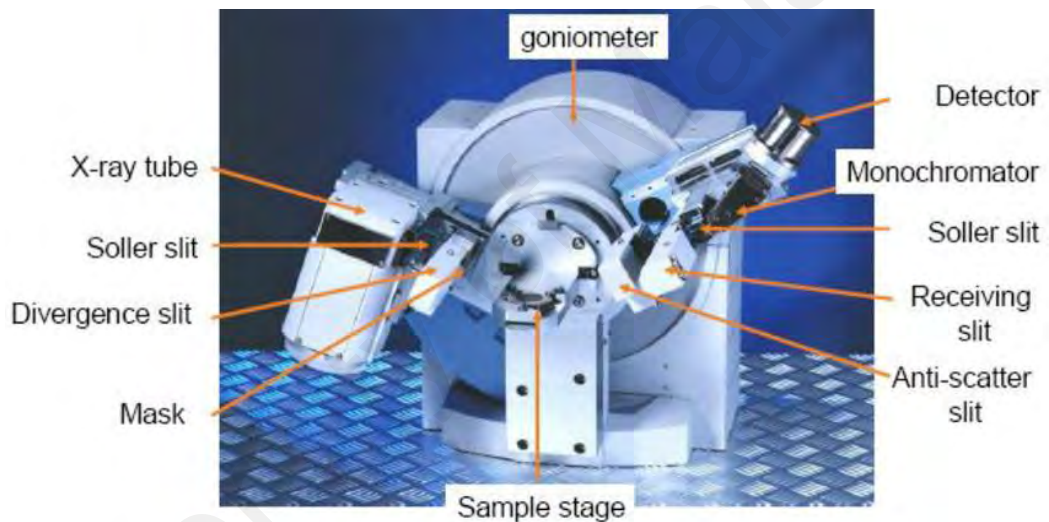


Figure 3.5: X-ray diffraction (Paper et al., 2011).

All diffraction methods are based on the generation of X-rays in an X-ray tube which beam directed at the sample and the diffracted rays are collected. The principle of powder x-ray diffraction experiments is the random orientation of powder sample for all sets of planes (h k l) will be in the horizontal orientation with respect to the X - ray source to satisfy Bragg's law for the proper angle θ .

X - ray diffraction is based on constructive interference of monochromatic X - rays from a powder sample. When a focused X - ray beam interacts with these planes of atoms, the beam undergoes various modifications like absorption, transmission, scattering, refraction and diffraction.

A key component of all diffraction is the angle between the incident and diffracted rays. The diffracted beam can provide information about the d - spacing by applying Bragg's law given by,

$$n \lambda = 2d \sin \theta \quad (3.1)$$

where n is an integer, λ is the wavelength of the incident wave, d is the spacing between the planes in the atomic lattice and θ is the angle between the incident ray and the scattering planes.

The spectra were recorded using $Cu K\alpha$ radiation at 40 kV and 30 mA with scanning at a 2θ of 10° to 50° . The crystallinity index (CI) was calculated using the Segal method, given by Equation 3.2,

$$CI (\%) = (I_{200} - I_{am}) / I_{200} * 100 \quad (3.2)$$

where I_{200} is the intensity of the (2 0 0) peak and I_{am} is the intensity of the amorphous minimum region between the (2 0 0) and (1 0 1) peaks.

The crystallite size (CS) was calculated using Scherer's equation, given by Equation 3.3,

$$CS = K\lambda / \beta_{1/2} \cos \theta \quad (3.3)$$

where K is the Scherer constant (0.94), λ is the X-ray wavelength (0.154060), $\beta_{1/2}$ is the full width at the half maximum (FWHM) of the deflection peak and θ is the Bragg's angle ($^\circ$).

3.4.1.3 Fourier Transform Infrared Spectroscopy (FTIR)

Fourier transform infrared spectroscopy (FTIR) was performed using FTIR spectrometer (FTIR-Spectrum 400, Perkin Elmer, Wokingham, UK) at a resolution of 4 cm^{-1} and in the range of 400 to 4000 cm^{-1} . Figure 3.6 illustrates the diagram of FTIR used in this study. Fourier transform infrared spectroscopy is an analytical technique used to identify functional groups present in the sample by standard KBr pellet method. By analysing the features of a recorded infrared spectrum, the composition or the structure of chemical components can be determined.

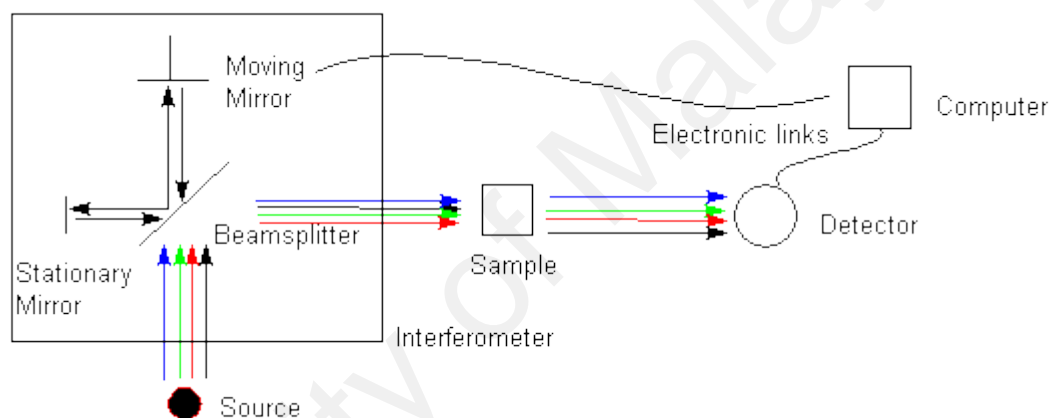


Figure 3.6: Fourier transform infrared spectroscopy (Gable, 2013).

When infrared light passes through a sample of organic compounds, some frequencies are absorbed and other frequencies are transmitted without being absorbed. The transition involved in infrared absorption is related to the change in vibration in the molecule. Functional groups have different oscillation frequencies and therefore the presence of these bonds in the molecule can be detected by identifying this characteristic frequency as an absorption band of the infrared spectrum. As the results, the plot of the transmittance versus frequency is called the infrared spectrum which analysed by using Ohmic32 software programmer.

3.4.2 Ultraviolet-Visible (UV-Visible) analysis of nanocomposite films

Ultraviolet-visible (UV-Vis) analysis of the nanocomposite films was performed using a UV-3101PC (Shimadzu, Kyoto, Japan) UV-Vis spectrometer in transmission mode and a wavelength range of 300 to 800 nm. Slit size was 2 nm in width and medium speed as set in the parameter. Noted that the film samples were coated on a glass plate and dried for 7 days at room temperature. The main purpose of UV-vis measurement was to evaluate the percentage changed of the film transparency due to additional of nanofiller. The UV-3101PC is illustrated in Figure 3.7.

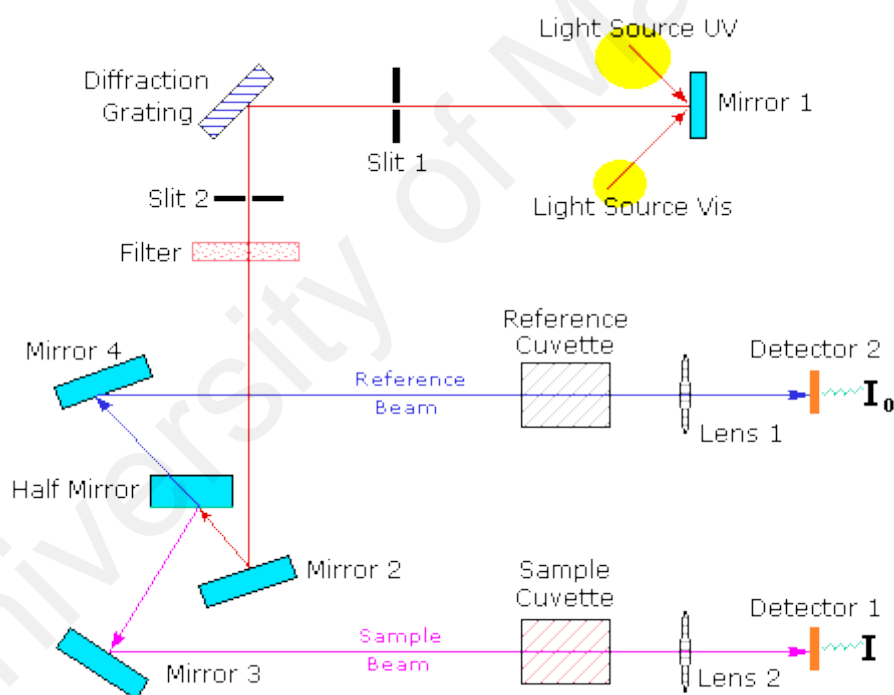


Figure 3.7: Ultraviolet-visible spectroscopy (Reusch, 2015).

An optical spectrometer records the wavelengths at which light transmittance occurs with the percentage of transmission at each wavelength. The resulting spectrum is presented as a graph of percentage versus wavelength. The optical properties of materials can be studied with the help of UV - Vis spectra.

3.4.3 Thermal properties analyses of nanocomposite films

3.4.3.1 Thermogravimetric Analysis (TGA)

The thermal stability of the nanocomposite samples was analysed by thermogravimetric analysis (TGA). The TGA tests were conducted using a Mettler Toledo TGA Q500 (Columbus, USA). The samples were heated from room temperature to 800 °C at a rate of heating of 50 °C/min under nitrogen gas with a flow rate of 60 mL/min. Free film samples were cast from Teflon® after 7 days cured at room temperature. The instrument is illustrated as shown in Figure 3.5.

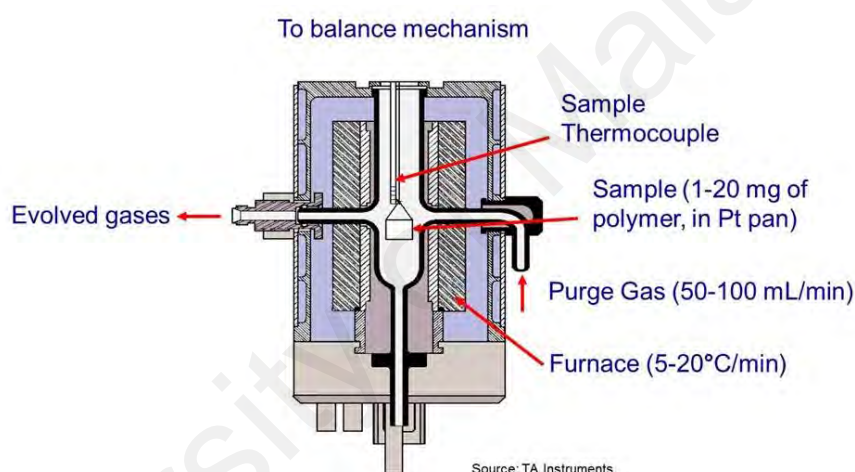


Figure 3.8: Thermogravimetric analysis (Prime, 2014).

Thermogravimetric analysis is a method for evaluating decomposition temperature, absorbed moisture content, levels of inorganic and organic components in materials, decomposition point of solvent residue and corrosion kinetics at high temperature. TGA measures increasing or decreasing weight of a sample as the sample is cooled or heated. Subsequently, the mass is monitored in a controlled atmosphere and at a controlled temperature.

3.4.3.2 Differential Scanning Calorimetry (DSC)

Differential scanning calorimetry (DSC) analysis was performed to investigate the influence of the reinforcement filler on the thermal properties of the coating systems. The DSC tests were performed using a TA Instruments Q200 DSC (New Castle, USA) under nitrogen flow. Free film samples were cast from Teflon® after 7 days cured at room temperature. The instrument is illustrated as shown in Figure 3.6. Each sample was heated from -30 to 300 °C at a heating rate of 10 °C/min.

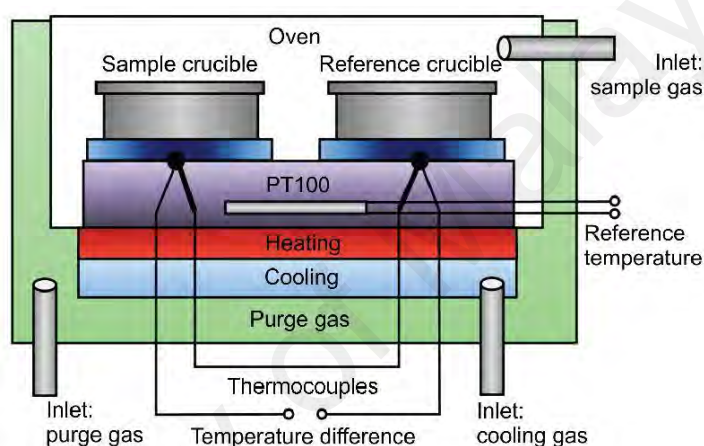


Figure 3.9: Differential scanning calorimetry (Steinmann et al., 2013).

The thermal behaviour of polymers can be studied based on differential scanning calorimetry (DSC) analysis. This technique provides information on heat flow, miscibility, crystallinity and transition temperature in a controlled atmosphere as a function of time. DSC measurements also provide information on physical changes such as melting, depolymerization and decomposition. Moreover, chemical changes such as heat of fusion or enthalpy in the form of heat of reaction can also be analysed. The curve obtained by DSC describes all endothermic or exothermic processes involved in the material analysed.

3.4.4 Electrochemical Impedance Spectroscopy (EIS)

The electrochemical response, barrier performance and corrosion protection of all the prepared coating systems with up to 30 days of immersion in 3.5 % NaCl solution were investigated using EIS. Figure 3.10 illustrates a set electrochemical cell with an exposed area of 3 cm² as the working electrode (WE), a saturated calomel electrode as the reference electrode (RE) and a graphene electrode as the counter electrode (CE) were utilized to perform the EIS tests after placement in a Faraday cage to reduce the noise during measurement.

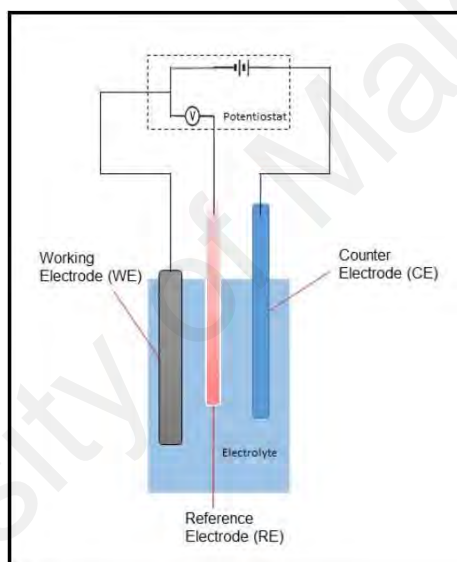


Figure 3.10: Set of an electrochemical cell.

A Gamry PC14G300 potentiostat (Warminster, PA, USA) with a frequency range of 300 kHz to 10 MHz and an amplitude of the sinusoidal voltage at 10 mV was utilised for data measurement. All the EIS data were analysed by the software Gamry Echem Analyst, Version 6.03 (Warminster, PA, USA).

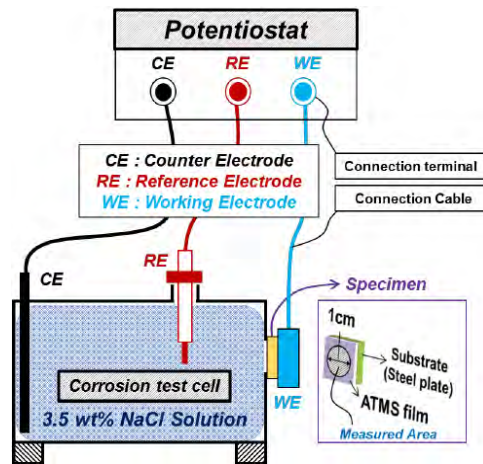


Figure 3.10: Schematic diagram of the experimental setup for EIS (Choe et al., 2015).

EIS is an electrochemical technique with the involvement of an AC potential to an electrochemical cell which obeys Ohm's law equation and then measuring the current through the cell. Ohm's law defined as resistance, R in terms of the ratio between voltage, V and current, I as show in Equation (3.4);

$$R \equiv \frac{V}{I} \quad (3.4)$$

EIS is useful when we want to tailor the system parameter in order to obtain a desirable effect on a surface such as applications in corrosion and coating characterization. The advantages of using EIS, it is useful on high resistance materials such as paints and coatings and the collective data dependent on time. However, it goes gives complex data analysis for qualification.

CHAPTER 4: RESULTS AND DISCUSSION OF EPOXY/NANOCELLULOSE NANOCOMPOSITE COATING SYSTEMS

4.1 Introduction

This chapter presents the results for the preparation of nanocellulose (NC) from commercial microcrystalline cellulose (MCC) and used as an enhancing agent in epoxy/diamine pre-polymer solution which then used for coating on mild steel surface. The contents of nanocellulose loaded into epoxy/diamine were designed as ENC0, ENC1.0, ENC1.5 and ENC2.0 for neat epoxy, 1.0 wt.%, 1.5 wt.% and 2.0 wt.% of NC, respectively. The mixing ratio of epoxy/diamine is 4:1 and followed by corresponded NCs content and dried at room temperature for seven days.

This chapter consists of discussion on the surface morphology by FESEM, chemical structure by FTIR and XRD for prepared nanofillers and epoxy/nanocellulose (ENC) nanocomposite samples. Also, thermal analysis employed by TGA and DSC test on free film of nanocomposite samples, transparency test by UV-Vis spectroscopy on coated glass plates and electrochemical impedance study for all nanocomposite coated on mild steel panels. All these analysis methods are to investigate the effect of NC in the neat epoxy matrix and to evaluate the corrosion performance within 30 days immersed in 3.5 wt.% NaCl solution.

4.2 Field Emission Scanning Electron Microscope (FESEM) Analysis

4.2.1 Preparation of nanocellulose from raw microcellulose

Figure 4.1 shows the morphology by FESEM images of raw microcrystalline with different magnifications. Note that the raw MCC was extracted commercially from softwood pulp and the particle size is estimated to be in an average of 50 μm . As shown in Figure 4.1(a), substantial agglomerations of raw MCC granules were observed and they were seemingly in fiber form. This indicated the strong composition of the hydrogen bonding within the cellulose microfibrils (Kumar et al., 2014) and partially amorphous nature of MCC can be seen as the magnification of FESEM images were enlarged (Figure 4.1(b) and (c)).

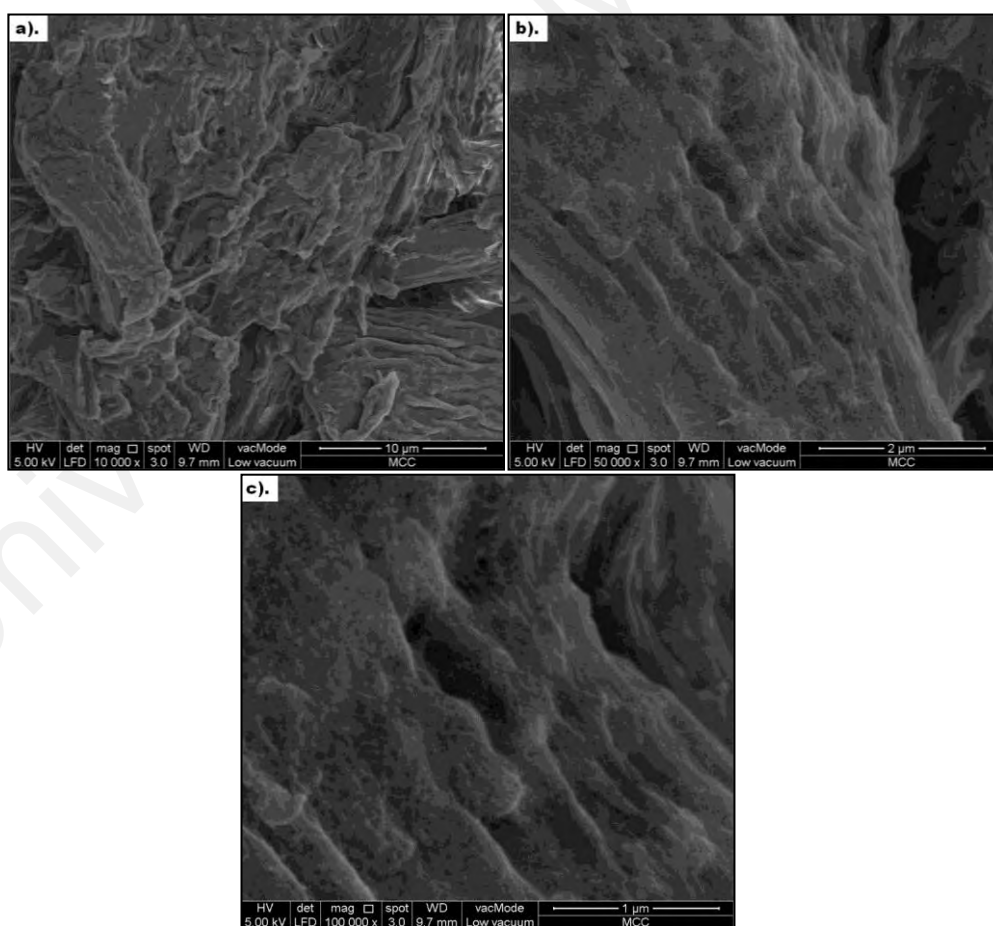


Figure 4.1: FESEM images of MCC at scale (a) 10 000 \times (b) 50 000 \times and (c) 100 000 \times of magnification.

Nanocellulose were prepared from raw MCC by an acid hydrolysis treatment with sulfuric acid solution. The morphology of the prepared NC was observed by FESEM, as shown in Figure 4.2, in which, after the acid hydrolysis treatment, the size of MCC decreased and NC was produced with an average length and width of 80 to 100 nm and 10 to 70 nm, respectively. Also, Figure 4.2 shows that the NC had a rod-like shape due to losing of an amorphous region on the microfibrils of MCC and as the image magnifications were enlarged, wrinkled rod-like shapes were seen attributed to amorphous nature of NC and strong bonding within the molecules. Consequently, the results indicated a favourable reaction due to the acidic treatment.

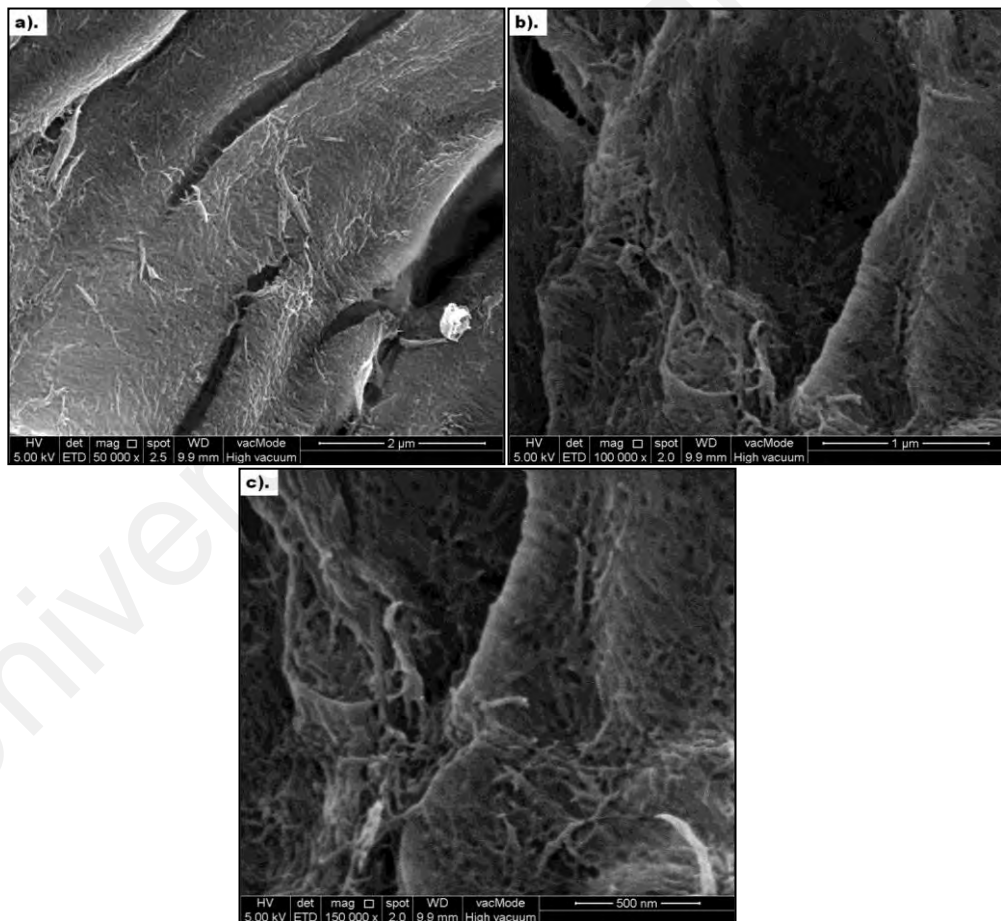


Figure 4.2: FESEM images of NC at scale (a) 50 000× (b) 100 000× and (c) 150 000× of magnification.

4.2.2 Epoxy/nanocellulose nanocomposite coating systems

Subsequently, the NC in powder form was incorporated into the epoxy/diamine polymer, hence, the morphology of the epoxy/nanocellulose (ENC) nanocomposite films were further characterized by FESEM, as shown in Figure 4.3 and Figure 4.4. Note that the neat epoxy coating was designed as ENC0 and followed by additional NC content as ENC1.0, ENC1.5 and ENC2.0 corresponds to 1.0 wt.%, 1.5 wt.% and 2.0 wt.% of NC contents, respectively.

Figure 4.3(a) shows a featureless surface of the neat epoxy film and reveals a rough surface characteristic of the film in which the NC particles were embedded in the epoxy matrix (Shi et al., 2009).

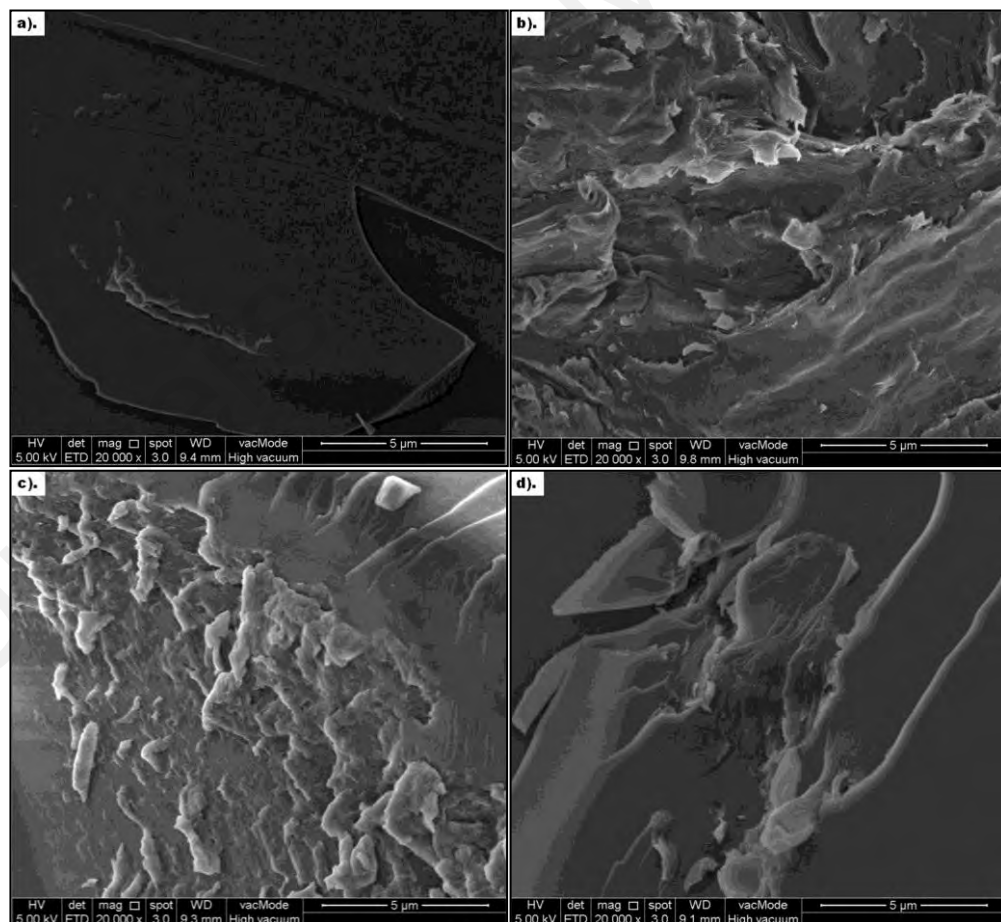


Figure 4.3: FESEM images of ENC at scale 20 000× of magnification (a) neat epoxy, (b) 1.0 wt.%, (c) 1.5 wt.% and (d) 2.0 wt.% NCs.

The surface of the ENC nanocomposites was observed to be relatively rough and eventful compared to the neat resin. The reason may have been that the NCs embedded in the resin caused a cross-linking reaction, which resulted in the matrix surface to become more abrasive during dispersion. Because of this changed in abrasiveness, the NCs may have limited the smoothness of the surface of the nanocomposite films as clearly seen in Figure 4.4, the enlarged magnification scale on FESEM images of Figure 4.3. The surface roughness indicated the occurrence of deformation when NCs were added with some forces applied during the dispersion through sonication. As shown in Figure 4.3(b), the surface roughness was homogeneous and less aggregated, which meant that the dispersion of 1 wt.% of NCs were good enough for the NC to be embedded within the EP matrix.

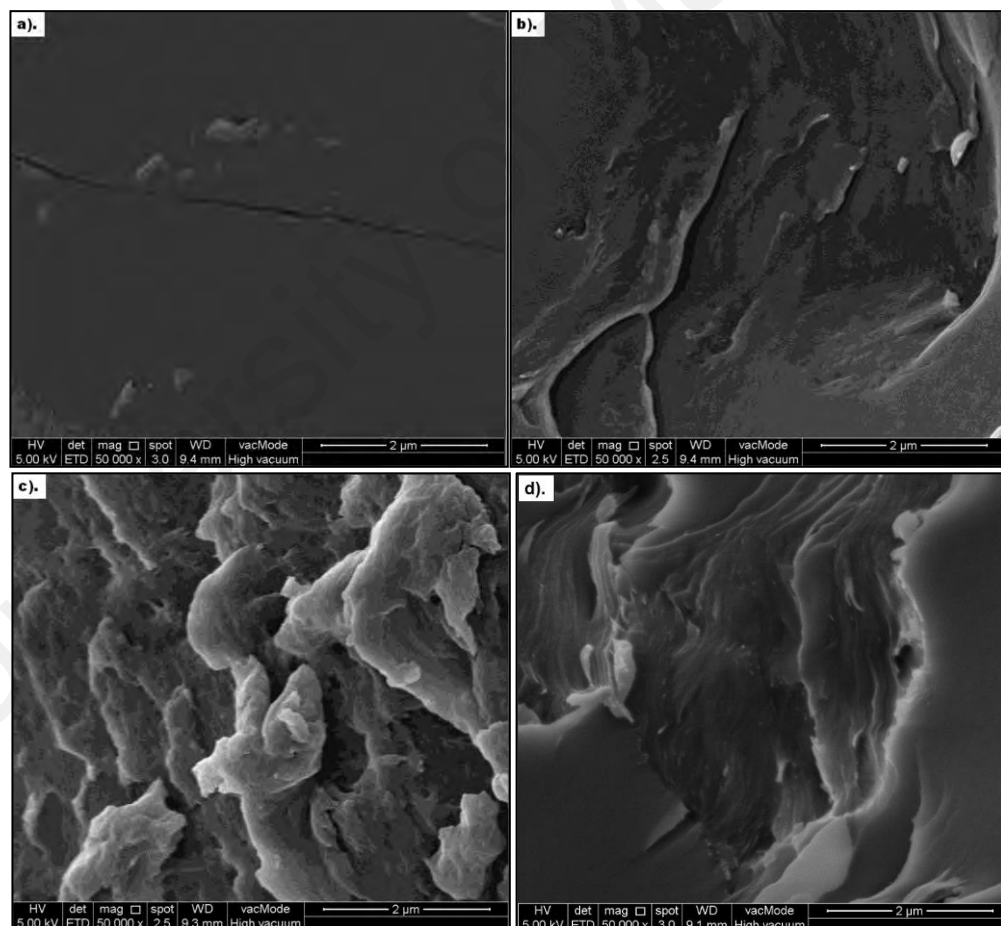


Figure 4.4: FESEM images of ENC at scale 30 000 \times of magnification (a) neat epoxy, (b) 1.0 wt.%, (c) 1.5 wt.% and (d) 2.0 wt.% NCs.

That, in turn, could be considered as a straightforward evidence of the competence of the sonication process in developing an acceptable level of nanoparticles dispersion within the utilised polymeric matrix.

In spite of that, the agglomeration of nanoparticles can be due to the heterogeneous reaction between the NC and epoxy matrices when more NC was added. This was because the resin had enough force to strengthen the bonding in the NC, which caused difficulty with dispersion in the epoxy surface. Moreover, as the loading ratio of NC filler exceeded 1.0 wt.% up to 1.5 wt.% and 2.0 wt.%, the number of the nanoparticles in the unit area increased (Figure 4.3(c) and 4.4(c)), therefore, the tendency of the utilised nanoparticles to be attracted to each other increased.

It is worth mentioning that a good dispersion of nanoparticles in the epoxy matrix led to have a stabilised cross-linking network (Kadhim et al., 2013) when more nanoparticles were added. However, this explanation does not fully clarify the nanocellulose systems seen in Figure 4.3(d). The surface morphology of the 2.0 wt.% NC nanocomposite (ENC2.0) was found to be relatively smooth and rough in the same vicinity. This observation indicated that the stiffness of the surface, which led to the adhesion behaviour of the films, was increased due to the strong intermolecular bonding within the cross-linking networks (Lu & Hsieh, 2010; Preghenella et al., 2005).

However, agglomeration remained within the matrix, even though both the mechanical mixing and ultrasonication were performed in this work. Sufficient energy force to disperse the particles could not be exerted. The ultrasonic mixing technique could help dispersion of NCs into epoxy and blend them homogeneously if the compatibility between the NC surfaces and matrix was adequate. Thus, only ENC1.0 showed good dispersion in epoxy/diamine pre-polymer.

4.3 Structural Analysis

4.3.1 X-ray Diffraction (XRD)

The crystallite size and nature of the NC produced from the MCC were determined by XRD and the materials further characterised with ENC nanocomposite coatings, as shown in Figure 4.5. The MCC and NC exhibited characteristic crystalline peaks around a 2θ of 14.6° , 16.5° , 20.0° , 22.6° and 34.6° , which are considered to be characteristic peaks of typical cellulose structures that correspond to (-110), (110), (102), (200) and (004) on the lattice plane, respectively (Ciolacu et al., 2011; Johar et al., 2012; Sheltami et al., 2012).

Furthermore, the crystalline index of the MCC and NC were 88 % and 79 %, respectively, which showed that the NC possessed a greater crystalline index because of the isolation from water dispersion during acid hydrolysis and alkaline neutralisation (Nam et al., 2016; Shankar & Rhim, 2016).

The crystallinity index (CI) of the MCC and NC was calculated using the Segal method, given by Equation (4.1),

$$CI (\%) = (I_{200} - I_{am}) / I_{200} * 100 \quad (4.1)$$

where I_{200} is the intensity of the (2 0 0) peak and I_{am} is the intensity of the amorphous minimum region between the (2 0 0) and (1 0 1) peaks.

On the other hand, the crystallite sizes (CS) of the MCC and NC, calculated using Equation (4.2), were 18.39 and 11.03 nm, respectively. This indicated that the crystallite size of the MCC decreased after treatment with acid hydrolysis using sulfuric acid dissolution. The Scherer's equation, given by Equation (4.2),

$$CS = K\lambda / \beta_{1/2}\cos\theta \quad (4.2)$$

where K is the Scherer constant (0.94), λ is the X-ray wavelength (0.154060), $\beta_{1/2}$ is the full width at the half maximum (FWHM) of the deflection peak and θ is the Bragg's angle ($^{\circ}$).

XRD micrographs were also obtained for ENC nanocomposites with variation in NC contents (Figure 4.5). The control film of the neat epoxy showed a broad amorphous peak from 12.2° to 28.5° , thus exhibiting the amorphous nature of epoxy. However, no change in the peak position of the neat epoxy was observed with the presence of NCs in the nanocomposite systems, which might have been because of the smaller concentration of NCs in the epoxy matrix. Pan et al., 2012 reported that no obvious peak was seen in the 2.0 wt.% ENC nanocomposite spectra because of the low content of nanofiller and visible peaks were observed in the nanocomposites that were 4 wt.% to 8 wt.% of loaded nanofiller. The disappearance of all the maxima ($2\theta = 14.6^{\circ}$, 16.5° , 20.0° , 22.6° and 34.6°) from the layered structure of the NC indicated the intercalation or exfoliation of the nanofiller to form the nanocomposite with the EP matrix.

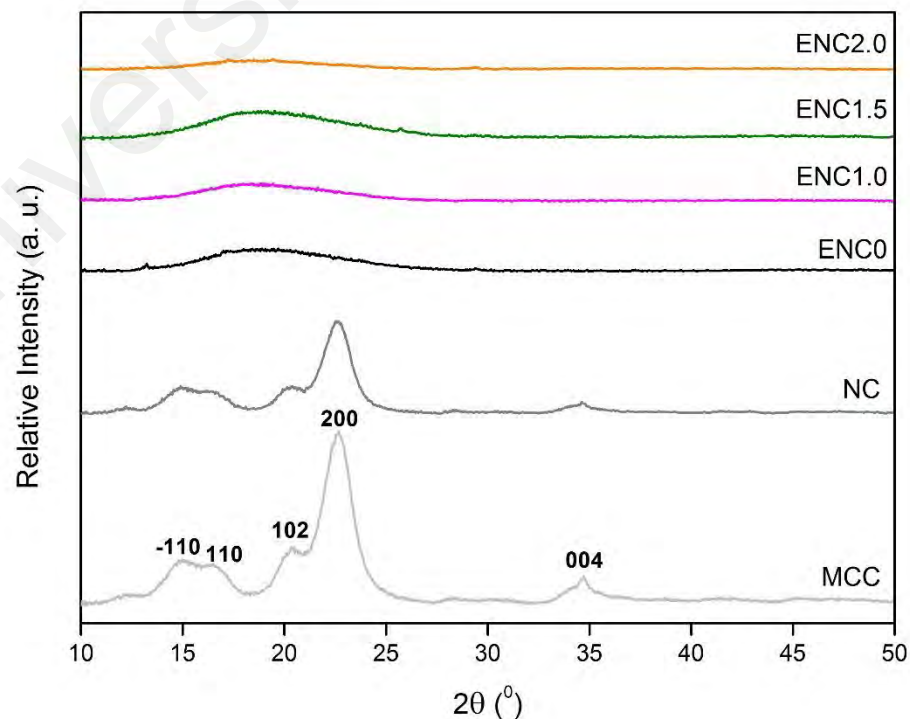


Figure 4.5: XRD spectra of MCC, NC and ENC nanocomposite coating systems.

4.3.2 Fourier Transform Infrared (FTIR)

FTIR was performed to understand the change in the chemical structures of the NC, neat epoxy and ENC nanocomposite samples, as shown in Figure 4.6. In general, the change in the crystalline structure of the cellulose led to the disappearance or reduction in intensity of certain FTIR peaks of the crystalline domains of the cellulose. In the functional region of the FTIR, the broad band located in the ranges of 3000 to 3500 cm^{-1} and 2790 to 2982 cm^{-1} correspond to the hydroxyl (O-H) and aliphatic alkyl (C-H) stretching vibrations, respectively (Lani et al., 2014).

In contrast, the amorphous band was assigned to the peak at 895 cm^{-1} , which was attributed to the C-O-C stretching vibration at the β -(1,4)-glycosidic linkages of cellulose (Ciolacu et al., 2011; Xu et al., 2013) and the disappearance of the band at 1062 cm^{-1} was attributed to the symmetrical C-O-S vibration resulting from the presence of H_2SO_4 in the acid hydrolysis treatment.

All of the infrared-active modes, such as deformation, twisting and wagging of the anhydroglucopyranose unit, were observed in 1800 to 700 cm^{-1} regions. The absorption peaks at 1315, 1160, 1108 and 1054 cm^{-1} were due to H-C-H wagging, the C-C ring stretching band, the C-O-C glycosidic ether band and the C-O-C pyranose ring stretching, respectively (Kumar et al., 2014; Lu & Hsieh, 2010; Sheltami et al., 2012; Voronova et al., 2012). The peak at 1642 cm^{-1} was attributed to the OH bending of the absorbed water, due to the strong water interaction in the cellulose (Flauzino et al., 2013; Morán et al., 2008). No difference was found in the spectrum of the NC compared with that of the MCC, which suggested that in the case of acid hydrolysis, the molecular structure of the cellulose did not undergo any vital changes. However, a slight reduction in the absorption number indicated that the change in the size of the NC was accompanied by a decreased degree of crystallinity, as shown by the XRD and FESEM.

In the fingerprint region, the crystallinity band at 1428 cm^{-1} was attributed to the CH_2 -bending vibration, which indicated the reduction in the degree of crystallinity of the cellulose due to the decrease in the absorption. Figure 4.6 depicts the FTIR spectra obtained from the unreacted epoxy, IPDA and neat cured epoxy (ECH0). The absorption peaks at 950 and 3100 cm^{-1} were attributed to the presence of the C-O deformation and the C-H stretching of the oxirane group in the epoxy matrix, respectively. The bands located at 1032 cm^{-1} corresponded to a C-O-C linkage because of the unreacted epoxide group. Fraga et al. (2008) reported that the bands at 1507 and 820 cm^{-1} could be assigned to the p-phenylene groups in the unreacted epoxide group. The disappearance of bands, as observed in the neat epoxy (ENC0), indicated that all of the epoxide groups reacted during curing and were well blended with the isophorone diamine curing agent (Fraga et al., 2008).

In the ENC nanocomposites, the epoxide group could react with the hydroxyl groups on the NC surfaces. If an epoxide group reacted with a NC hydroxyl group, the result would be an ether group and a hydroxyl group. The band at 3200 to 3450 cm^{-1} of the ENC nanocomposite spectrum confirmed that an interaction occurred within the hydroxyl group and suggested there was an increase in hydrogen bonding between the NC nanofiller and epoxy matrix. The band at 1606 cm^{-1} was possibly due to the overlapping of the C=C stretching of the epoxide group and the $-\text{NH}_2$ scissoring of the amine group. It is worth noting that the observed peaks of the N-H stretching (3283 cm^{-1}) and the N-H deformation (1602 cm^{-1}) of the diamine group quantitatively appeared because of the strong -OH absorption bands and corresponded to the other organic band region.

Also, the peak at 1032 cm^{-1} clearly showed a change in the peak intensity attributed the stretching of ether linkage between the epoxy matrix and the glycosidic ether linkages of the NC. Other bands at 895 , 1229 , 1455 and 1606 cm^{-1} increased in intensity after the addition of the NC nanofiller and these bands were attributed to the C-O-C stretching vibration, H-C-H wagging, CH_2 -bending vibration and C=C stretching, respectively. Since

the band at 895 cm^{-1} was attributed to the C-O-C stretching vibration of NCs due to the presence of β -(1,4)-glycosidic linkages, so it can be considered as an “amorphous band” (Shankar & Rhim, 2016). Therefore, the result on the different in the CS of NCs as measured by the XRD test settled too by FTIR test.

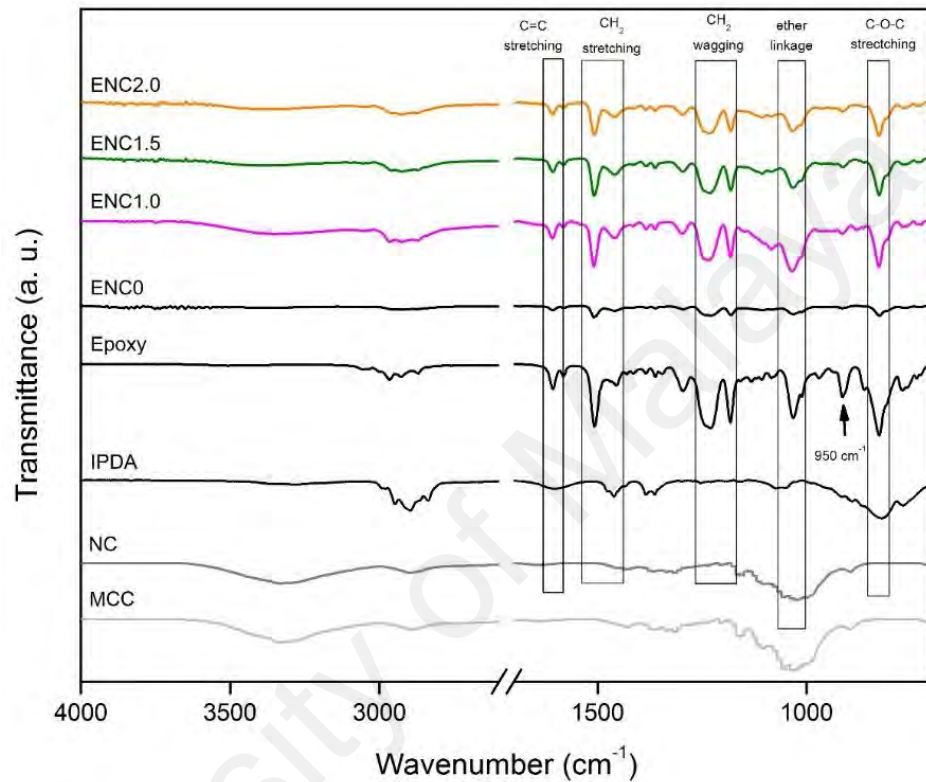


Figure 4.6: FTIR of the MCC, NC, IPDA, Epoxy and ENC nanocomposite coating systems.

4.4 UV-Visible Spectroscopy

The UV-Vis transmittance spectra of the neat epoxy/nanocellulose nanocomposite specimens in the visible wavelength range of 300 to 800 nm at 2.0 nm intervals are shown in Figure 4.7. The transmittance of the 2.0 wt.% NC nanocomposite (ENC2.0) was the lowest, with less than 20 % light transmittance. Incidentally, the specimen with 1 wt.% NC nanocomposite (ENC1.0) was clearly transparent, with the highest light transmittance of 73% at 400 nm. The transparency of the nanocomposites was dependent upon the amount of the nanofillers. The light transmission rates of the specimens with 1.5 wt.% and 2.0 wt.% NC nanocomposite (ENC1.5 and ENC2.0) were reduced to 43 % and 45 %, respectively. It has been reported by Pan et al., 2012 that the transmittance of epoxy/nanocellulose nanocomposites was reduced with the increase of the content of cellulose nanocrystalline and claimed that all nanocomposites still retained high transparency at above 60 % of transmittance. Hence, only ENC1.0 and ENC1.5 are considered to be transparent film while ENC2.0 can be classified as a translucent film due to the homogeneity of nanocellulose and epoxy matrices.

Figure 4.7 shows the drop off on the light transmission for all of the samples was observed at approximately 300 to 350 nm, which meant there was high light absorption at this point and that no light reflection occurred in the ultraviolet region (300 to 400 nm). The high transparency of the 1.0 wt.% NC in the ENC nanocomposite possibly resulted from the difference in the refractive index between the nanofiller and the epoxy matrix, which suppressed light transmission through the epoxy/NC interphase. This indicated that the difference in the refractive index of the filler and matrix also played a significant role in controlling the optical transmittance of the composite films. According to Shimazaki et al., 2007, the high transparency of the nanocomposites results from the small diameter of nanofibril of cellulose which leads to a small difference in refractive index between the

nanofibers cellulose and the epoxy matrix, as result suppressed scattering of the photons at the interface of nanocellulose/epoxy resin.

Furthermore, a nanocomposite film due to the incorporation of nanocellulose with its superior properties such as small diameter, high strength and modulus that utilised the transparency film are believed to improve in mechanical properties relative to the optical properties (Iwamoto et al., 2005; James et al., 2012). Since the fibrillar shape-like was aggregated in nanocellulose chains, this morphology kind actually contributes to a significant improvement in the thermal stability properties as will be discussed in the next section of this chapter. Therefore, the size effect plays such an important role in this study of how a biopolymer nanofiller can lead to better improvement of many kinds of properties. As one of the most abundantly organic resources on earth plants, celluloses in nanoscale size enormously have potential as a future resource.

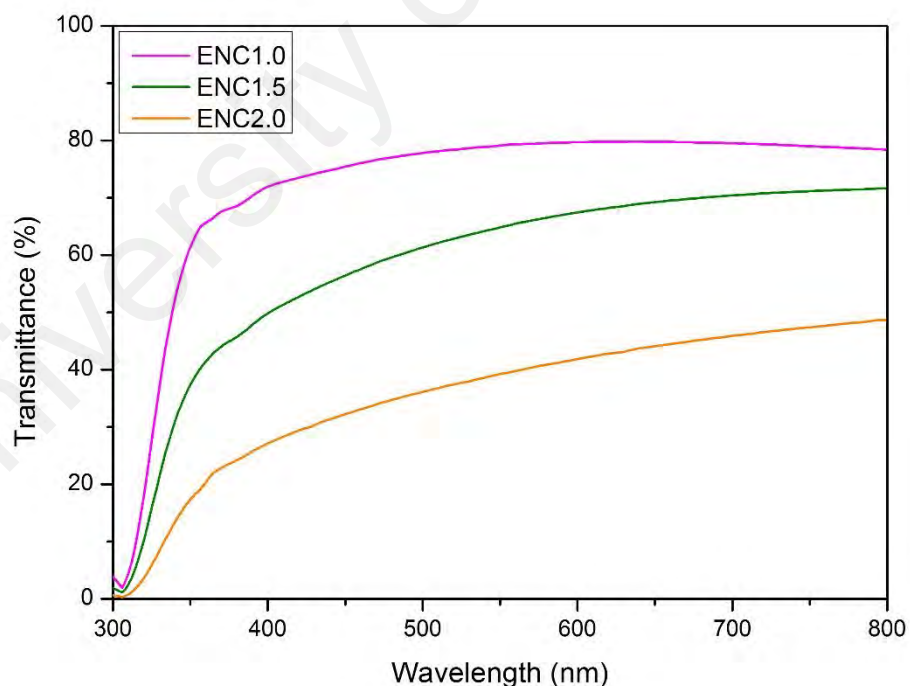


Figure 4.7: UV-Vis spectra for the ENC nanocomposite specimens.

4.5 Thermal Analysis

4.5.1 Thermogravimetric Analysis (TGA)

The TGA results of the neat epoxy and ENC nanocomposite coating samples are given in Figure 4.8, which consists of weight loss and derivative thermogravimetric (DTG) versus temperature. The initial degradation temperature (T_{IDT}), the temperature at the maximum weight loss rate (T_{max}) and residue at 700 °C were extracted using TA universal analysis programme. By the action of heat, carbonisation removes hydrogen and oxygen from the solid and the remaining residue predominantly consists of carbon (Kumar et al., 2014).

Herein, T_{IDT} is used as the thermal stability indicator and defined as the temperature corresponded to the 5 wt.% loss in weight. Figure 4.8 shows that there was less than 5 % weight loss at approximately 65 to 160 °C of all coating systems and the water or small molecule loss in this range was considered to be minimal. The NC nanocomposite coating samples exhibited about 5 wt.% weight loss in between approximately 300 and 390 °C, which corresponded to the initial degradation temperature, but the overall thermal stability showed slight change due to the NC contents. Also, the thermal decomposition of the neat epoxy consisted of one step (Ammar et al., 2016).

Furthermore, the T_{IDT} for thermal degradation for the ENC nanocomposite coating samples increased from approximately 367 to 384 °C, which was relatively high compared to the neat epoxy coating. The change in the temperature may have been due to dehydration and decomposition of the glycosyl unit accompanied by char formation. The drastic weight loss that occurred up to 460 °C could be attributed to the breakdown and oxidation of the char residue.

Many studies have been done on the thermal properties of NC and reported that at lower temperature corresponds to the dehydration of the cellulose network chains catalysed by the acidic groups present during the sulfuric hydrolysis. Meanwhile, at higher temperature attributed to the decomposition of the solid unsulfated interior and residues (Pan et al., 2012; Shimazaki et al., 2007; Xu et al., 2013).

Figure 4.8 also show DTG curves, as the NC content increased, the temperature at the maximum weight loss rate for the first degradation step decreased, but overall was still greater than for the neat epoxy coating. Thus, the maximum decomposition temperature of nanocomposites was insignificantly increased compared to neat epoxy resin.

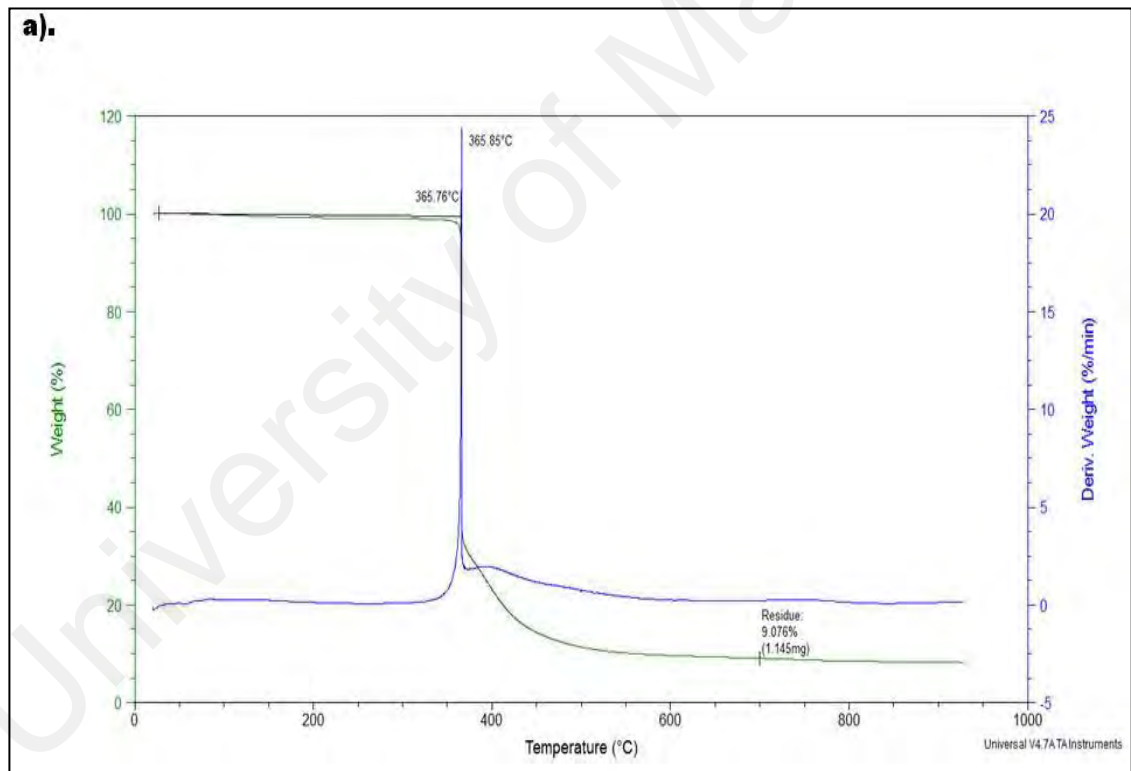


Figure 4.8: TGA thermograms of the (a) neat epoxy (ENC0) and ENC nanocomposite coating systems (b) ENC1.0, (c) ENC1.5 and (d) ENC2.0.

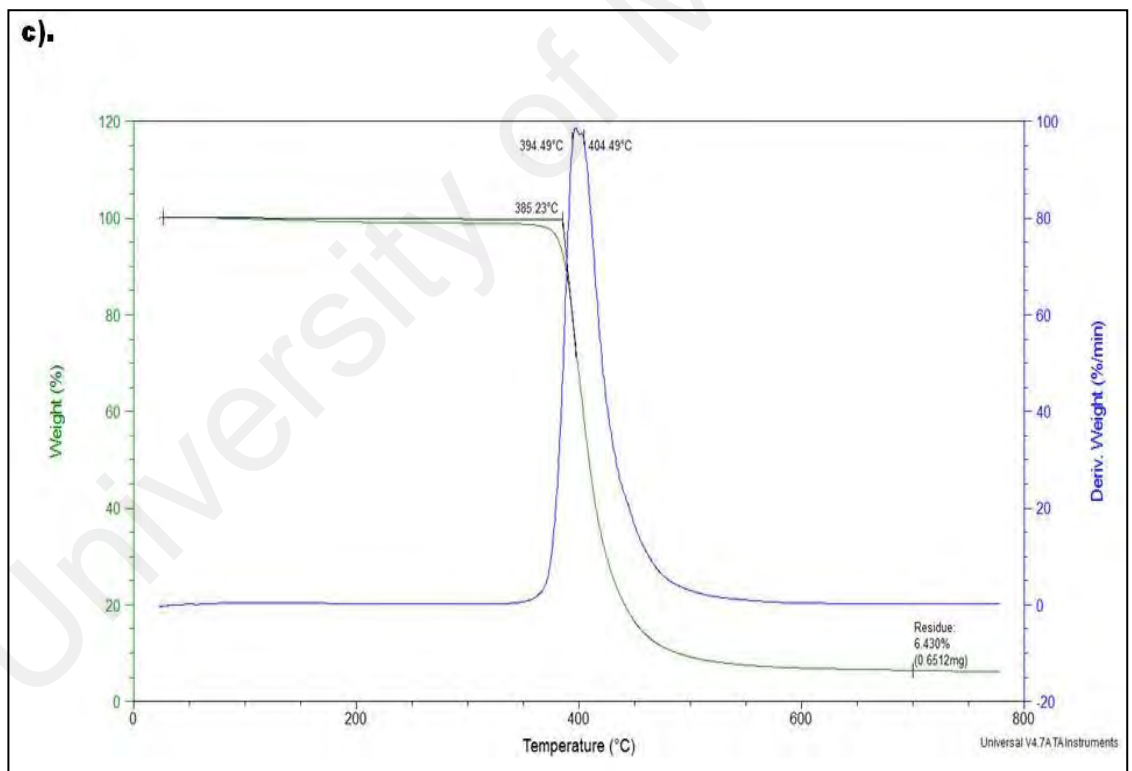
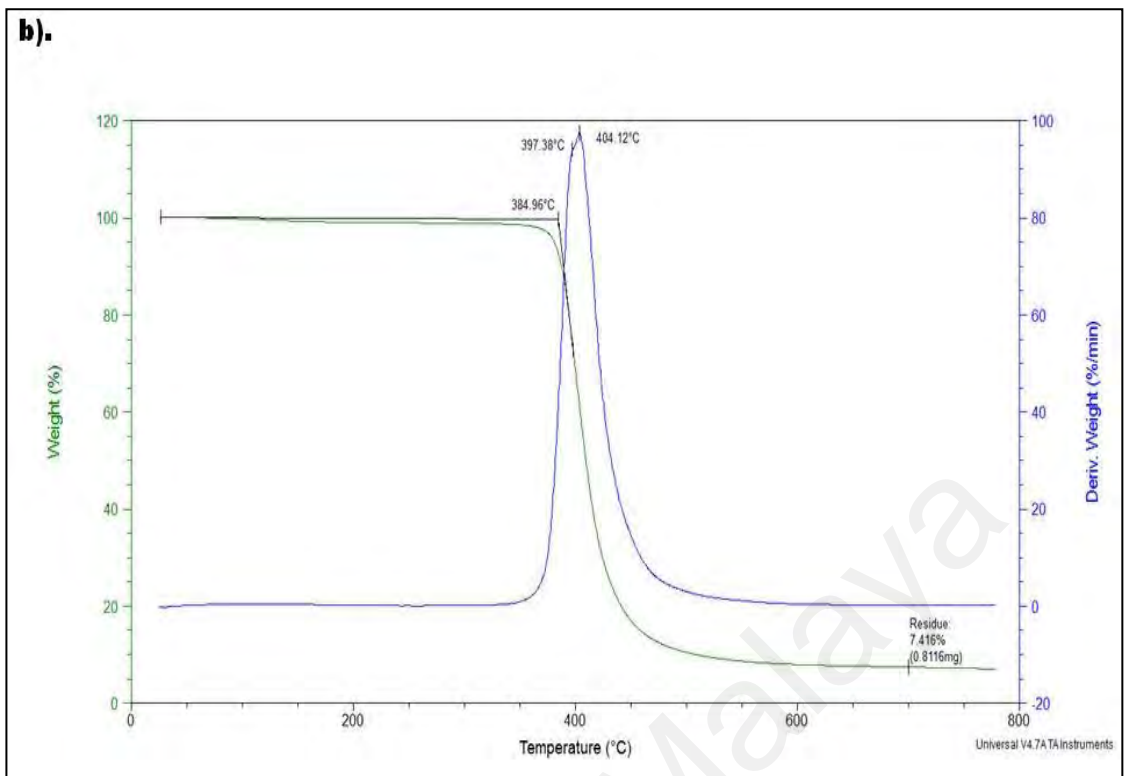


Figure 4.8: Continued.

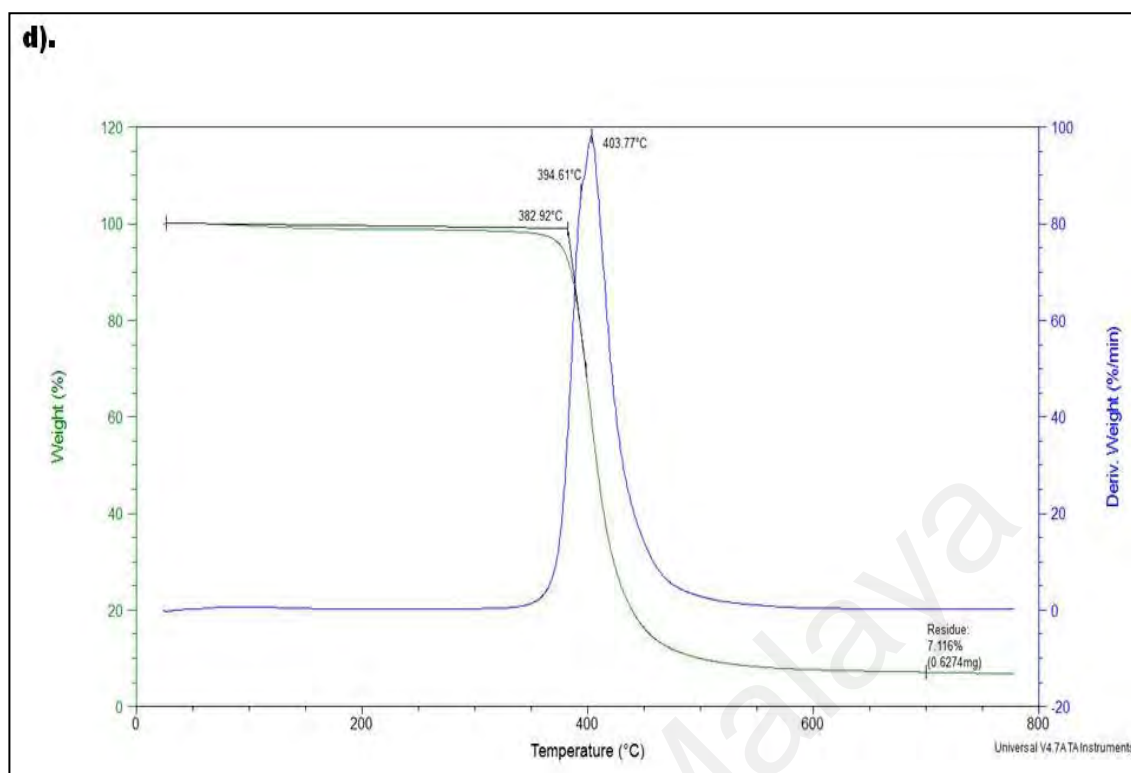


Figure 4.8: Continued.

4.5.2 Differential Scanning Calorimetry (DSC)

The DSC thermograms with glass transition temperature (T_g) values for the second cycle scanning of the endothermic measurement for all of the coating systems are shown in Figure 4.9. Note that, the two-cycle scanning was adopted to eliminate the moisture content of the samples, which might affect the DSC measurements or the thermal degradation. Data information and graphs were extracted by using TA universal analysis software programme.

In this study, the T_g was approximately 135 to 150 °C, although the baseline step was somewhat small. The baseline step may have been small because of the anhydroglucopyranose units in the NC. From the changes of T_g due to the additional NC may infer more information about the component interactions.

A maximum increase of approximately 15 °C of the T_g was observed at a NC loading of 1.0 wt.% and 1.5 wt.% and the T_g slightly decreased for the 2.0 wt.% loading. Overall, the T_g of nanocomposite samples were insignificantly increased relative to the neat epoxy samples. This trend of an increased T_g corresponded with the good bonding system between the polymer network and reinforced filler. This indicated the good physical or chemical mobility interactions between the epoxy matrix and the inclusion of NC particles. Nonetheless, associated with polysaccharide based material concerned to their high moisture absorption which can affect the epoxy physical properties. Investigate the behaviour of water contact to the coating surface or measure the water content being absorbed by the films are much necessary for the future study to know the impact of the coating properties.

Xu et al., 2013 have concluded that the presence NC did not introduce any additional water or moisture to the composite systems even though neat NC consist 60 % water content compared to the neat epoxy resin. It was found that the water content of the composites decreased insignificantly with the additional of NC contents. This suggested that the interaction of nanocomposites is able to block the access of water to the hydrophilic hydroxyl groups on the surface.

However, other possibilities should be noted. Firstly, the possibility that the inclusion of NCs in epoxy surface might prevent or delay the diffusion of water due to the aggregation. Next, it is possible that NC provides barriers to water transport that prevent them from accessing with moisture in the time scale of measurements. Unfortunately, it is not possible to differentiate these alternatives due to limit of collected data and probably bring the investigation on the furtherance.

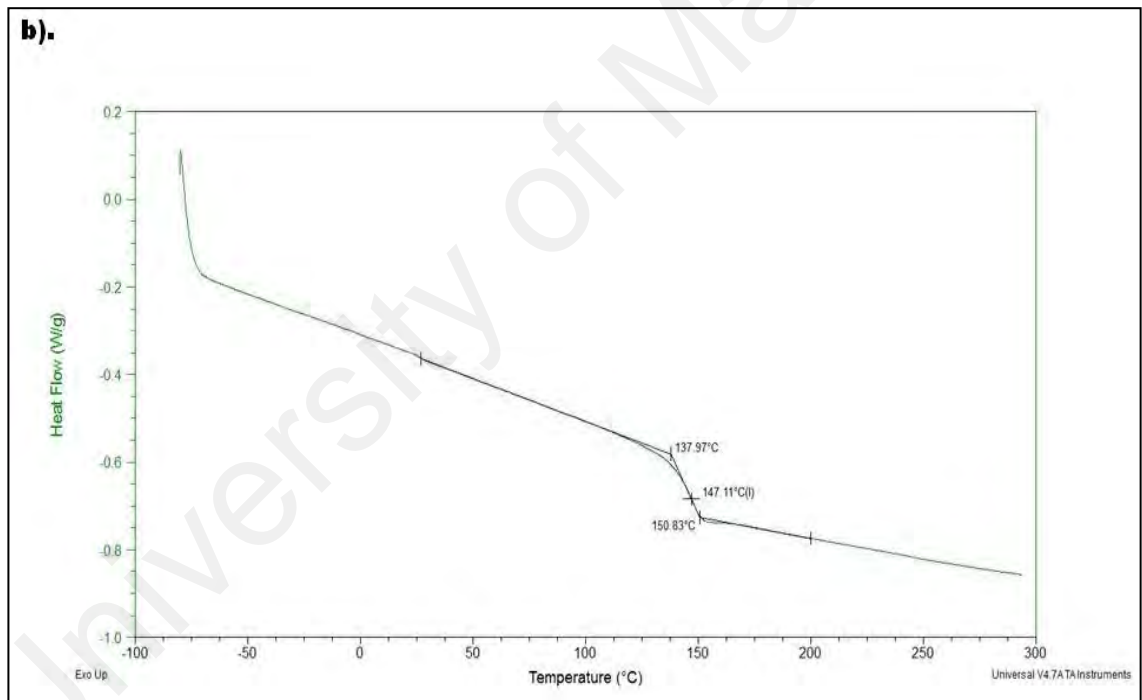
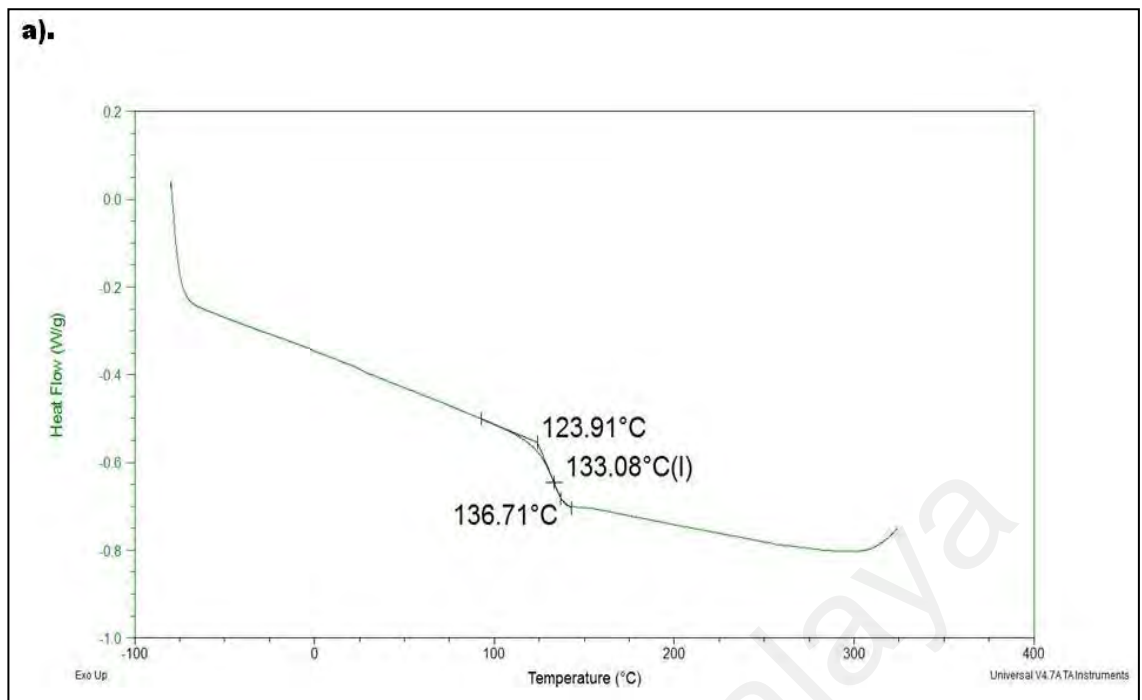


Figure 4.9: DSC thermograms of the (a) neat epoxy (ENC0) and ENC nanocomposite coatings (b) ENC1.0, (c) ENC1.5 and (d) ENC2.0.

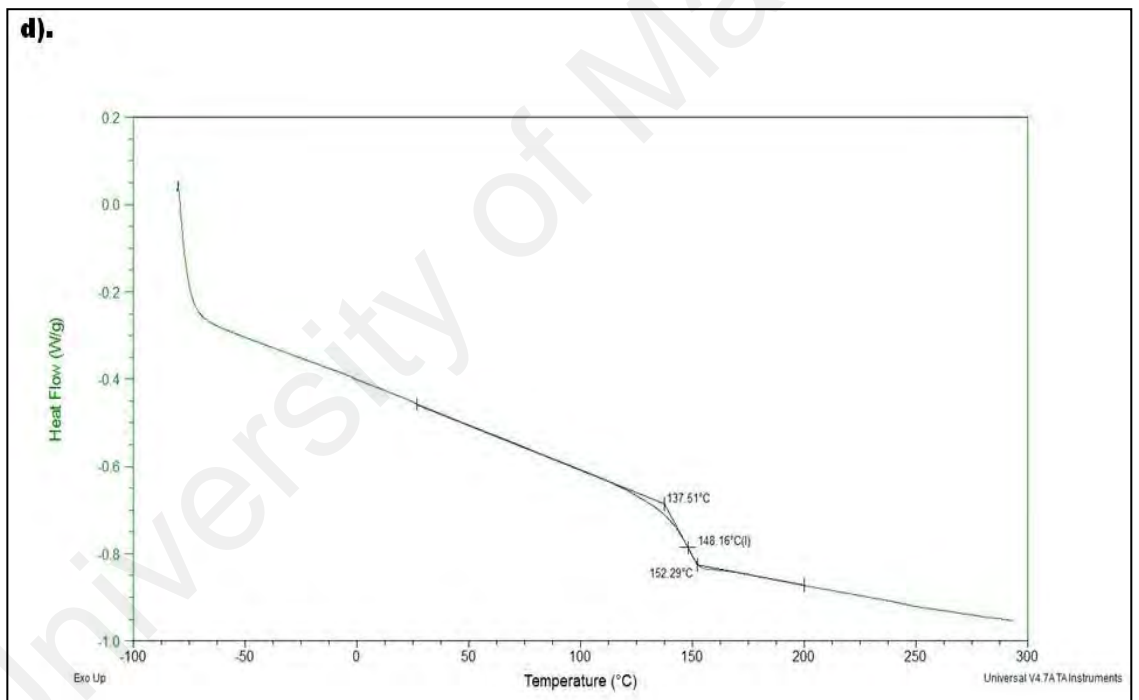
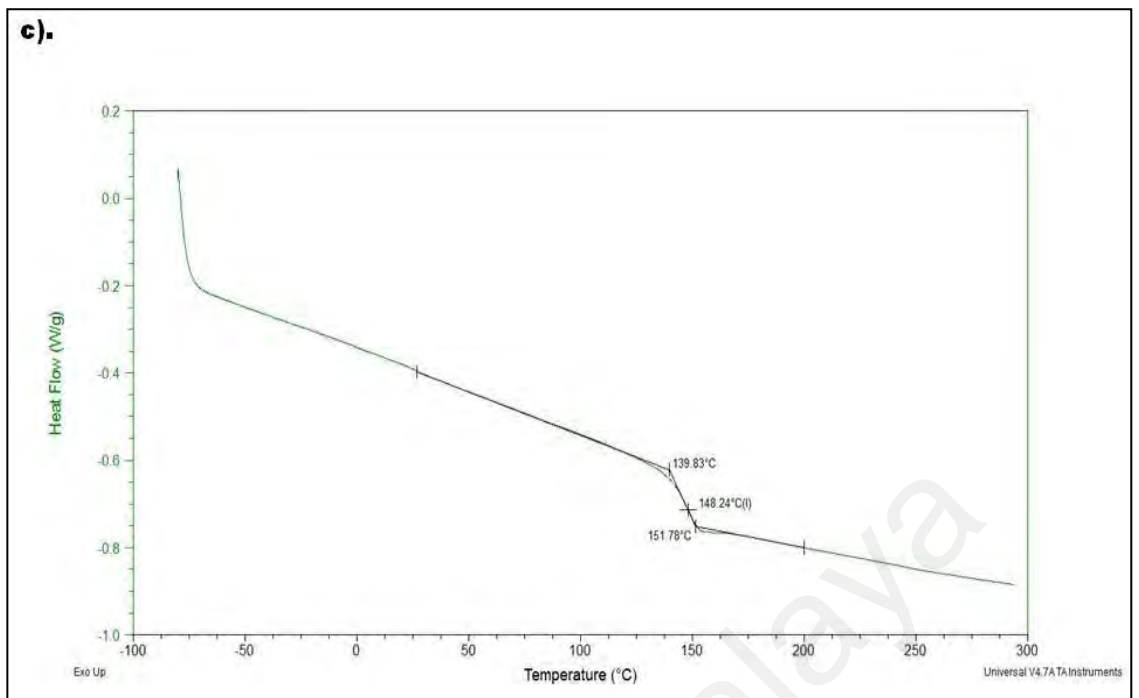


Figure 4.9: Continued.

4.6 Electrochemical Impedance Spectroscopy (EIS)

Figures 4.10 and 4.11 present the Bode plots of the epoxy coating and the coatings reinforced with various amounts of NC after 1 day and 30 days of immersion, respectively. To study the influence of NCs as the filler on the corrosion protection performance of the epoxy, EIS measurements were conducted periodically after exposing the coated steel panels to the 3.5 % NaCl solution. The obtained results were expressed graphically using Bode plots fitted by using two models of the equivalent circuit.

After 1 day of immersion, as shown in Figure 4.10, the electrochemical responses of all prepared coating systems, revealed that only the neat epoxy coating system, ENC0, demonstrated a Bode plot with two-time constants. The ENC0 also demonstrates lower phase angle at on frequency range (Figure 4.10(b)). This finding could be considered as a clear evidence that the coating film of the unmodified polymeric matrix suffered penetration of electrolytes towards the substrate surface with the weakest barrier ability. The electrochemical behaviour of the ENC0 coating system at this stage of degradation could be perfectly described with model A of the equivalent circuit (Figure 4.12).

In contrast, all of the prepared coating systems reinforced with different loading rates of NCs demonstrated better corrosion protection properties after the 1 day of immersion. The good anticorrosion performance of the NC nanocomposite coatings was confirmed by the Bode plots illustrated in Figure 4.10. The impedance plots demonstrated an one-time constant and the EIS data was fitted with model A of the equivalent circuit (Ammar et al., 2016; Mostafaei & Nasirpouri, 2013).

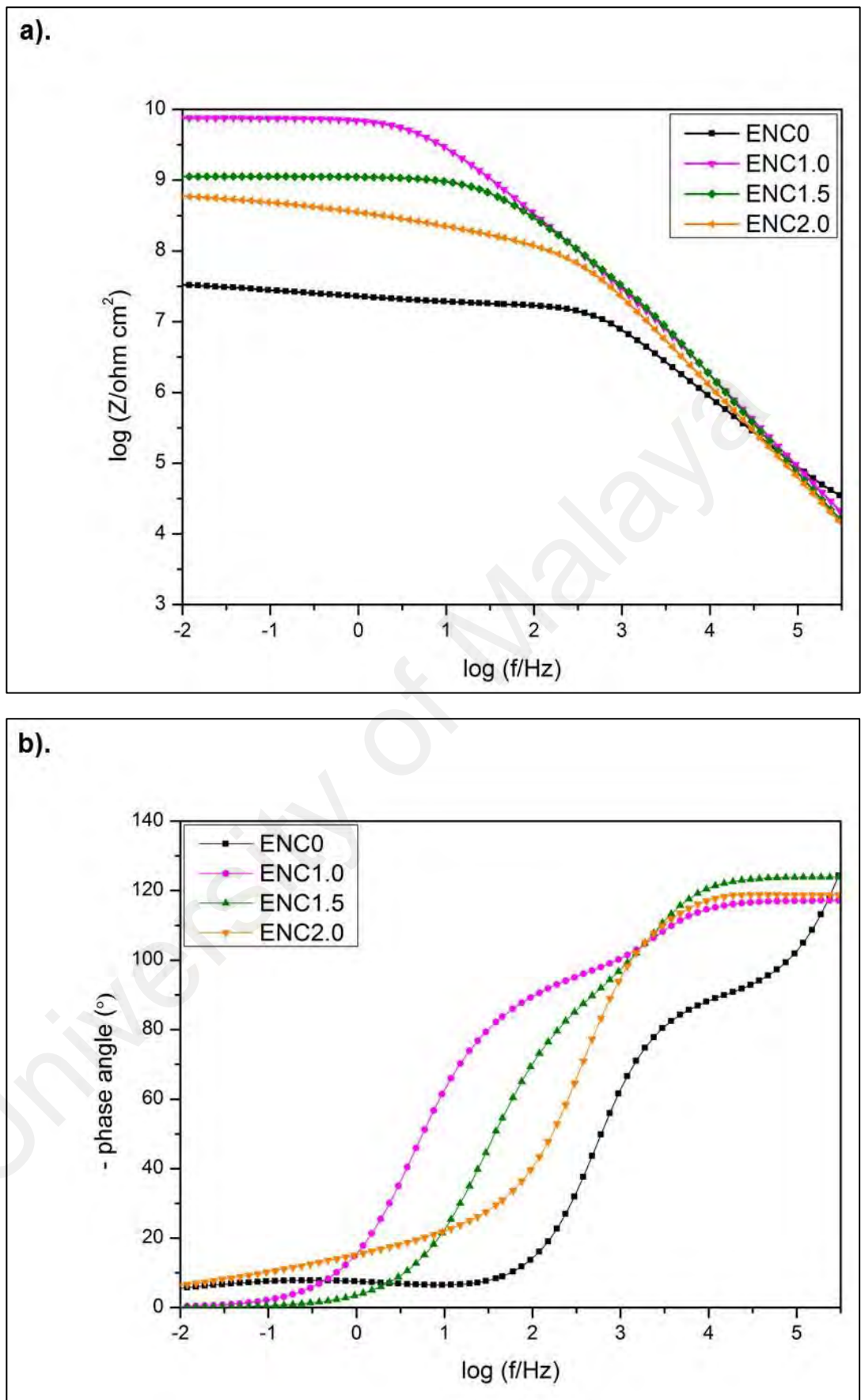


Figure 4.10: Representative Bode plots in terms of (a) impedance and (b) phase angle of the neat epoxy (ENC0) and ENC nanocomposite coating after 1 day of immersion.

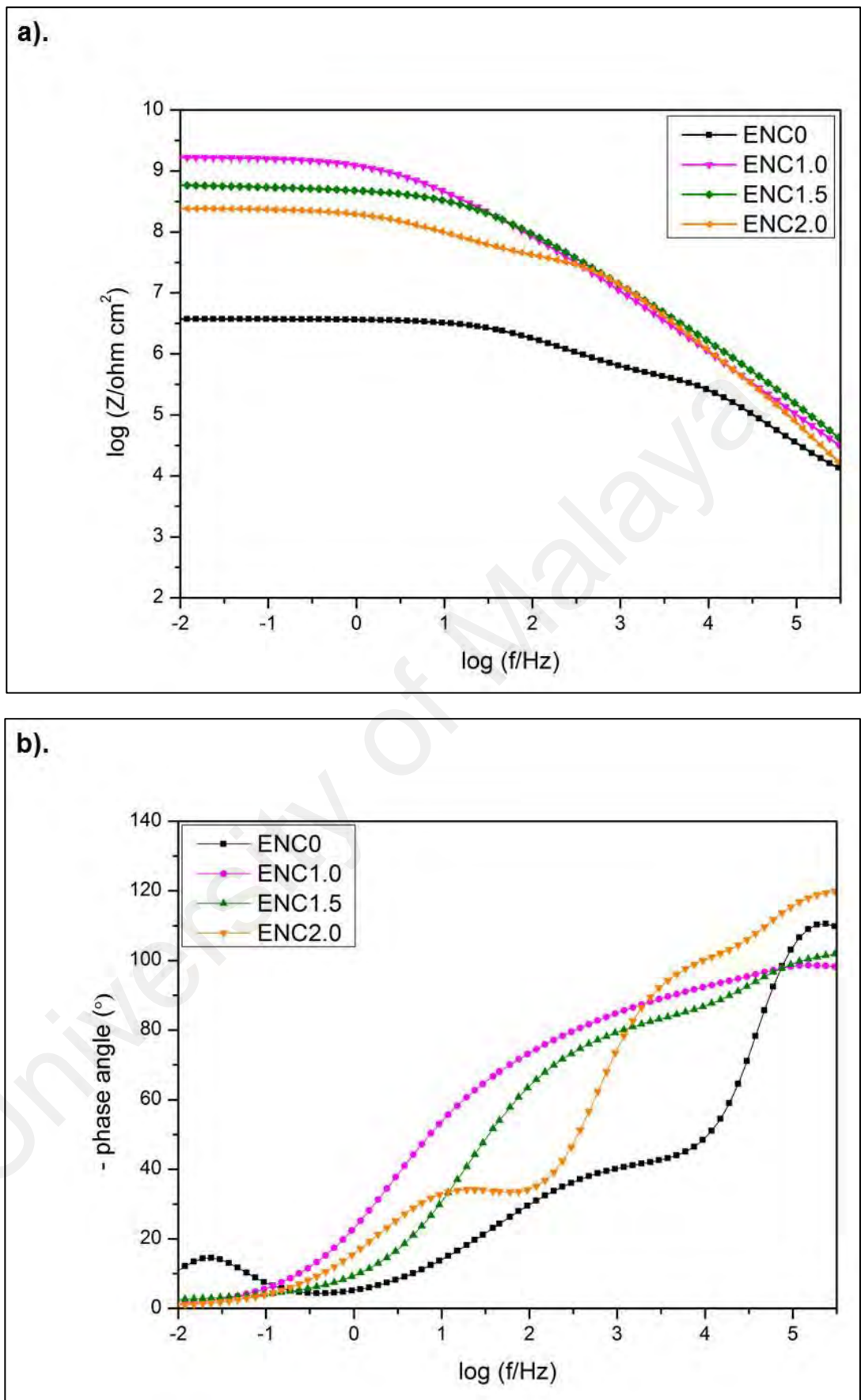


Figure 4.11: Representative Bode plots in terms of (a) impedance and (b) phase angle of the neat epoxy (ENC0) and ENC nanocomposite coating after 30 days of immersion.

To further investigate the ability of the NCs to enhance the corrosion protection performance of the epoxy coating systems, the EIS studies continued up to 30 days of immersion and the Bode plots were recorded and illustrated in Figure 4.11. Also, shown in Figure 4.11, the plotting of the ENC0 coating system continued to demonstrate two-time constants with the lowest coating resistance and phase angle, which indicated that the unmodified polymeric matrix of the epoxy did not withstand the exposure to the aggressive corrosive medium. This resulted in the creation of diffusion pathways and the penetration of the corrosive agents towards the substrate surface and therefore, corrosion occurred.

However, the 1.0 wt.% NC and 1.5 wt.% NC coating systems demonstrated a remarkable stability against the corrosion initiation over up to 30 days of immersion, as their respective Bode plots continued with the one time constant and remained well-fitted with model A of the equivalent circuit. Ammar et al., 2016b and other researchers (Ramezanzadeh et al., 2016; Zhou et al., 2014) have attributed the better corrosion protection performance of the nanocomposite coating systems, compared to the unmodified polymeric systems, to the ability of the NCs to fill up the porosity of the polymeric matrices and further enhance the quality of the coating film by promoting the possibility of achieving the optimal defect-free coating film. This forced the corrosive agents to travel longer distances to reach the surface of the substrate. However, it is worth noting that as the loading ratio of the NCs increased up to 2.0 wt.%, the coating resistance value decreased and two-time constants were observed with the impedance plot after 30 days of immersion. This was due to the degradation of the film coating and was a sign that the corrosion occurred at the coating-substrate interface. The performance of the 2.0 wt.% NC coating system could be attributed to the tendency of NCs to agglomerate at high loading ratios (Ammar et al., 2016c, d).

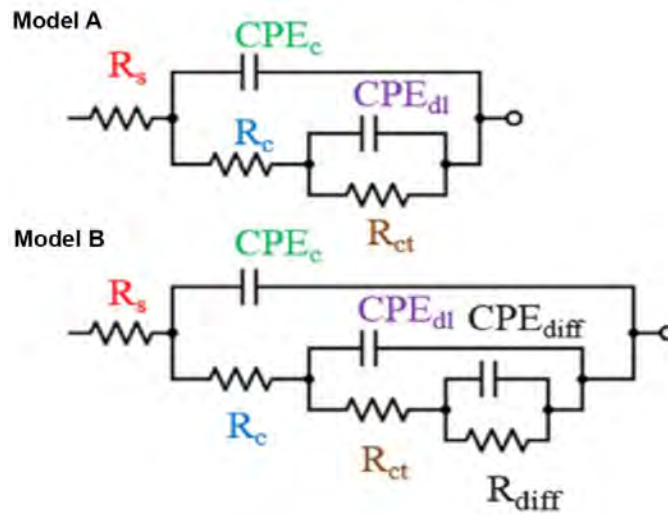


Figure 4.12: The equivalent circuits used for fitting the EIS Bode plots.

As aforementioned, Figure 4.12 highlights two different model of the equivalent circuit were utilised to achieve the best numerical fitting of the recorded EIS data over the different periods of immersion and the corresponded coating resistance values for all the resistance components of the utilised equivalent circuit models are tabulated in Table 4.1 and Table 4.2. Model A consists of two resistances, which known as solution resistance (R_s), coating resistance (R_c) and the charge transfer resistance (R_{ct}). Also, two capacitors, that is, CPE_c is the constant phase element of coating capacitance, CPE_{dl} is the constant phase element of double layer capacitance. As an extension of Model A, equivalent circuit Model B was created, which includes CPE_{diff} is the constant phase element of diffusion capacitance and R_{diff} is the diffusion resistance.

Table 4.1: Fitted parameter values of the equivalent circuit elements along with the utilised model for ENC nanocomposite coatings after 1 days of immersion.

System	R_c ($\Omega \text{ cm}^2$)	R_{ct} ($\Omega \text{ cm}^2$)	The equivalent circuit model used in fitting EIS data
ENC0	$(1.58 \pm 0.05) \times 10^7$	$(2.56 \pm 0.34) \times 10^7$	A
ECH0.5	$(3.55 \pm 0.05) \times 10^9$	$(1.99 \pm 0.12) \times 10^9$	A
ENC1.0	$(2.60 \pm 0.34) \times 10^7$	$(1.10 \pm 0.01) \times 10^9$	A
ENC1.5	$(5.06 \pm 0.13) \times 10^7$	$(0.18 \pm 0.02) \times 10^9$	A

Table 4.2: Fitted parameter values of the equivalent circuit elements along with the utilised model for ENC nanocomposite coatings after 30 days of immersion.

System	R_c ($\Omega \text{ cm}^2$)	R_{ct} ($\Omega \text{ cm}^2$)	R_{diff} ($\Omega \text{ cm}^2$)	The equivalent circuit model used in fitting EIS data
ENC0	$(4.55 \pm 0.18) \times 10^4$	$(8.69 \pm 0.23) \times 10^5$	$(7.32 \pm 0.98) \times 10^5$	B
ENC1.0	$(2.28 \pm 0.27) \times 10^8$	$(1.52 \pm 0.04) \times 10^9$	-	A
ENC1.5	$(1.33 \pm 0.97) \times 10^7$	$(5.47 \pm 0.34) \times 10^8$	-	A
ENC2.0	$(6.24 \pm 0.95) \times 10^5$	$(3.87 \pm 0.14) \times 10^7$	$(1.96 \pm 0.03) \times 10^8$	B

CHAPTER 5: RESULTS AND DISCUSSION OF EPOXY/NANOCHITOSAN NANOCOMPOSITE COATING SYSTEMS

5.1 Introduction

This chapter presents the results for the preparation of nanochitosan (NCH) from the high molecular weight of chitosan (CHI) and used as enhancing agents in epoxy/diamine pre-polymer solution. The contents of NCH loaded into epoxy/diamine were designed as ECH0, ECH0.5, ECH1.0 and ECH1.5 correspond to neat epoxy, 0.5 wt.%, 1.0 wt.% and 1.5 wt.% of NCH contents, respectively. The mixing ratio of epoxy/diamine is 4:1 and followed by corresponded NCHs load. Accordingly, all the results obtained are discussed analytically as in chapter 4 followed by corrosion study in an electrolyte, 3.5 wt.% NaCl, for 30 days.

This chapter consists of discussion on the surface morphology by FESEM, chemical structure by FTIR and XRD for prepared nanofillers and epoxy/nanochitosan nanocomposite (ECH) samples. Also, thermal analysis employed by TGA and DSC test on free film of nanocomposite samples, transparency test by UV-Vis spectroscopy on coated glass plates and electrochemical impedance study for all nanocomposite samples coated on mild steel panel. All these analyses methods are to investigate the effect of NC in the neat epoxy matrix and to evaluate the corrosion performance within 30 days immersed in 3.5 wt.% NaCl solution.

5.2 Field Emission Scanning Electron Microscope (FESEM) Analysis

5.2.1 Preparation of nanochitosan from high molecular weight of chitosan

Figure 5.1 shows the morphology at different magnification scales of commercial chitosan exhibited irregular plain membrane-like shape. Unlike cellulose, chitosan consists of amino and hydroxyl group as reactive sites which make it more versatile in a chemical reaction (Dutta et al., 2004). Chitosan is one of the most abundant biopolymers on earth and it contains primary amine and hydroxyl groups exhibit chelating agent properties. For morphological images, CHI in coarse ground flakes and powder form were used without further purification and commercially extracted from shrimp crustacean shell with a molecular weight of 310 000-375 000 Da.

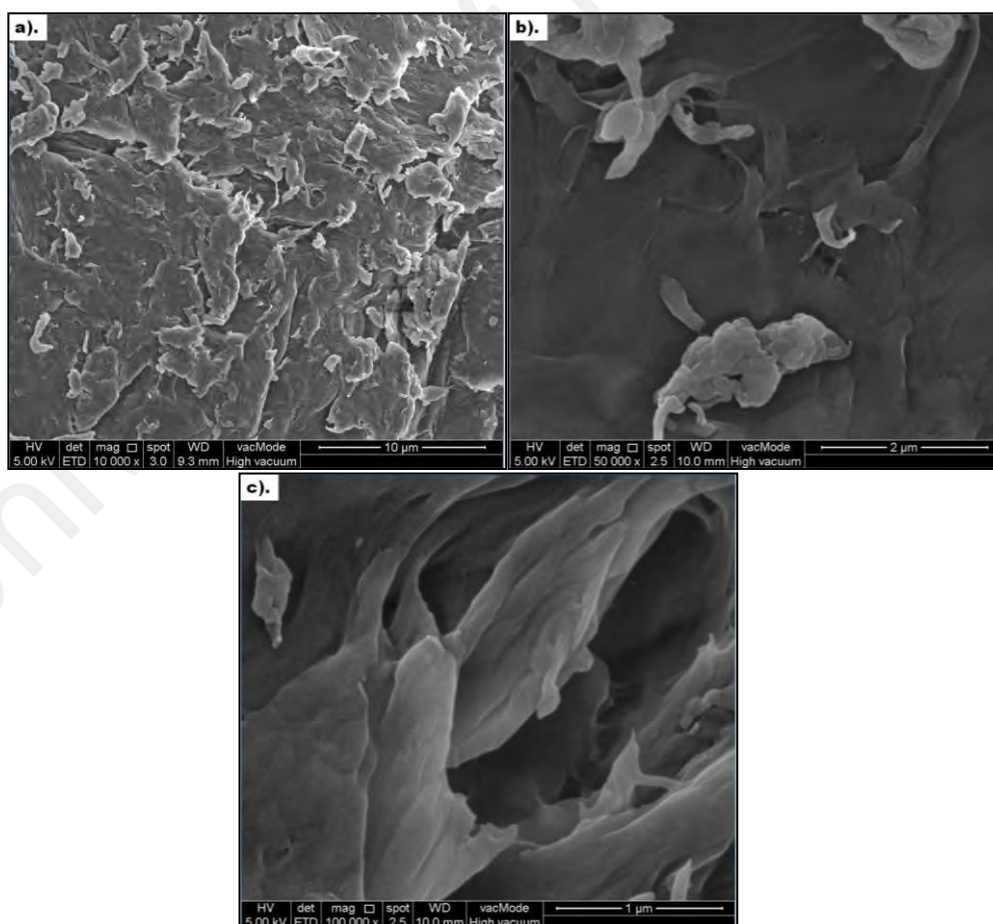


Figure 5.1: FESEM images of CHI scale at (a) 10 000 \times (b) 50 000 \times and (c) 100 000 \times of magnification.

This CHI was then hydrolyzed with 85 % of phosphoric acid with further treatment for purification was implemented to obtain the low molecular weight of chitosan. Subsequently, loosen chitosan molecular weight can help in scissoring particle size of chitosan due to the intermolecular entanglement of hydrogen bonding. According to Jia and Shen (2002), the homogeneous hydrolysis of chitosan with 85 % phosphoric acid was dependent on temperature and time of reaction. They also claimed that 19 000-200 000 Da of CHI molecular weight can be obtained through this acid hydrolysis method within 1-15 hours at 60 °C. Hence, in this study, hydrolysed CHIs with 85 % of H₃PO₄ at 60 °C for 4 hours were believed yield molecular weight in range 70 000 - 200 000 Da which can be considered as a low range of molecular weight chitosan (Jia & Shen, 2002).

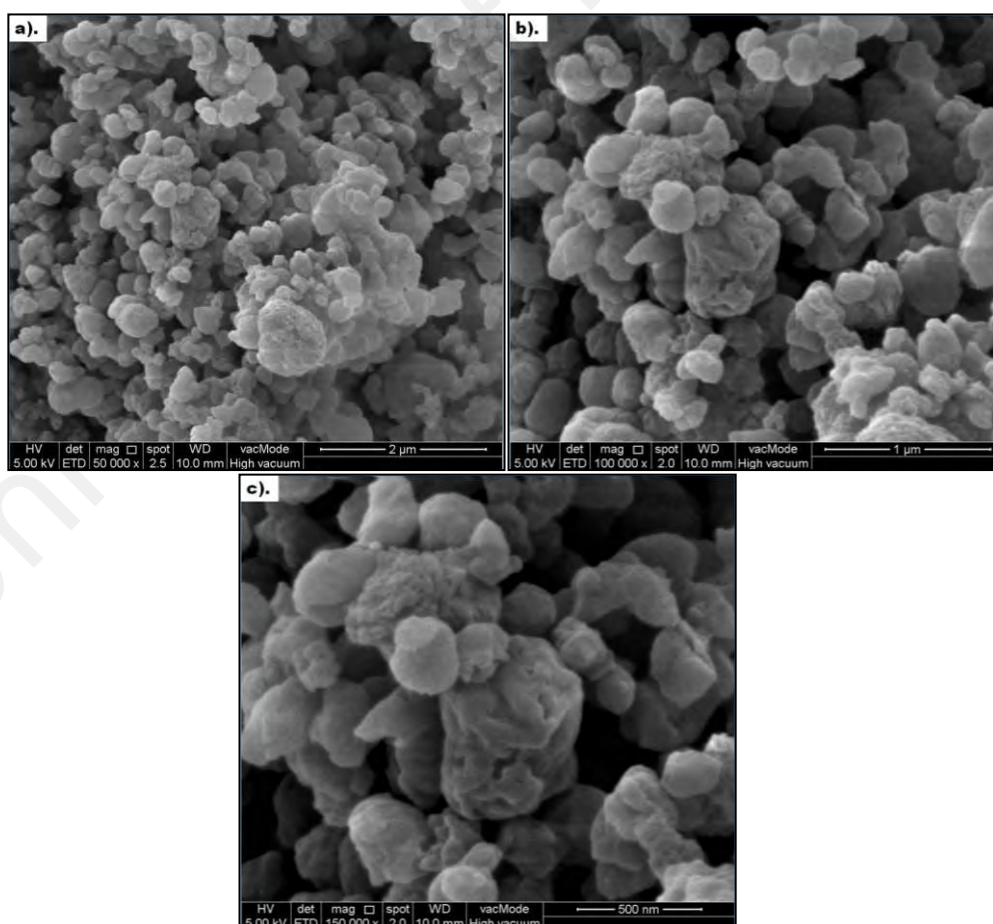


Figure 5.2: FESEM images of NCH at scale (a) 50 000× (b) 100 000× and (c) 150 000× of magnification.

Nanochitosans (NCHs) were prepared using acetic acid and sodium tripolyphosphate (TPP) which carry five negative charges per molecule which crosslinked with the reactive sites of chitosan. In this method, TPP solution is added to acidic chitosan solution in a dropwise manner upon a constant motion for homogeneity mixture. Apparently, spherical shape particles are formed spontaneously during the mixing. Huang et al., 2009 were degraded low weight CHI using different concentrations of H₂O₂ and of TPP for the preparation of NCHs. They concluded that the formation of NCH depended on the TPP concentration. When the TPP concentration was excessively low or high, it failed to react with the chitosan to form nanochitosan. A lower molecular weight of low weight CHI led to a tailored the particle. Hence, with the incorporation of TPP cross-linked with CHI resulting reduction in size and morphology.

As shown in Figure 5.2, spherical morphology of NCHs was formed well and fine, whereabouts, the size of NCHs in the range of 80 – 120 nm. This result exhibit the NCHs were derived from the CHI and TPP reaction due to the association of the charge stability of the hydrogen bond of CHI particles. Worth to note that chitosan contains cationic polysaccharide of (1,4)-linked 2-amino- 2-deoxy- β -D-glucose and 2-acetamido-2- β -D-glucose units which interact with negative charges of TPP. Hence, with the presence of these glucosic units, NCHs tend to agglomerate due to strong hydrogen bond attraction to the water during the gelation process and swelling still can form in the trend of compactness as shown in Figure 5.2(c) with respect to the initial particles of NCHs. As a consequence, swelling can be caused by osmosis of water inflow with the presence of TPP and agglomeration might be due to the nature of the rendered size of NCHs.

5.2.2 Epoxy/nanochitosan nanocomposite coating systems

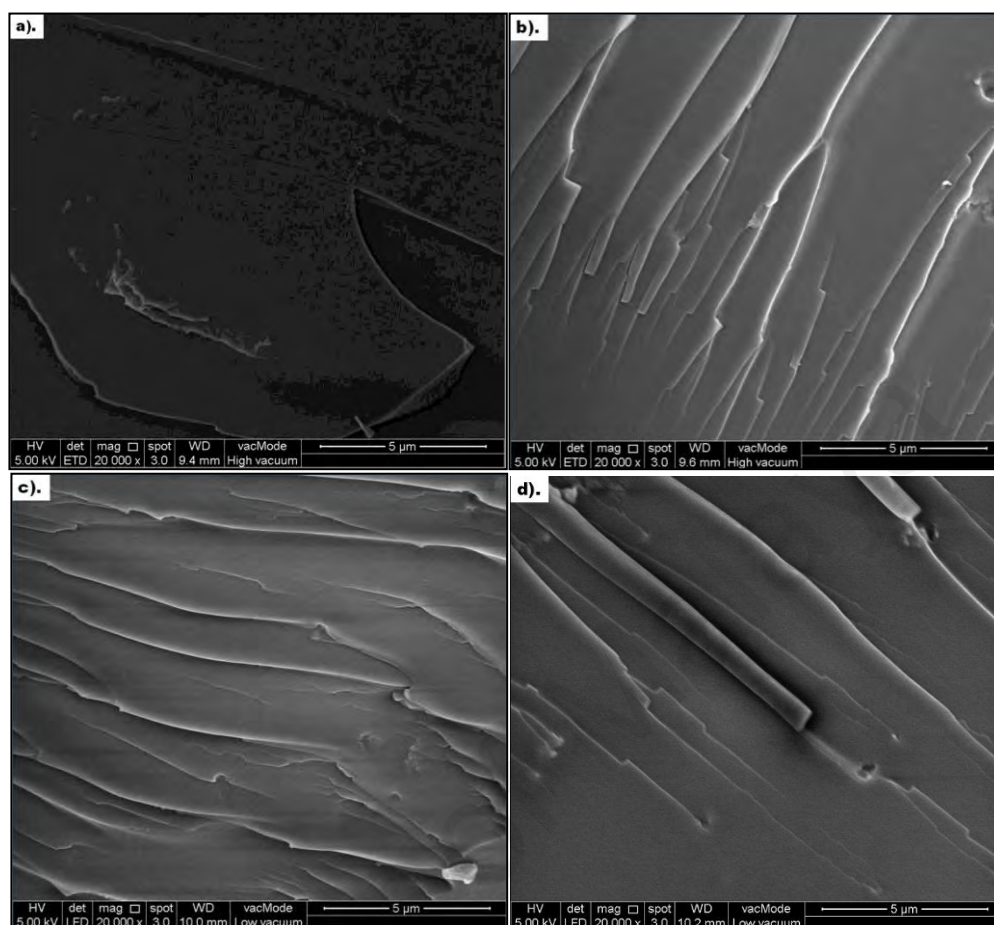


Figure 5.3: FESEM images of ECH at scale 20 000 \times of magnification (a) neat epoxy, (b) 0.5 wt.%, (c) 1.0 wt.% and (d) 1.5 wt.% NCHs.

Figures 5.3 and 5.4 show the FESEM images of epoxy/nanochitosan at scale 20 000 and 50 000 of magnification, respectively, for all coating systems. Figure 5.3(a) and 5.4(a) indicate the featureless of neat epoxy coating morphology in which can be attributed to its surface behaviour as the cured film coating. In these figures, (b) and (c) belonging to epoxy/nanochitosan nanocomposite with 0.5 wt.% and 1.0 wt.% NCHs contents, respectively, describe the cross section of NCH presence in an epoxy matrix. NCHs were incorporated into epoxy/diamine, apparently, homogeneous nanocomposites were produced, resulted smooth surfaces were obtained.

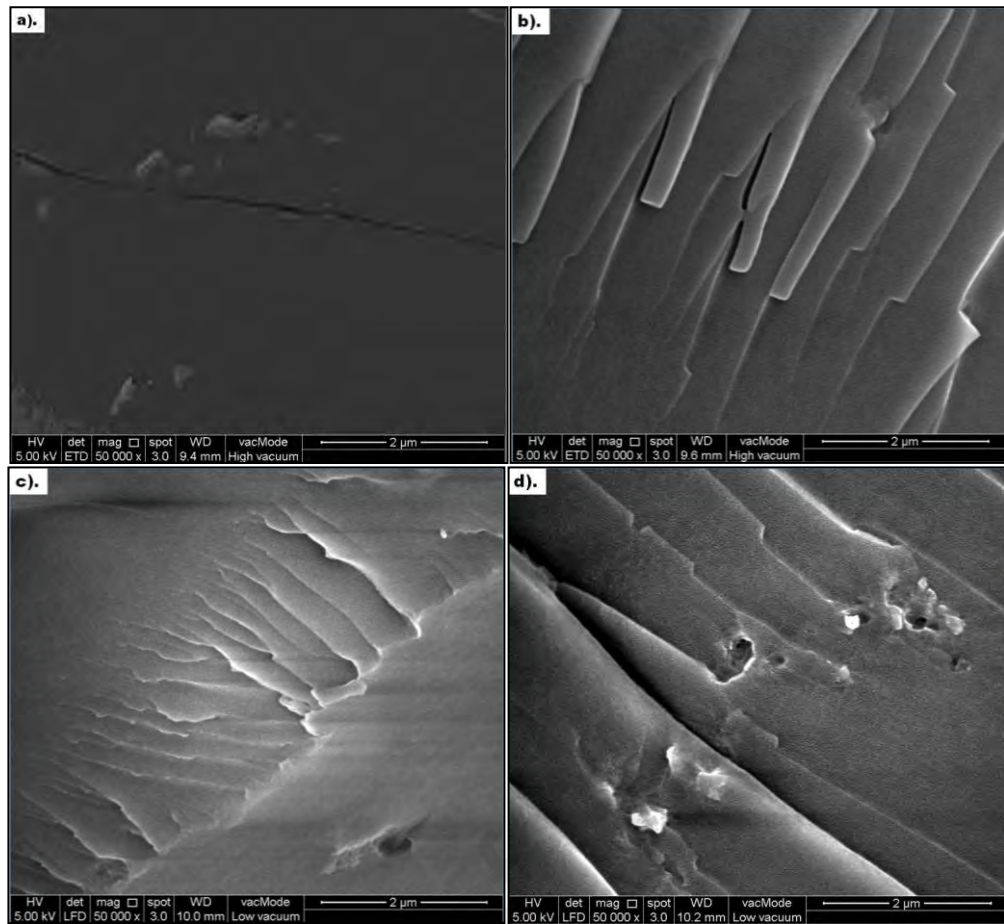


Figure 5.4: FESEM images of ECH at scale 50 000 of magnification (a) neat epoxy, (b) 0.5 wt.%, (c) 1.0 wt.% and (d) 1.5 wt.% NCHs

It is worth to note that NCH is versatile due to the presence of glucosamine units and reacts homogeneously with the epoxy matrix as a binder, thus, the appearances of NCH on epoxy surfaces cannot be observed clearly. However, it is very difficult to avoid the agglomeration of NCHs corresponds to their amount loaded. Figure 5.3(d) and 5.4(d) related to the epoxy/nanochitosan nanocomposites of 1.5 wt.% NCH contents, evinced the occurrences of agglomeration at a certain part of the epoxy surface.

5.3 Structural Analysis

5.3.1 X-ray Diffraction (XRD)

Figure 5.5 shows the X-ray diffraction patterns of chitosan and nanochitosan. Chitosan gives characteristic peaks at $2\theta = 20^\circ$. In contrary, XRD spectra of nanochitosan showed the disappearance of the peak at 20° from the raw chitosan indicating the increased of its amorphous nature, thus the crystal structure of chitosan is decreased after cross-linking with sodium tripolyphosphate (TPP). Moreover, there are no apparent peaks on neat epoxy spectra, however, the difference in EP/NCH nanocomposite can be observed as the broad band at range $10^\circ - 23^\circ$ varied with the amount of nanochitosan attributed the amorphous nature of nanocomposite systems increased with the additional NCHs.

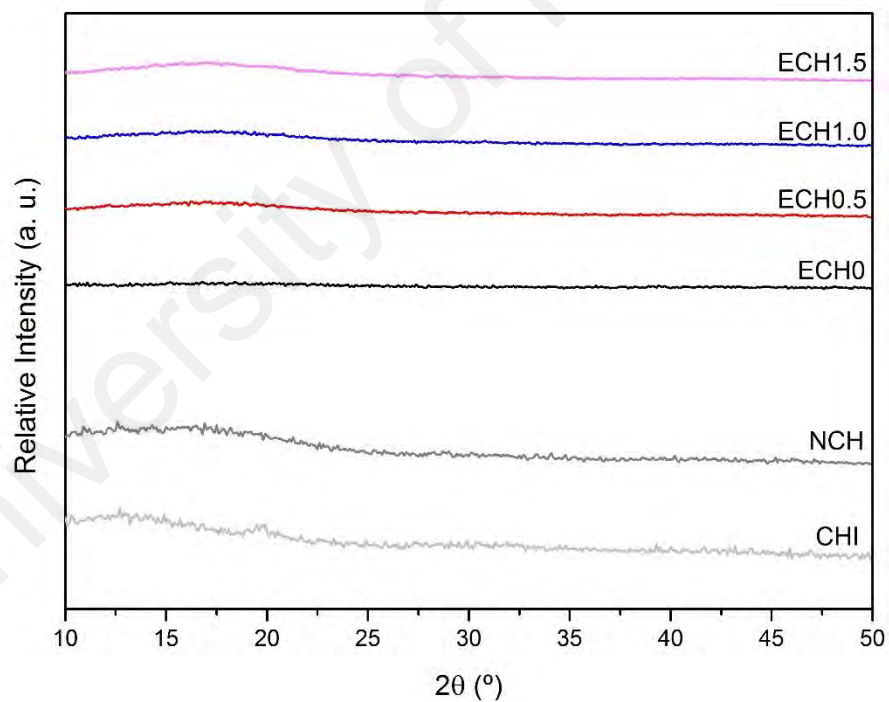


Figure 5.5: XRD spectra of CHI, NCH and ECH nanocomposite coating systems.

5.3.2 Fourier Transform Infrared (FTIR) Spectroscopy

Figure 5.6 depicts the FTIR images of all main components in nanocomposite coating systems. The absorbance peak at 826 cm^{-1} is very probable, as the peak is increased with the additional of NCH loaded into each coating system. This peak attribute to C-O-C stretching. The absorbance peak at 915 cm^{-1} corresponds to the C-O deformation in the oxirane group of epoxy resin. The band at 1032 cm^{-1} correspond to the stretching vibration of C-O-C linkages in the ether linkage of the epoxy matrix and glucosamine ring of nanochitosan.

NCH shows an absorption peak at 1235 cm^{-1} which is related to stretching of phosphate group also attributed of C = C wagging in epoxide group. At 1383 cm^{-1} and 1362 cm^{-1} are related to the C - CH₃ deformation in amide groups and the oscillations of OH and CH groups. These peaks can be observed in IPDA and NCH spectra confirming that amino groups involved in nanocomposite matrices with additional of NCH.

The NCH spectrum shows peaks at 1608 and 1582 cm^{-1} correspond to the reaction of free -NH₂ group due to the acetylated residues and pyranose ring structure (Dudhani & Kosaraju, 2010; Zheludkevich et al., 2011), which indicate strong intermolecular bond is formed between epoxy and NCHs. This can be seen as the intensity band increases with the additional NCHs contents where the intermolecular bonding inherently allowing to some extent.

The band at $2790 - 2982\text{ cm}^{-1}$ related to the symmetrical and asymmetrical -CH stretching in neat epoxy and overlapping with NH₃⁺ of nanochitosan for the composite matrix. The absorption band at about 2900 cm^{-1} is attributed to methoxyl groups presence in both epoxy and NCH. Meanwhile, shoulder peak at 3400 cm^{-1} is associated with O-H stretching due to hygroscopic properties of NCHs.

Nevertheless, it is difficult to differentiate the peaks of nanochitosan and epoxy in the FTIR analysis because both are polymers and, thus, some of the epoxy bands may overlap with nanochitosan bands correspond to their individual characteristics as an organic compound. It shows new peaks appeared for chitosan after crosslinking reaction indicating that epoxy has reacted with the hydroxyls of the glucosamine rings due to acetalization and in good agreement with other studies. Overall, the aforementioned bands indicate the existence of good miscibility between epoxy and NCHs, which is most likely caused by the formation of intermolecular hydrogen bonds between the amino and hydroxyl groups in NCHs and the hydroxyl groups in epoxy.

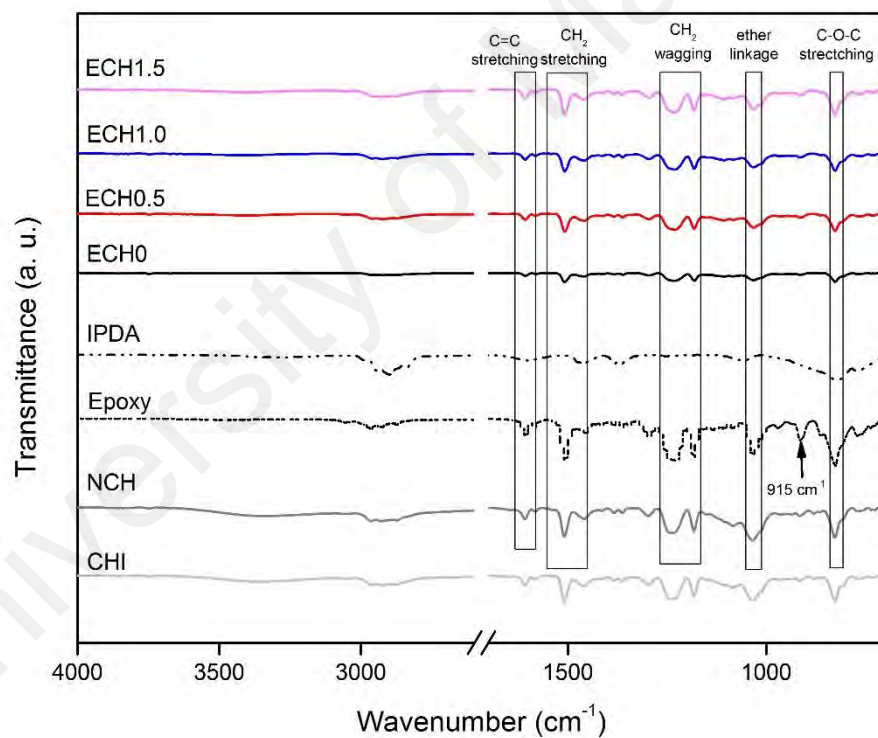


Figure 5.6: FTIR of the CHI, NCH, neat epoxy and ECH nanocomposite coating systems.

5.4 UV-Visible Spectroscopy

The UV-vis transmittance spectra of the ENC nanocomposite specimens in the visible wavelength range of 300-800 nm at 2.0 nm slit intervals are shown in Figure 5.7. ECH 0.5 shows the highest light transmittance, 72 % at 400 nm which indicates most transparent specimen than the neat epoxy and nanocomposite specimens. However, the transparency of ECH nanocomposite specimens reduced with more additional NCH contents as observed in Figure 5.7 whereas ECH1.0 and ECH1.5 reduced to 60 % and 50 % of light transmittance, respectively.

Up to 500 nm of visible wavelength showing that all the nanocomposite films are at 60 to 80 % of transmittance. This indicated even at high loading of NCH contents, the films optically transparent probably due to the spherical morphology of NCH. The size effect of NCH allowed light to pass and transmit more light. On the other hand, the drop off in the light transmission at 350 - 300 nm attributed to the high light absorption at this range. Hence, the NCH nanofiller enhanced the optical transmission of the neat epoxy resin due to its capability influencing the transparency of epoxy matrix.

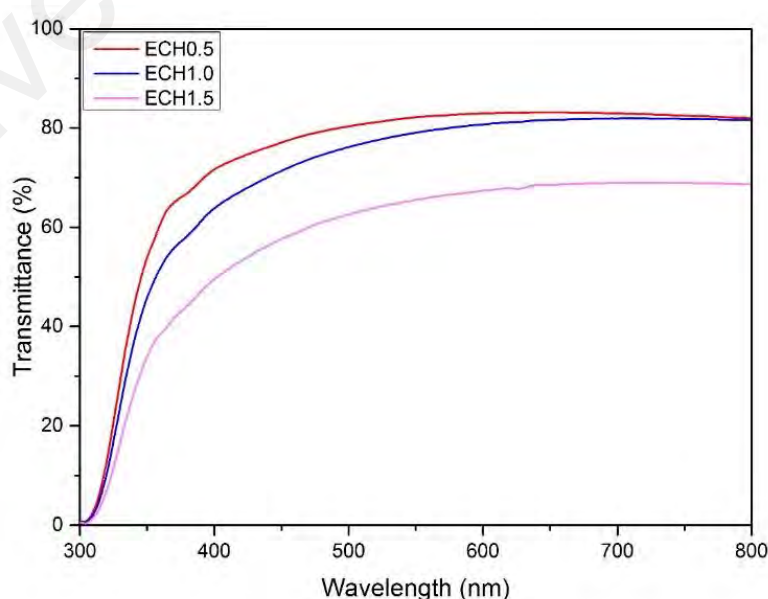


Figure 5.7: UV-Vis spectra for the ECH nanocomposite specimens.

5.5 Thermal Analysis

5.5.1 Thermogravimetric Analysis (TGA)

The TGA results of the neat epoxy and ENC nanocomposite coating samples are given in Figure 5.8, which consists of weight loss versus temperature and also included the derivative thermogravimetric (DTG) graph. The initial degradation temperature (T_{IDT}), the temperature at the maximum weight loss rate (T_{max}) and residue at 700 °C were extracted using TA universal analysis software programmer. The TGA curves in Figure 5.8 show that there was about 1 % weight loss, corresponding to water loss that occurred at first stage, below 100 °C, which is associated with the loss of moisture in the nanocomposite. The second stage of the TGA curves at the range after 200 °C corresponds to the degradation of the molecular networks of the nanocomposite due to the decomposition of the composite. These results suggest that the entire polymer network was present in the epoxy matrix so that the NCH remained stable without aggregating.

Herein, T_{IDT} is used as the thermal stability indicator and defined as the temperature corresponded to the 5 wt.% loss in weight. The highest T_{IDT} and T_{max} corresponded to the temperature at which the rate of weight loss reaches degradation and a maximum pronounced on ECH 0.5, that is, 380.13 °C and 396.79 °C, respectively.

Also, Figure 5.8 (b – d) shows that less than 9 % of the sample remains as a residue at 700 °C attributed to the dissociation process of NCH molecules in the resin matrix at a higher temperature. These results demonstrate that the present of NCH increased the degradation temperature due to the strong interchain bonding in the polymer matrix. Hence, it is noteworthy that the significant changes with NCH loaded were more thermally stable compared to neat epoxy sample.

Moreover, TG curve is a smooth curve with only one weight loss step and that there is only one peak on the DTG curve, indicating that the thermal degradation of nanocomposites in a nitrogen atmosphere is simple and is a one-step reaction. Both TG and DTG curves shift toward high temperatures along with the rising of the heating rate. The TGA thermogram of nanochitosan shows that around less than 7 % of the sample remained as a residue. On comparing results of thermogram details of nanocomposites with neat epoxy resin, it was concluded that the ECH nanocomposites were found to be thermally more stable and this was confirmed from the initial decomposition temperatures and the amount of residue remained at the end of the experiment.

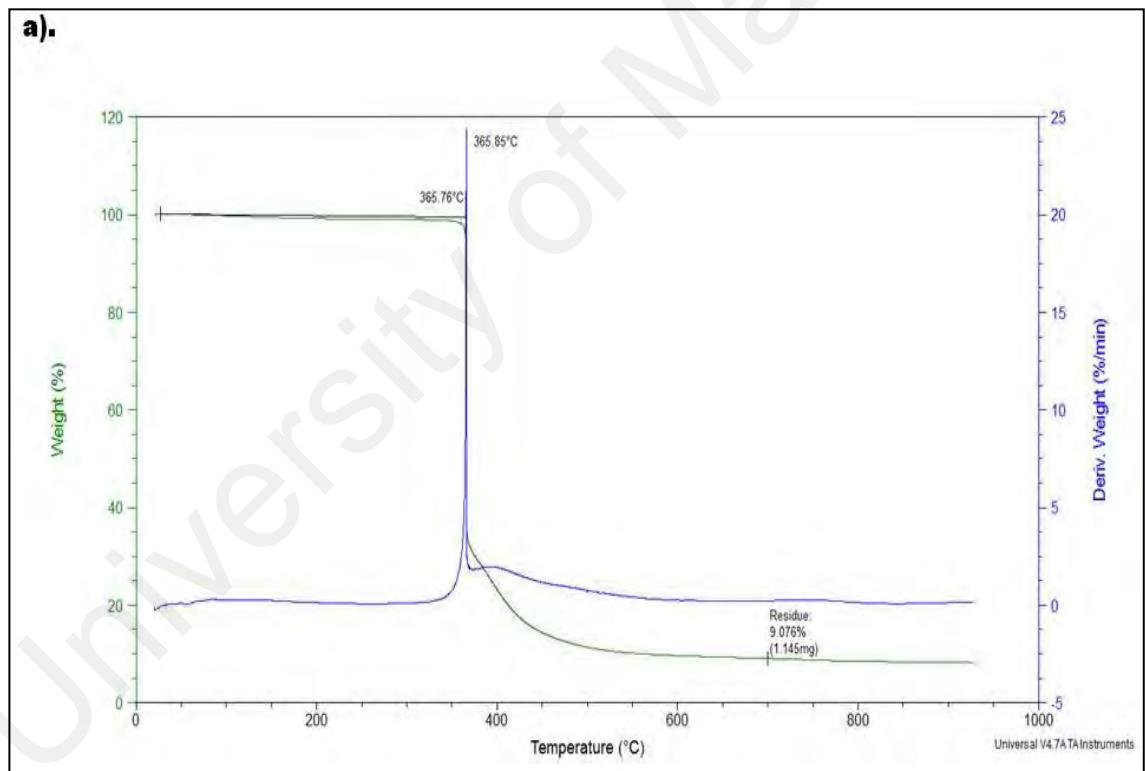


Figure 5.8: TGA thermograms of the (a) neat epoxy (ECH0) and ECH nanocomposite coating systems (b) ECH0.5, (c) ECH1.0 and (d) ECH1.5.

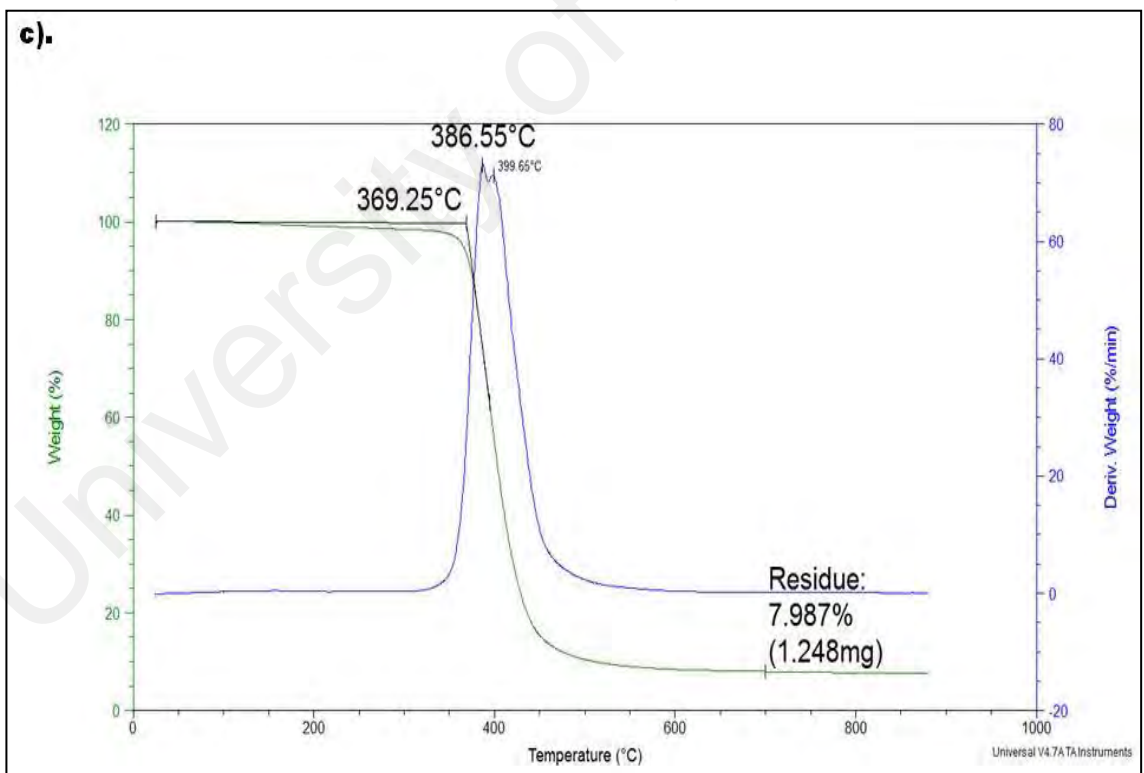
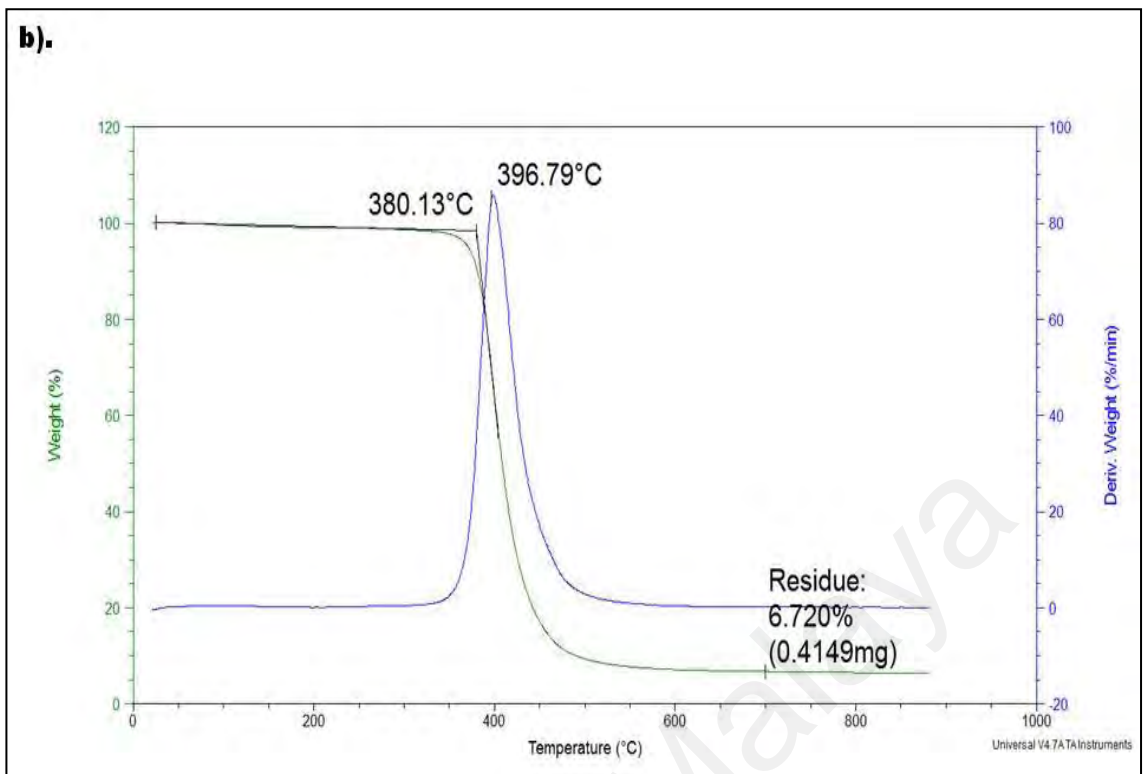


Figure 5.8: Continued.

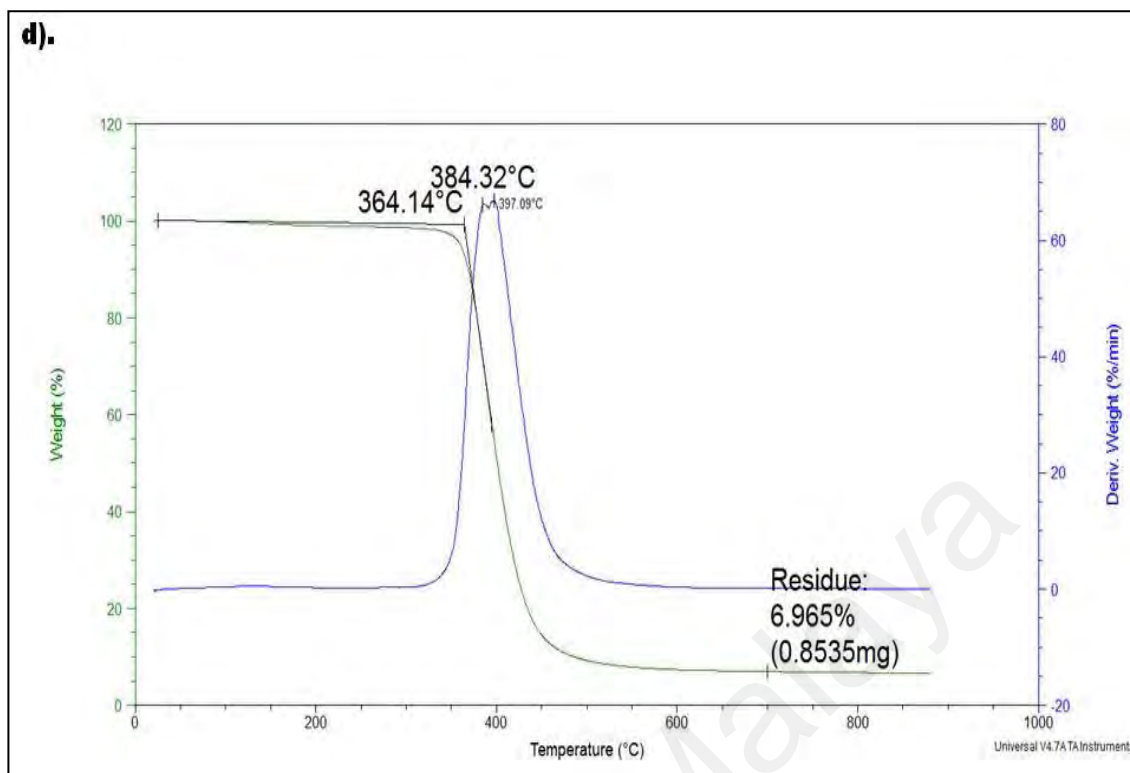


Figure 5.8: Continued.

5.5.2 Differential Scanning Calorimetry (DSC)

The DSC thermograms with glass transition temperature (T_g) values for the second cycle scanning of the endothermic measurement for all of the coating systems are shown in Figure 5.9. Note that, the two-cycle scanning was adopted to eliminate the moisture content of the samples, which might affect the DSC measurements or the thermal degradation. Data information and graphs were extracted by using TA universal analysis software programmer.

The differential scanning calorimetric (DSC) curves with glass transition (T_g) values of neat epoxy and epoxy/nanochitosan nanocomposite samples are shown in Figure 5.9, the DSC thermogram for second cycles scanning of endothermic measurement for all the coating samples for the purpose of moisture elimination and avoid insignificant thermal measurement. Very often, only heating measurements are performed when DSC is used to analyse materials.

In many cases, however, heating measurements alone are not sufficient to understand and characterise the properties and behaviour of a sample. Cooling measurements are then a simple way to gain valuable additional information. However, in this study, no information gain from cooling measurement. The rapid drop at $-25\text{ }^{\circ}\text{C}$ correspond to the second cycle scanning or also recycled materials which mean thermal history are not included in this measurement. Since there is no information of crystallisation, therefore, glass transition temperature of second cycle scanning has no different with thermal history. Herein, the glass transition temperature is about $\sim 135\text{ }^{\circ}\text{C}$ of neat epoxy to $154\text{ }^{\circ}\text{C}$ with a maximum increased of $\sim 20\text{ }^{\circ}\text{C}$ was observed at NCH loading of $0.5\text{ wt.}\%$ which attributes to the highest value of T_g as a function of NCH content compared as observed higher NCH contents. The increase of T_g value indicates the good incorporation of NCH in the epoxy matrix through their mobility interaction physically or chemically which is more pronounced on $0.5\text{ wt.}\%$ of NCH loaded.

The additional of NCH up to $1.0\text{ wt.}\%$ shows reduction of T_g value, that is, $137.15\text{ }^{\circ}\text{C}$, at much lower to $134.17\text{ }^{\circ}\text{C}$ of $1.5\text{ wt.}\%$ of NCH. This reduction of T_g attributes to the aggregation of NCHs at the epoxy surface due to the strong interaction between the $-\text{NH}_2$ and $-\text{OH}$ bonding of NCH. The embedding NCH into the epoxy polymer can cause aggregation as the amount of NCH contents increased. With aggregation at some part of the surface, increased the free volume on the vicinity surface, which then caused weak interaction between the network chains of NCH and epoxy. This aforementioned weak interaction leads to reduce the ability of nanocomposites properties.

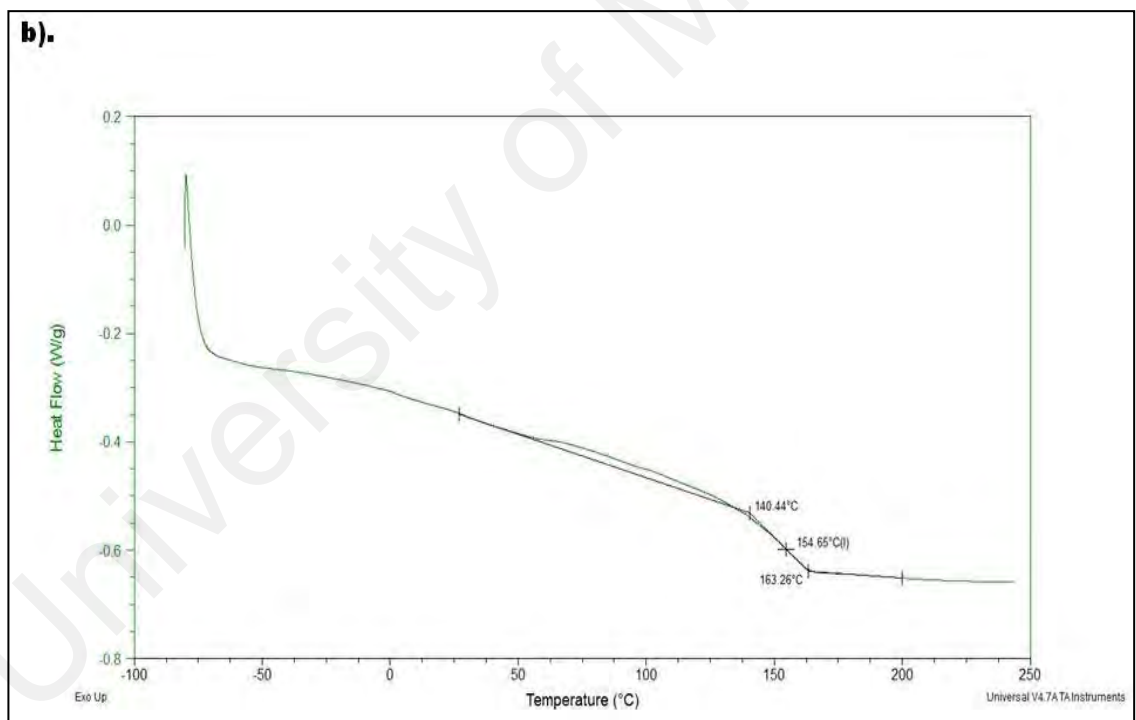
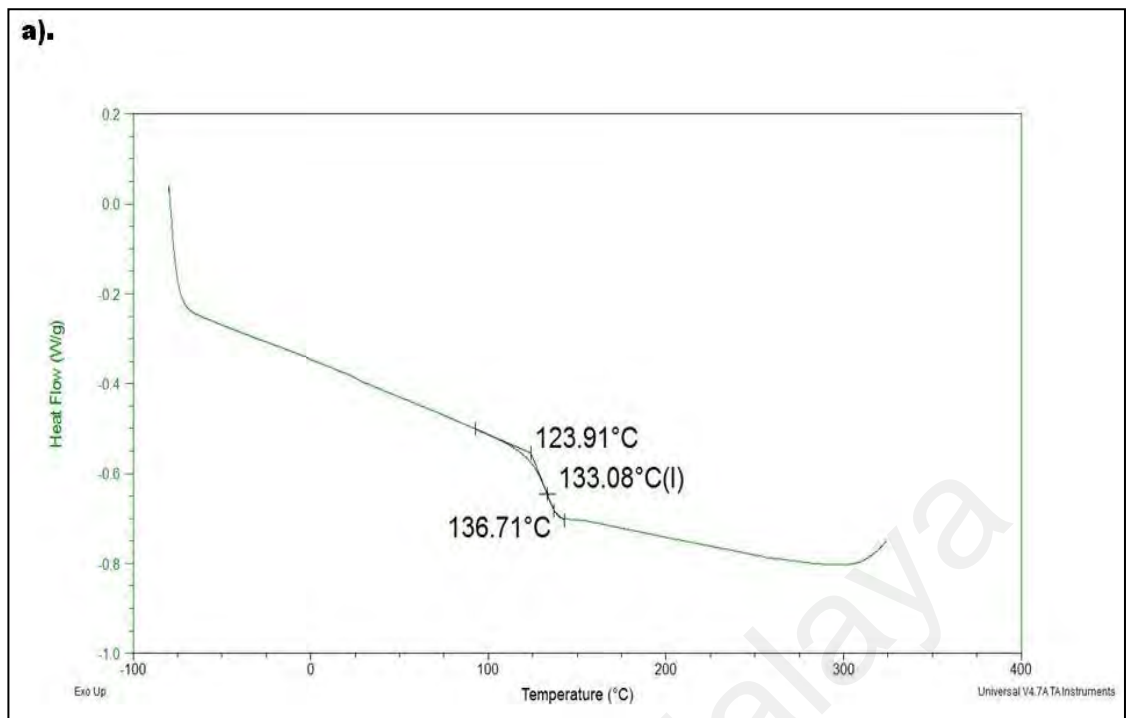


Figure 5.9: DSC thermograms of the (a) neat epoxy (ECH0) and ECH nanocomposite coatings (b) ECH0.5, (c) ECH1.0 and (d) ECH1.5.

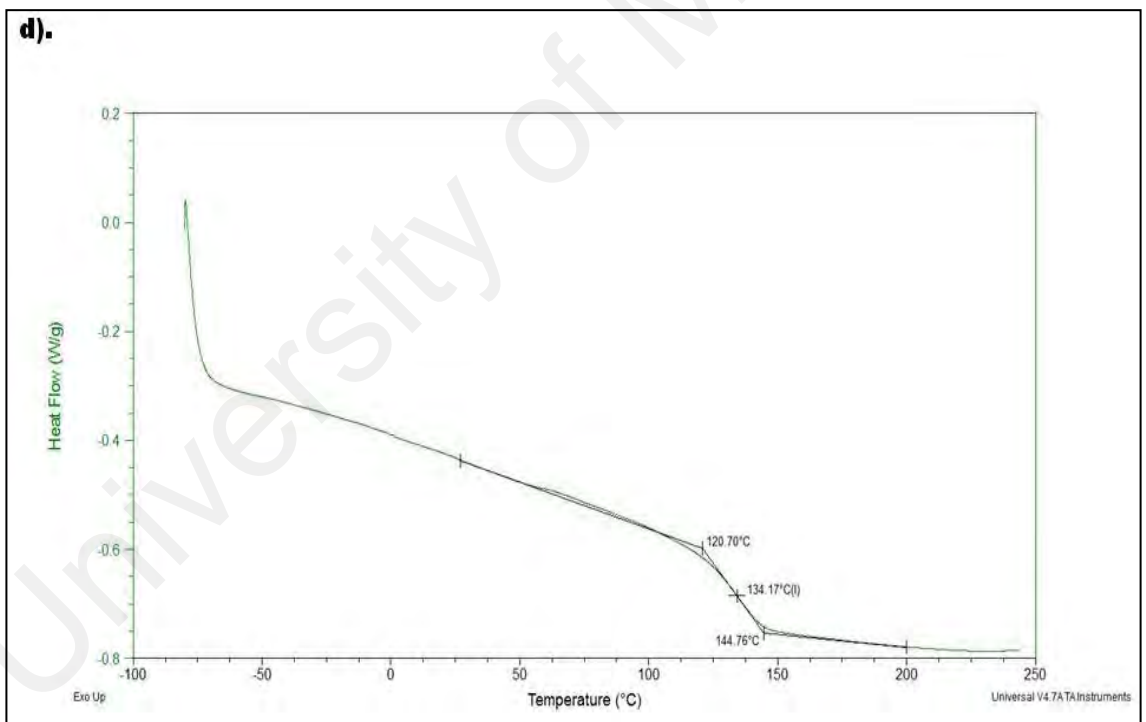
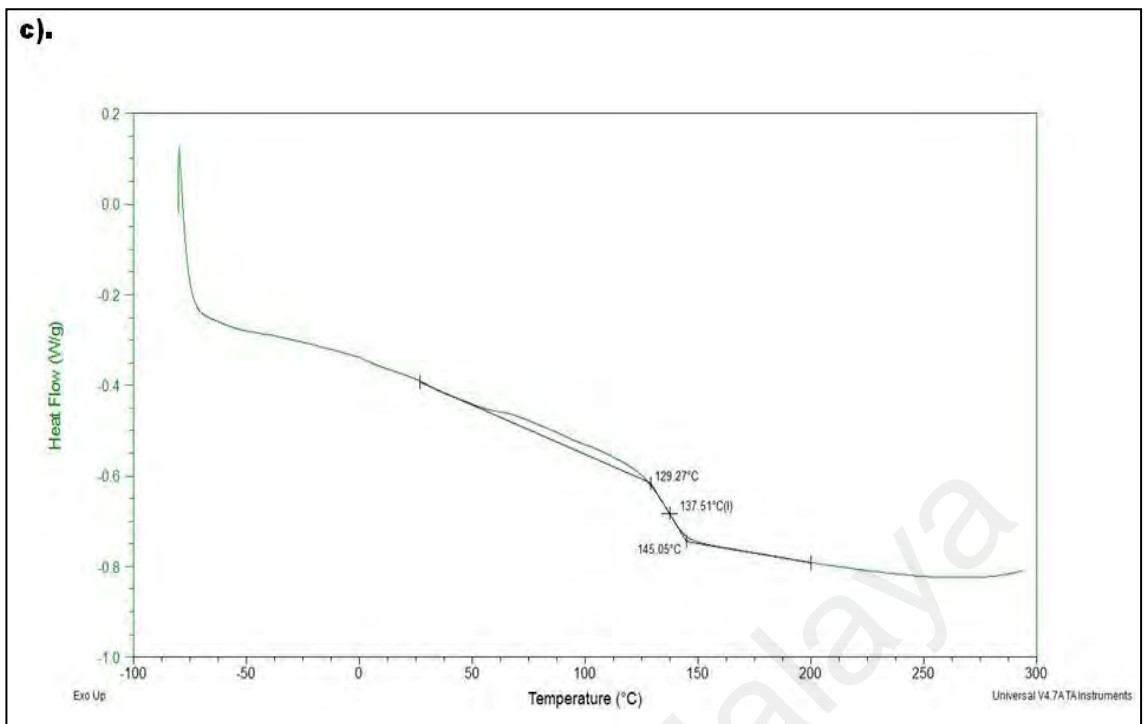


Figure 5.9: Continued.

5.6 Electrochemical Impedance Spectroscopy (EIS)

Figures 5.10 and 5.11 present the Bode plots of the epoxy coating and the coatings reinforced with various amounts of NCH after 1 day and 30 days of immersion, respectively.

To study the influence of NCHs on the corrosion protection performance of the EP, EIS measurements were conducted periodically after exposing the coated steel panels to 3.5 % NaCl solution. The obtained results were expressed graphically using Bode plots after 1 day and 30 days of immersion and fitted with two models of equivalent circuits. Electrochemical impedance spectroscopy (EIS) is a powerful tool for studying anticorrosion performance and coating degradation on coated surface. When used in conjunction with proper equivalent circuit model, EIS can provide valuable information about the electrochemical behavior of the coating film such as the creation of coating defects and coating delamination during any time of the exposure period.

EIS results at the first day of immersion, as shown in Figure 5.10, revealed the poor corrosion protection ability of all prepared coating systems as the penetration of the electrolyte occurred at the early stage of the immersion, first 24 hours of exposure time. The electrochemical responses of all prepared coating systems were recorded in the form of Bode plots and the numerical fitting of all the resistance components of the equivalent circuit was carried out via utilizing model A of the equivalent circuit and the resistance values were tabulated in Table 5.1. However, ECH nanocomposite coatings showed the barrier properties with higher coating resistance values than the neat epoxy coating. Also, the high frequency phase angle values also indicate that the coatings containing NCH remain intact. This finding could be considered as clear evidence that the electrolyte reaches the coating film but still not yet reached the coating/substrate interface.

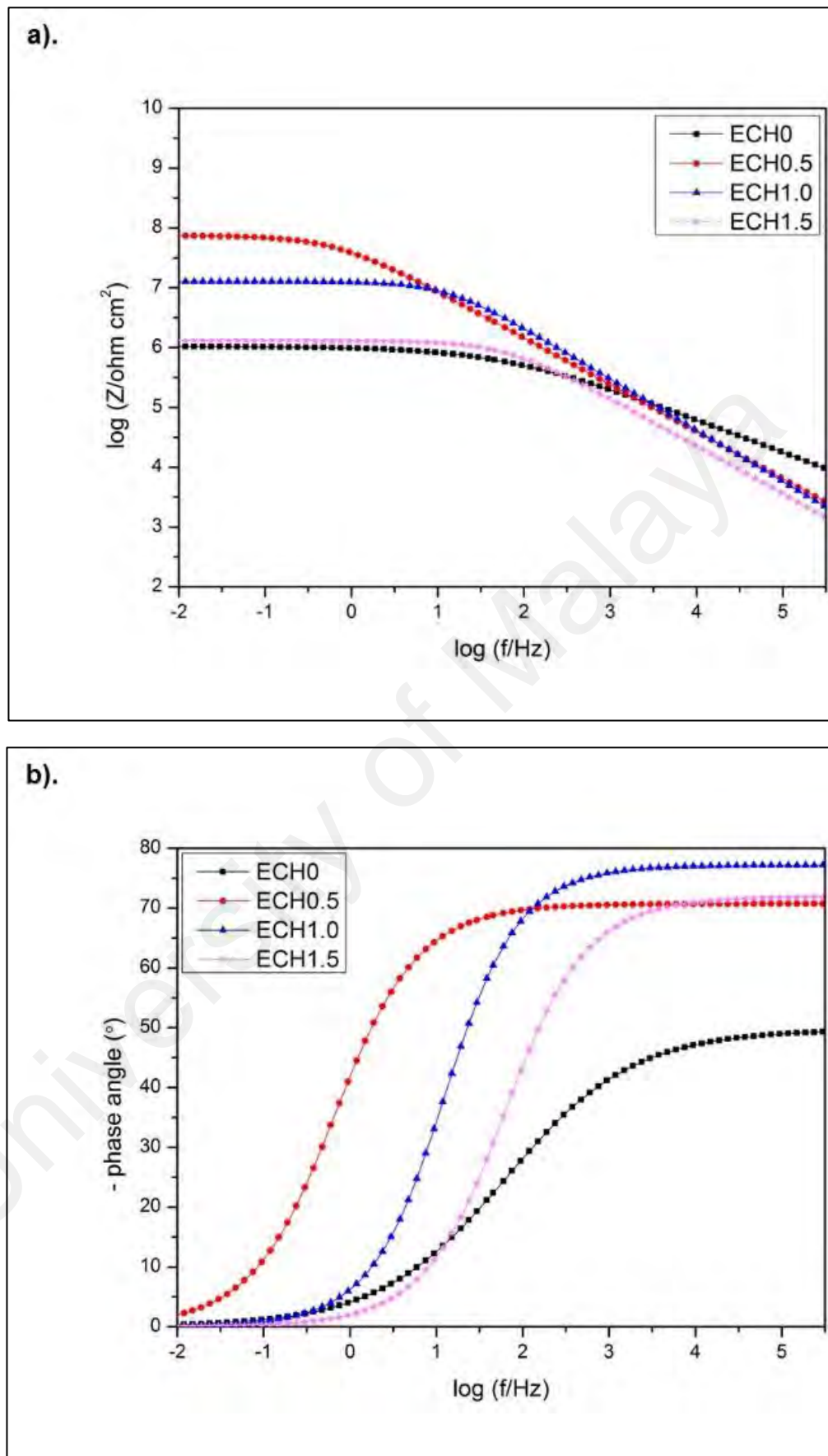


Figure 5.10: Representative Bode plots in terms of (a) impedance and (b) phase angle of the neat epoxy (ECH0) and ECH nanocomposite coating after 1 day of immersion.

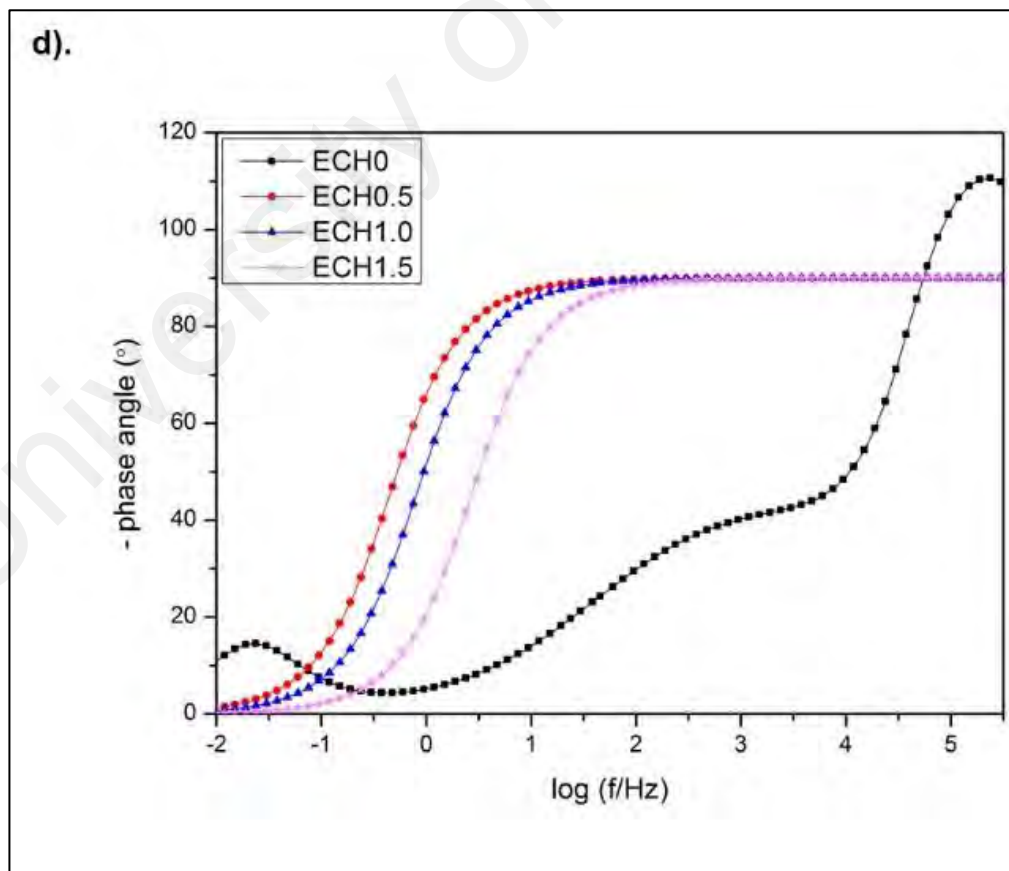
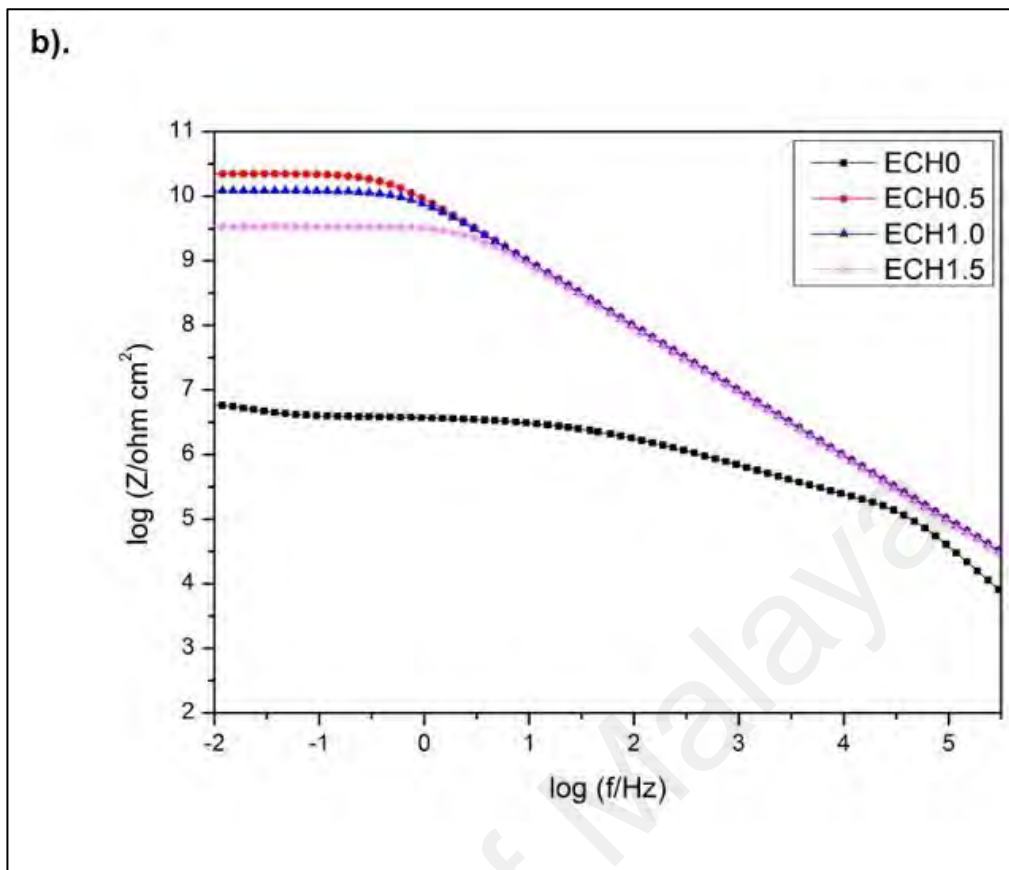


Figure 5.11: Representative Bode plots in terms of (a) impedance and (b) phase angle of the neat epoxy (ECH0) and ECH nanocomposite coating systems after 30 days of immersion.

Figure 5.12 shows two equivalent circuit models, that is, Model A and Model B. Model A consist of R_s as solution resistance, the coating resistance (R_c), CPE_c as the constant phase element of coating capacitance, the charge transfer resistance (R_{ct}) and CPE_{dl} as the constant phase element of double layer capacitance. An extended equivalent circuit of Model A so-called Model B consists of CPE_{diff} is the constant phase element of diffusion capacitance and diffusion resistance (R_{diff}).

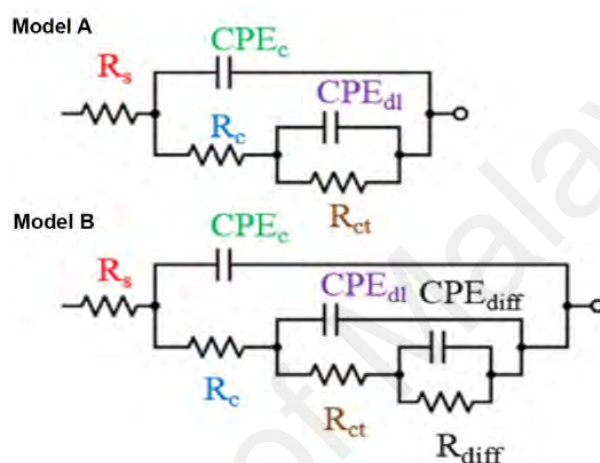


Figure 5.13: The equivalent circuits used for fitting the EIS Bode plots.

Technically, the decrease in coating resistance resulted during the immersion period could be attributed to many reasons such as the diffusion of moisture, ions and corrosive agents through the coating film toward the coating/substrate interface (Ammar et al., 2016).

As the time elapsed, the electrochemical responses of all prepared coating systems were illustrated in Figure 5.11. Furthermore, Table 5.2 highlights the values of all resistance components at this stage on immersion time. Neat epoxy coating (ECH0) demonstrated a significant degradation as its respective Bode plot was found to be fitted perfectly with Model B of the equivalent circuit and the coating resistance (R_c) value drops to approximately $10^4 \Omega \text{ cm}^2$. That, in turn, indicates the delamination of the coating upon the interface of coating/metal surface and resulted in blister formation and corrosion initiation

(Ammar et al., 2016). Meanwhile, coating resistance of nanocomposite coating systems increased as shown in Figure 5.11 and Table 5.2, which could be explained as the corrosive species were prohibited from reaching the coating/metal interface by the coating film.

Table 5.1: Fitted parameter values of the equivalent circuit elements along with the utilised model for ECH nanocomposite coatings after 1 days of immersion.

System	R_c (Ω cm ²)	R_{ct} (Ω cm ²)	The equivalent circuit model used in fitting EIS data
ENC0	$(1.11 \pm 0.09) \times 10^6$	$(2.56 \pm 0.34) \times 10^7$	A
ECH0.5	$(7.53 \pm 0.06) \times 10^7$	$(1.11 \pm 0.02) \times 10^8$	A
ENC1.0	$(1.27 \pm 0.75) \times 10^7$	$(1.91 \pm 0.26) \times 10^7$	A
ENC1.5	$(1.31 \pm 0.08) \times 10^6$	$(1.16 \pm 0.06) \times 10^7$	A

Table 5.2: Fitted parameter values of the equivalent circuit elements along with the utilised model for ECH nanocomposite coatings after 30 days of immersion.

System	R_c (Ω cm ²)	R_{ct} (Ω cm ²)	R_{diff} (Ω cm ²)	The equivalent circuit model used in fitting EIS data
ENC0	$(4.55 \pm 0.18) \times 10^4$	$(8.69 \pm 0.23) \times 10^5$	$(7.32 \pm 0.98) \times 10^5$	B
ECH0.5	$(2.22 \pm 0.16) \times 10^{10}$	$(0.59 \pm 0.89) \times 10^{10}$	-	A
ECH1.0	$(1.21 \pm 0.08) \times 10^{10}$	$(1.19 \pm 0.13) \times 10^{10}$	-	A
ENC1.5	$(3.36 \pm 0.02) \times 10^9$	$(2.49 \pm 0.23) \times 10^9$	-	A

As stated in Table 5.2, ECH0.5 and ECH1.0 exhibit more than 10^{10} Ω cm² of R_c attributed to the improvement of corrosion protection for the steel substrate probably due to the good dispersion of NCHs embedding into the epoxy matrix.

Nevertheless, the higher loading of nanofiller contents is influential to the anticorrosion performance of protection coating. The Bode plots of ENC1.5 (Figure 5.11(a)) after 30 days of measurement resulting in the lowest coating resistance among the nanocomposite coating systems. This is due to the aggregation of the epoxy/nanochitosan network chains which is contributed by the strong hydrogen bonding of nanochitosan leading to weakening the interconnection with epoxy matrix and leading to the creation of small pores at the matrices vicinity. As a result, allowing the diffusion of corrosive agents from the permeable pores to reach the coating/metal interface.

Also, the phase angle of ECH coating systems are lower than neat epoxy (Figure 5.11(b)) due to the occurrence of NCHs agglomeration but more stable corresponds to the barrier properties of nanocomposite coatings. This result confirming that the diffusion of electrolyte into the coating is delayed by the NCHs.

The incorporation of nanofiller increased the R_c and the R_{ct} values as shown in Table 5.2 which in turn contributed to the enhancement of corrosion protection of nanocomposite coating systems. Hence, several advantageous can be listed through the obtained EIS studies. First, chitosan nanofiller not only improved the quality of the cured epoxy coating but also reduced the permeable of the coating matrix resulting in a decrement of porosity matrices. Secondly, the deferment of delamination through zigzagged the diffusion path by superior properties of the nanofiller against corrosive agents. As a result, leading to improved barrier performance of the epoxy coating. Last but not least, the inclusion of this spherical nanochitosan improved the of the adhesion of the neat epoxy coating to the underlying substrate and enhanced the physiochemical properties of the coating/steel interface.

In comparison, the nanocomposite coating samples could maintain relatively high values of corrosion resistance at low-frequency range throughout the whole period of immersion time. However, it was interesting to notice that after 30 days of immersion time the Bode plots of all prepared nanocomposite coating systems tend to demonstrate better corrosion protection properties comparing to the performance of the same coating systems after 1 day of immersion time. This observation can be attributed due to the vital role of the NCHs that assist in filling up the diffusion pathways with the assist of the corrosion product that resulted from the corrosion reaction after some time of exposure. This mechanism could be explained as the electrolyte started to penetrate within the coating film and at the time it reached the substrate surface, corrosion reaction started and produced corrosion products. These corrosion products together with the incorporated NCHs tend to fill the newly produced channels of the electrolyte penetration and block these pathways against any more transformation of ions which in turn led to stop the corrosion reaction and observing an increment with the resistance values after 30 days of immersion as be stated in Table 5.2.

CHAPTER 6: DISCUSSION

In this work, the anticorrosion coatings using epoxy/diamine pre-polymer contains nanocellulose (NC) and nanochitosan (NCH) have been implemented. The coating systems were employed with the additional of nanocellulose and nanochitosan separately have been developed in different ratios.

The formation of NC and NCH via acid hydrolysis and ionic gelation, respectively, were confirmed by the changed in the surface morphology studied by FESEM. Acid hydrolysis leads to the isolation of micro and nanofibers with a high degree of crystallinity by removing the amorphous regions of the raw cellulose material. Applying this method, a negatively charged surface of the cellulose fibers can be obtained, through the esterification of hydroxyl groups by the sulphate ions. On the other hand, ionotropic gelation method was used to prepare nanochitosan with the presence of tripolyphosphate (TPP) but was protonated in phosphoric acid for -NH_3^+ formation. It is known that under acidic conditions, there is electrostatic repulsion between chitosan molecules due to the protonated amino groups of chitosan, meanwhile, there also exist interchain hydrogen bonding interactions between chitosan molecules. The size reduction of raw MCC and CHI were further characterised by XRD spectra. The disappearance of the peak decreased in intensity and increased broad shoulder showing the amorphous nature of nanofiller as they are originally polysaccharide polymer in nature. Moreover, the chemical compound of nanofiller shown by FTIR spectra that there are no changes of existence peak for NC and NCH. This confirmed the chemical bonding of the same as raw material that not affected by preparation methods. However, the decrease of peak intensity shows the size reduction of the particle.

Also, the surface morphology and structure of nanocomposite coating systems were studied by FESEM, XRD and FTIR. FESEM images show the surface cross-section with and without nanofiller. The agglomeration in nanocomposite systems is quite challenging to avoid as it increased with the additional load, strongly due to the forming of hydrogen bonding in the network chain (Rafieian & Simonsen, 2015). This undesirable agglomeration causes the nanofiller lose their large surface area and might affect the properties of coating (Gaur & Khanna, 2015).

On the other hand, XRD and FTIR spectra clearly show the composition results in nanocomposite coating systems. As much as, 2.0 wt.% of highest nanofiller loading relatively shown in XRD spectra that not much different as neat epoxy indicated the amorphous nature of coating system (Pan et al., 2012). The crosslinking between nanofiller, epoxy/diamine and epoxy resin were identified by FTIR with the evidence of C=C stretching, CH₂ stretching and wagging and C-O-C stretching clearly seen in the spectra.

The thermal analyses of nanocomposite systems were evaluated by TGA and DSC clearly, explains the increase of the thermal stability relatively to the neat coating. The TG curve of all coating systems is a smooth curve with only one weight loss step and that there is only one peak on the DTG curve, indicating that the thermal degradation of nanocomposites in a nitrogen atmosphere is simple and is a one-step reaction. Thermal decomposition of neat epoxy is considered as one step stage as reported by Ammar et al., 2016c which is due to dehydration, depolymerization and decomposition of the glycosyl unit accompanied by char formation. The little change of the initial degradation temperature in nanocomposite systems signified the overall thermal stability.

DSC is used to study the thermosetting behaviour of nanocomposite coating system by determining the glass transition temperature (T_g). T_g of nanocomposite systems was higher than neat epoxy attributed to the adherence behaviour of nanofiller incorporation. The increase of T_g value indicates the good incorporation of nanofiller in the epoxy matrix through their mobility interaction physically or chemically. However, the T_g trend significantly decreased up to 1.0 wt.% of nanofiller contents, this may due to the aggregation in the crosslinking of the network chains. Thus, the exceeding of optimum nanofiller contents possibly to reduce physical properties of the coating.

The transparency of the nanocomposite films was examined by UV-vis transmission spectroscopy. Apparently, incorporation of biopolymer nanofiller increased the transparency of coating film, which means the nanocomposite film has the capability of transmitting light. The purpose of having transparent coating film is to obtain a clear image on material surface that can see by naked eyes. This show that biopolymer nanofiller has the effect in which allowing light passing through the films or might be due to the size of particle which able to scatter light and produce transparent films. However, this case is not that simple because light scattering is depending on the refractive index (Xu et al., 2013), that is, the difference between the nanofiller and pre-polymer. Subsequently, the optical transparency of these nanocomposite films was decreased significantly due to the agglomeration of those nanofillers incorporation (Cross et al., 2013; James et al., 2012). The transmittance of nanocomposite systems was reduced with the increase of the content of nanofillers, but all nanocomposites still retained more than 60 % of transparency. Thus, the elimination of nanocomposite films transparency percentage due to the agglomeration of nanofillers and the particle size of filler.

Electrochemical impedance spectroscopy (EIS) was employed with two type of equivalent circuit consists R_s as solution resistance, the coating resistance (R_c), CPE_c as the constant phase element of coating capacitance, the charge transfer resistance (R_{ct}) and

CPE_{dl} as the constant phase element of double layer capacitance. Then an extended equivalent circuit of which consists of CPE_{diff} is the constant phase element of diffusion capacitance and diffusion resistance (R_{diff}).

Anticorrosion behaviour was studied by EIS and tested in the 3.5 wt.% NaCl medium for 30 days. All nanocomposite coating systems have enhanced the protection properties compared the coatings without nanofiller incorporation. These results were confirmed with the increased of coating resistance and charge transfer resistance. Moreover, incorporation of NC and NCH also decreased the rate of corrosion due to their strong intercalation bonding with epoxy matrix delaying the diffusion flow. By their high surface area properties with smaller size, these nanofillers were able to fill the free volume spaces in the coating/metal interface which mean protection also occur at the underlying coating.

It is interesting to note that NC and NCH were previously reported to alter the mechanical and thermal properties of epoxy resin as well (Cross et al., 2013; Dehnad et al., 2014; Dutta et al., 2004; Rafieian & Simonsen, 2015). Generally, pigment with macro- or micro- grain sizes was used incorporation with protective coating as corrosion inhibitor and resulted improve in its physical properties rather than chemical due to the mechanically strengthening of the coating film (Musil, 2000; Navarchian et al., 2014; Polcar et al., 2007; Stratmann et al., 1994; Zubielewicz & Gnot, 2004). Hence, long-term anticorrosive performance can be achieved with the improvement of the dispersion method either mechanical or sonication in the epoxy matrix.

CHAPTER 7: CONCLUSION AND RECOMMENDATION

The obtained results indicated that the deposition of biopolymers can successfully modify the anticorrosion performance on mild steel surface. The addition of biopolymer nanofiller into epoxy/diamine pre-polymer improved the coating properties without worsening their optical properties and these improvements can be attributed to the thermophysical characteristics of the biopolymers used. It is worth mentioning that the thickness of the coatings was $60 \pm 5 \mu\text{m}$.

The results obtained are concluded as follows;

1. This study reported the preparation of anticorrosive reagent from the raw biopolymer resource, that is, cellulose and chitosan. Cellulose was treated via acid hydrolysis to obtain nanocellulose (NC) in form of powder, whereas, chitosan was hydrolyzed with phosphoric acid before undergone ionotropic gelation method to obtain nanochitosan (NCH). Both biopolymer nanofillers were then used to develop an organic coating against corrosive environment.
2. NC and NCH in powder form acted as reinforcement nanofiller in epoxy/diamine pre-polymer solution. The effect of the reinforcement nanofillers on the corrosion protection properties of the epoxy/diamine coatings was studied.
3. The results showed that embedding the nanofiller into the epoxy/diamine pre-polymer enhanced not only the physical and chemical properties but also in thermal and optical properties.
4. The T_{IDT} and T_g increased as the content of nanofiller increased, corresponding to the thermal stability of nanocomposite coating relative to the neat coating. This indicated that the water content and thermal stability were not degraded and thus show the improvement of epoxy/diamine matrices with the presence of nanofiller.

5. The transparency of the film coating decreased with higher nanofiller loadings into the epoxy matrices due to aggregation of nanofiller. These results are worthy of further investigation in future studies.
6. EIS studies were performed with immersion in a 3.5 % NaCl solution up to 30 days to investigate the corrosion protection performance and the barrier properties of all the developed coating systems. The results of EIS studies revealed the ability of nanofiller to alter the corrosion protection performance of the coating film. Higher impedance values were recorded for the coating systems that contain NC even after 30 days of immersion time.
7. The best barrier properties and the most pronounced enhancement over the corrosion protection performance were observed for the 1.0 wt.% NC and 0.5 wt.% NCH coating systems.
8. The nanofiller incorporated into the epoxy matrices helped to improve their properties physically and chemically. In that regard, epoxy/nanocellulose and epoxy/nanochitosan nanocomposite coatings enhanced the barrier properties as anticorrosion protection.
9. Overall, these results indicated that the nanocomposite or another type of polymer nanocomposite might support the assertion that such structure-property relationships can be applied in a broad range of applications in the future.

Faced with these encouraging results, some other possibilities for improvement on the incorporation of active additives in the film formulation such as scratch-resistant, hydrophobic or antimicrobials to produce an active pre-polymer that interacts with the steel surface. Moreover, looking forward to industrial scale, intensive research need to be carried out fast cured coating instead for seven days curing time without damaging the material surface.

REFERENCES

- Ahmad, Z. (2006). *Principles of Corrosion Engineering and Corrosion Control* (1st ed.). UK: Elsevier Science.
- Ahmed, R. A., Farghali, R. A., & Fekry, A. M. (2012). Study for the stability and corrosion inhibition of electrophoretic deposited chitosan on mild steel alloy in acidic medium. *International Journal of Electrochemical Science*, 7(8), 7270–7282.
- Aliofkhazraei, M. (2014). Smart nanocoatings for corrosion detection and control. In A. S. H. Makhoulf (Ed.), *Handbook of Smart Coatings for Materials Protection* (pp. 198–223). UK: Elsevier.
- Ammar, S., Ramesh, K., Vengadaesvaran, B., Ramesh, S., & Arof, A. K. K. (2016). Amelioration of anticorrosion and hydrophobic properties of epoxy/PDMS composite coatings containing nano ZnO particles. *Progress in Organic Coatings*, 92, 54–65.
- Ashworth, V. (2010). Principles of cathodic protection. In V. Ashworth (Ed.), *Shreir's Corrosion* (3rd ed., pp. 2747–2762). Elsevier B.V.
- Bagherzadeh, M. R., & Mahdavi, F. (2007). Preparation of epoxy-clay nanocomposite and investigation on its anti-corrosive behavior in epoxy coating. *Progress in Organic Coatings*, 60(2), 117–120.
- Bahadori, A. (2014). *Cathodic Corrosion Protection Systems*. Cathodic Corrosion Protection Systems. Elsevier Inc.
- Bierwagen, G. P. (1996). In Organic Reflections on corrosion control by organic coatings, 9440(95).
- Chang, C., & Zhang, L. Cellulose-based hydrogels: Present status and application prospects, 84. *Carbohydrate Polymers* (2011).
- Chang, C., Zhang, L., Zhou, J., Zhang, L., & Kennedy, J. F. (2010). Structure and properties of hydrogels prepared from cellulose in NaOH/urea aqueous solutions. *Carbohydrate Polymers*, 82(1), 122–127.
- Choe, H. B., Lee, H. S., Ismail, M. A., & Hussin, M. W. (2015). Evaluation of electrochemical impedance properties of anti-corrosion films by Arc thermal metal spraying method. *International Journal of Electrochemical Science*, 10(11), 9775–9789.
- Ciolacu, D., Ciolacu, F., & Popa, V. I. (2011). Amorphous Cellulose – Structure and Characterization. *Cellulose Chemistry and Technology*, 45(1–2), 13–21.
- Cornell, R. M., & Schwertmann, U. (2003). *Products of Iron Metal Corrosion*. (R. M. Cornell & U. Schwertmann, Eds.), *The Iron Oxides: Structure, Properties, Reactions, Occurrences and Uses* (2nd ed.). Weinheim: Wiley.
- Cross, L., Schueneman, G., Mintz, E., Xu, S., Girouard, N., Shofner, M., & Service, U. S. F. (2013). Nanocellulose Reinforced Epoxy Elastomer. *Annual Meeting of the Adhesion*, 25–27.
- Dash, M., Chiellini, F., Ottenbrite, R. M., & Chiellini, E. (2011). Chitosan - A versatile semi-synthetic polymer in biomedical applications. *Progress in Polymer Science (Oxford)*, 36(8), 981–1014.

- Davis, J. (2000). *Corrosion: understanding the basics*. Corrosion. United States: ASM International.
- Dehnad, D., Emam-Djomeh, Z., Mirzaei, H., Jafari, S. M., & Dadashi, S. (2014). Optimization of physical and mechanical properties for chitosan- nanocellulose biocomposites. *Carbohydrate Polymers*, 105(1), 222–228.
- Dehri, I., & Erbil, M. (2000). The effect of relative humidity on the atmospheric corrosion of defective organic coating materials: An EIS study with a new approach. *Corrosion Science*, 42(6), 969–978.
- Dudhani, A. R., & Kosaraju, S. L. (2010). Bioadhesive chitosan nanoparticles: Preparation and characterization. *Carbohydrate Polymers*, 81(2), 243–251.
- Dutta, P. K., Duta, J., & Tripathi, V. S. (2004). Chitin and Chitosan: Chemistry, properties and applications. *Journal of Scientific and Industrial Research*, 63(1), 20–31.
- El-Haddad, M. N. (2013). Chitosan as a green inhibitor for copper corrosion in acidic medium. *International Journal of Biological Macromolecules*, 55, 142–149.
- Elmore, J. D., Kincaid, D. S., Komar, P. C., & Nielsen, J. E. (2002). Waterborne epoxy protective coatings for metal. *Journal of Coatings Technology*, 74(8), 63–72.
- Fan, W., Yan, W., Xu, Z., & Ni, H. (2012). Formation mechanism of monodisperse, low molecular weight chitosan nanoparticles by ionic gelation technique. *Colloids and Surfaces B: Biointerfaces*, 90(1), 21–27.
- Fekry, A. M., & Mohamed, R. R. (2010). Acetyl thiourea chitosan as an eco-friendly inhibitor for mild steel in sulphuric acid medium. *Electrochimica Acta*, 55(6), 1933–1939.
- Flauzino Neto, W. P., Silvério, H. A., Dantas, N. O., & Pasquini, D. (2013). Extraction and characterization of cellulose nanocrystals from agro-industrial residue - Soy hulls. *Industrial Crops and Products*, 42(1), 480–488.
- Fraga, F., Vazquez, E. C., Rodríguez-Núñez, E., & Martínez-Ageitos, J. M. (2008). Curing kinetics of the epoxy system diglycidyl ether of bisphenol A/isophoronediamine by Fourier transform infrared spectroscopy. *Polymers for Advanced Technologies*, 19(11), 1623–1628.
- Galliano, F., & Landolt, D. (2002). Evaluation of corrosion protection properties of additives for waterborne epoxy coatings on steel. *Progress in Organic Coatings*, 44(3), 217–225.
- Gaur, S., & Khanna, A. (2015). Functional Coatings by Incorporating Nanoparticles. *Nano Research & Applications*, 1(7), 1–8.
- Granath, J. (2010). Overview of Corrosion Protection with Volatile Corrosion Inhibitors. *ECS Transactions*, 25(30), 15–21.
- Iwamoto, S., Nakagaito, A. N., Yano, H., & Nogi, M. (2005). Optically transparent composites reinforced with plant fiber-based nanofibers. *Applied Physics A: Materials Science and Processing*, 81(6), 1109–1112.
- James, F., Josh, A., Richard, S., & Alan, W. (2012). Nanocellulose Reinforcement of Transparent Composites. In *Proceedings of SAMPE* (pp. 21–24). Baltimore.

- Jia, Z., & Shen, D. (2002). Effect of reaction temperature and reaction time on the preparation of low-molecular-weight chitosan using phosphoric acid. *Carbohydrate Polymers*, 49(4), 393–396.
- Johar, N., Ahmad, I., & Dufresne, A. (2012). Extraction, preparation and characterization of cellulose fibres and nanocrystals from rice husk. *Industrial Crops and Products*, 37(1), 93–99.
- John, S., Joseph, A., Jose, A. J., & Narayana, B. (2015). Enhancement of corrosion protection of mild steel by chitosan/ZnO nanoparticle composite membranes. *Progress in Organic Coatings*, 84, 28–34.
- Jones, D. (1993). Principles and prevention of corrosion. *Materials & Design*, 14, 207.
- Jusman, Y., Ng, S. C., & Abu Osman, N. A. (2014). Investigation of CPD and HMDS sample preparation techniques for cervical cells in developing computer-aided screening system based on FE-SEM/EDX. *Scientific World Journal*, 2014.
- Kadhim, M. J., Abdullah, A. K., Al-Ajaj, I. A., & Khalil, A. S. (2013). Mechanical Properties of Epoxy-Al₂O₃ Nanocomposites. *International Journal of Application or Innovation in Engineering & Management (IJAIEM)*, 2(11), 10.
- Karayannidou, E. G., Achilias, D. S., & Sideridou, I. D. (2006). Cure kinetics of epoxy-amine resins used in the restoration of works of art from glass or ceramic. *European Polymer Journal*, 42(12), 3311–3323.
- Kumar, A., Negi, Y. S., Choudhary, V., & Bhardwaj, N. K. (2014). Characterization of Cellulose Nanocrystals Produced by Acid-Hydrolysis from Sugarcane Bagasse as Agro-Waste. *Journal of Materials Physics and Chemistry*, 2(1), 1–8.
- Lamaka, S. V., Zheludkevich, M. L., Yasakau, K. A., Serra, R., Poznyak, S. K., & Ferreira, M. G. S. (2007). Nanoporous titania interlayer as reservoir of corrosion inhibitors for coatings with self-healing ability. *Progress in Organic Coatings*, 58(2–3), 127–135.
- Levy, A. V. (1995). Erosion and Erosion-Corrosion of Metals. *Corrosion*, 51(11), 872–883.
- Li, W., & Wang, F. (2011). Modeling of continuous drive friction welding of mild steel. *Materials Science and Engineering A*, 528(18), 5921–5926.
- Lim, S. H., & Hudson, S. M. (2004). Application of a fiber-reactive chitosan derivative to cotton fabric as an antimicrobial textile finish. *Carbohydrate Polymers*, 56(2), 227–234.
- Lin, J., Wu, X., Zheng, C., Zhang, P., Huang, B., Guo, N., & Jin, L. (2014). Synthesis and properties of epoxy-polyurethane/silica nanocomposites by a novel sol method and in-situ solution polymerization route. *Applied Surface Science*, 303, 67–75.
- Lince, J. R. (1991). Encyclopedia of tribology. *Wear* (Vol. 150). New York: Springer.
- Lu, P., & Hsieh, Y. Lo. (2010). Preparation and properties of cellulose nanocrystals: Rods, spheres and network. *Carbohydrate Polymers*, 82(2), 329–336.
- Materne, T., de Buyl, F., & Witucki, G. L. (2012). Organosilane Technology in Coating Applications : Review and Perspectives. *Dow Corning*, 1–16.

- McCafferty, E. (2010). *Introduction to corrosion science. Introduction to Corrosion Science*. New York: Springer.
- McMurray, H. N., & Williams, G. (2010). Under film/coating corrosion. In Tony J.A. Richardson (Ed.), *Shreir's Corrosion* (pp. 988–1004). UK: Elsevier.
- Morán, J. I., Alvarez, V. A., Cyras, V. P., & Vázquez, A. (2008). Extraction of cellulose and preparation of nanocellulose from sisal fibers. *Cellulose*, *15*(1), 149–159.
- Mostafaei, A., & Nasirpouri, F. (2013). Preparation and characterization of a novel conducting nanocomposite blended with epoxy coating for antifouling and antibacterial applications. *Journal of Coatings Technology Research*, *10*(5), 679–694.
- Musil, J. (2000). Hard and superhard nanocomposite coatings. *Surface and Coatings Technology*, *125*(1–3), 322–330.
- Nahla A. El-Wakil, M. L. H. (2008). Structural Changes of Regenerated Cellulose Dissolved in FeTNa, NaOH/thiourea and NMMO Systems. *Journal of Applied Polymer Science*, *109*(5), 2862–2871.
- Nam, S., French, A. D., Condon, B. D., & Concha, M. (2016). Segal crystallinity index revisited by the simulation of X-ray diffraction patterns of cotton cellulose I and cellulose II. *Carbohydrate Polymers*, *135*, 1–9.
- Navarchian, A. H., Joulazadeh, M., & Karimi, F. (2014). Investigation of corrosion protection performance of epoxy coatings modified by polyaniline/clay nanocomposites on steel surfaces. *Progress in Organic Coatings*, *77*(2), 347–353.
- Palimi, M. J., Rostami, M., Mahdavian, M., & Ramezanzadeh, B. (2014). Application of EIS and salt spray tests for investigation of the anticorrosion properties of polyurethane-based nanocomposites containing Cr 2O₃ nanoparticles modified with 3-amino propyl trimethoxy silane. *Progress in Organic Coatings*, *77*(11), 1935–1945.
- Pan, H., Song, L., Ma, L., & Hu, Y. (2012). Transparent Epoxy Acrylate Resin Nanocomposites Reinforced with Cellulose Nanocrystals. *Industrial & Engineering Chemistry Research*, *51*(50), 16326–16332.
- Paper, C., Corrosion, I., Series, C., Saudi, Z., Oil, A., Saudi, S., & Oil, A. (2011). Characterization of Corrosion Products In Oil And Gas Facilities Using X-ray Powder Diffraction Method. In *NACE - International Corrosion Conference*.
- Peng, B. L., Dhar, N., Liu, H. L., & Tam, K. C. (2011). Chemistry and applications of nanocrystalline cellulose and its derivatives: A nanotechnology perspective. *Canadian Journal of Chemical Engineering*, *89*(5), 1191–1206.
- Polcar, T., Nossa, A., Evaristo, M., & Cavaleiro, A. (2007). Nanocomposite coatings of carbon-based and transition metal dichalcogenides phases: A review. *Reviews on Advanced Materials Science*, *15*(2), 118–126.
- Pots, B. F. M., & Hendriksen, E. L. J. a. (2000). Corrosion 2000. In *Corrosion* (p. 31). Orlando: NACE International.
- Preghenella, M., Pegoretti, A., & Migliaresi, C. (2005). Thermo-mechanical characterization of fumed silica-epoxy nanocomposites. *Polymer*, *46*(26), 12065–12072.

- Presuel-Moreno, F., Jakab, M. A., Tailleart, N., Goldman, M., & Scully, J. R. (2008). Corrosion-resistant metallic coatings. *Materials Today*, 11(10), 14–23.
- Prime, R. B. (2014). Thermoset Characterization Part 12: Introduction to Thermogravimetric Analysis (TGA). *Polymer Innovation Blog*.
- Rafieian, F., & Simonsen, J. (2015). The effect of carboxylated nanocrystalline cellulose on the mechanical, thermal and barrier properties of cysteine cross-linked gliadin nanocomposite. *Cellulose*, 22(2), 1175–1188.
- Ramezanzadeh, B., Niroumandrad, S., Ahmadi, A., Mahdavian, M., & Moghadam, M. H. M. (2016). Enhancement of barrier and corrosion protection performance of an epoxy coating through wet transfer of amino functionalized graphene oxide. *Corrosion Science*, 103, 283–304.
- Rani, B. E. A., & Basu, B. B. J. (2012). Green inhibitors for corrosion protection of metals and alloys: An overview. *International Journal of Corrosion*, 2012, 1–15.
- Rinaudo, M. (2006). Chitin and chitosan: Properties and applications. *Progress in Polymer Science*, 31(7), 603–632.
- Roche, A. A., Bouchet, J., & Bentadjine, S. (2002). Formation of epoxy-diamine / metal interphases. *International Journal of Adhesion & Adhesives*, 22, 431–441.
- Saji, V. S. (2010). A Review on Recent Patents in Corrosion Inhibitors. *Recent Patents on Corrosion Science*, 2(1), 6–12.
- Sales, R. de C. M., & Brunelli, D. D. (2005). Luminescence spectroscopy applied to a study of the curing process of diglycidyl-ether of bisphenol-A (DGEBA). *Materials Research*, 8, 299–304.
- Shankar, S., & Rhim, J.-W. W. (2016). Preparation of nanocellulose from micro-crystalline cellulose: The effect on the performance and properties of agar-based composite films. *Carbohydrate Polymers*, 135, 18–26.
- Sheltami, R. M. E., Abdullah, I., & Ahmad, I. (2012). Structural Characterisation of Cellulose and Nanocellulose Extracted from Mengkuang Leaves. *Advanced Materials Research*, 545, 119–123.
- Shi, X., Nguyen, T. A., Suo, Z., Liu, Y., & Avci, R. (2009). Effect of nanoparticles on the anticorrosion and mechanical properties of epoxy coating. *Surface and Coatings Technology*, 204(3), 237–245.
- Shimazaki, Y., Miyazaki, Y., Takezawa, Y., Nogi, M., Abe, K., Ifuku, S., & Yano, H. (2007). Excellent thermal conductivity of transparent cellulose nanofiber/epoxy resin nanocomposites. *Biomacromolecules*, 8(9), 2976–2978.
- Steinmann, W., Walter, S., Beckers, M., Seide, G., & Gries, T. (2013). Thermal Analysis of Phase Transitions and Crystallization in Polymeric Fibers. *Applications of Calorimetry in a Wide Context - Differential Scanning Calorimetry, Isothermal Titration Calorimetry and Microcalorimetry*.
- Stratmann, M., Feser, R., & Leng, A. (1994). Corrosion protection by organic films. *Electrochimica Acta*, 39(8–9), 1207–1214.
- Tan, C. K., & Blackwood, D. J. (2003). Corrosion protection by multilayered conducting polymer coatings. *Corrosion Science*, 45(3), 545–557.

- Truong, V. T., Lai, P. K., Moore, B. T., Muscat, R. F., & Russo, M. S. (2000). Corrosion protection of magnesium by electroactive polypyrrole/paint coatings. *Synthetic Metals*, 110(1), 7–15.
- Tsai, M. L., Chen, R. H., Bai, S. W., & Chen, W. Y. (2011). The storage stability of chitosan/tripolyphosphate nanoparticles in a phosphate buffer. In *Carbohydrate Polymers* (Vol. 84, pp. 756–761).
- Uhlig, H. H. E. (2008). Corrosion Handbook. *Corrosion Handbook Online*, (Iii), 414–418. Retrieved from <http://doi.wiley.com/10.1002/9783527610433>
- Vijayalakshmi, K., Gomathi, T., & Sudha, P. N. (2014). Preparation and characterization of nanochitosan / sodium alginate / microcrystalline cellulose beads. *Der Pharmacia Lettre*, 6(4), 65–77.
- Voronova, M. I., Zakharov, A. G., Kuznetsov, O. Y., & Surov, O. V. (2012). The effect of drying technique of nanocellulose dispersions on properties of dried materials. *Materials Letters*, 68, 164–167.
- Wang, N., Ding, E., & Cheng, R. (2007). Thermal degradation behaviors of spherical cellulose nanocrystals with sulfate groups. *Polymer*, 48(12), 3486–3493.
- Xu, S., Girouard, N., Schueneman, G., Shofner, M. L., & Meredith, J. C. (2013). Mechanical and thermal properties of waterborne epoxy composites containing cellulose nanocrystals. *Polymer*, 54(24), 6589–6598.
- Yeh, J. M., Huang, H. Y., Chen, C. L., Su, W. F., & Yu, Y. H. (2006). Siloxane-modified epoxy resin-clay nanocomposite coatings with advanced anticorrosive properties prepared by a solution dispersion approach. *Surface and Coatings Technology*, 200(8), 2753–2763.
- Yuan, Y., Chesnutt, B. M., Haggard, W. O., & Bumgardner, J. D. (2011). Deacetylation of chitosan: Material characterization and in vitro evaluation via albumin adsorption and pre-osteoblastic cell cultures. *Materials*, 4(8), 1399–1416.
- Zareei, D., Sarabi, A. A., Sharif, F., Kassiriha, S. M., & Gudarzi, M. M. (2010). Preparation and Evaluation of Epoxy-Clay Nanocomposite Coatings for Corrosion Protection. *International Journal of Nanoscience and Nanotechnology*, 7(2), 126–136.
- Zhang, J., Hosemann, P., & Maloy, S. (2010). Models of liquid metal corrosion. *Journal of Nuclear Materials*, 404(1), 82–96.
- Zhang, S. Y., Li, S. J., Luo, X. W., & Zhou, W. F. (2000). Mechanism of the significant improvement in corrosion protection by lowering water sorption of the coating. *Corrosion Science*, 42(12), 2037–2041.
- Zheludkevich, M. L., Tedim, J., Freire, C. S. R., Fernandes, S. C. M., Kallip, S., Lisenkov, A., ... Ferreira, M. G. S. (2011). Self-healing protective coatings with ‘green’ chitosan based pre-layer reservoir of corrosion inhibitor. *Journal of Materials Chemistry*, 21(13), 4805.
- Zhou, C., Lu, X., Xin, Z., Liu, J., & Zhang, Y. (2014). Polybenzoxazine/SiO₂ nanocomposite coatings for corrosion protection of mild steel. *Corrosion Science*, 80, 269–275.

- Zorll, U. (1985). *Organic coatings* (3rd Ed., Vol. 13). New Jersey: John Wiley & Sons.
- Zubielewicz, M., & Gnot, W. (2004). Mechanisms of non-toxic anticorrosive pigments in organic waterborne coatings. *Progress in Organic Coatings*, 49(4), 358–371.
- Zugenmaier, P. (2008). History of Cellulose Research. In *Crystalline Cellulose and Derivatives* (1st ed., pp. 7–51). Verlag Berlin Heidelberg: Springer.

University of Malaya

LIST OF PUBLICATIONS AND PAPERS PRESENTED

Publications

Aema, I., Ma, W., Shafaamri, A., Kasi, R., Zaini, F. N., Balakrishnan, V., Ramesh, S., Arof, A. K. (2017). Anticorrosion Properties of Epoxy / Nanocellulose Nanocomposite Coating. *Bioresources*, 12(2), 2912–2929.

Ammar, S., Ramesh, K., **Ma, I. A. W.,** Farah, Z., Vengadaesvaran, B., Ramesh, S., & Arof, A. K. (2017). Studies on SiO₂-hybrid polymeric nanocomposite coatings with superior corrosion protection and hydrophobicity. *Surface and Coatings Technology*, 324, 536–545.

Conferences

Ma, I. A. W., Ramesh, K., Ammar, S., Farah, Z., Vengadaesvaran, B., Ramesh, S., Arof, A. K. (2016). Development of Biodegradable Coating by Using Natural Biopolymer Anti Corrosive Reagent. *In Proceeding National Physics Conference*. Kuala Lumpur, Malaysia.

Anticorrosion Properties of Epoxy/Nanocellulose Nanocomposite Coating

Iling Aema Wonnice Ma, Ammar Shafaamri, Ramesh Kasi,* Farah Nadia Zaini, Vengadaesvaran Balakrishnan, Ramesh Subramaniam, and Abdul Kariem Arof

Nanocellulose (NC) is an attractive reinforcement agent that can be incorporated into protective coatings because it is a renewable, biodegradable, and biocompatible polymer resource. In this study, a series of epoxy resin-based nanocomposites were prepared in the form of coatings with various amounts of NC loadings, and the coatings were applied onto mild steel at room temperature. The characterizations of the NC and nanocomposites were performed via X-ray diffraction (XRD), field-emission scanning electron microscopy (FESEM), and Fourier transform infrared spectroscopy (FTIR). The thermophysical properties of the nanocomposites were evaluated using differential scanning calorimetry (DSC) and thermogravimetry (TGA) analyses. The transparency of the nanocomposite specimens was examined by ultraviolet visible (UV-Vis) spectroscopy in the range of 300 to 800 nm. The corrosion protection properties of the coated mild steel substrates immersed in a 3.5% NaCl solution were studied comparatively by electrochemical impedance spectroscopy (EIS). The results showed that all of the nanocomposite coatings with NC noticeably influenced the epoxy-diamine liquid pre-polymer, both physically and chemically. Furthermore, the 1 wt.% NC nanocomposite coating system was found to have the most pronounced anti-corrosion properties, as confirmed by a 30-day EIS study.

Keywords: Nanocellulose; Nanocomposite; Corrosion; Coating; Electrochemical impedance spectroscopy (EIS)

Contact information: Center for Ionics University of Malaya, Department of Physics, University of Malaya, Kuala Lumpur, 50603, Malaysia; *Corresponding author: rameshkasi@um.edu.my

INTRODUCTION

The suitability of using biopolymer materials, such as polysaccharides, proteins, and lipids, in film production has been intensively studied recently for the production of biodegradable packaging materials. The development of biomaterials holds great promise to alleviate many sustainability problems and offers the potential of renewability, biodegradability, and a path away from harmful additives. Compared with other materials, cellulose is the most abundant natural carbohydrate biopolymer on earth that is renewable, biodegradable, and non-toxic. It is a hydrophilic polymer composed of repeating β -1,4-linked-D-glucopyranose units and consists of three hydroxyl groups per anhydroglucose unit (AGU), which allows the cellulose molecule to establish strong hydrogen bonds (Zugenmaier 2008).

Knowledge of the molecular structure of cellulose is crucial, as it explains the characteristic properties of cellulose, such as hydrophilicity, chirality, biodegradability, and high functionality. The morphology and the properties of the cellulose nanocrystals



Studies on SiO₂-hybrid polymeric nanocomposite coatings with superior corrosion protection and hydrophobicity



Sh. Ammar, K. Ramesh ^{*}, I.A.W. Ma, Z. Farah, B. Vengadaesvaran, S. Ramesh, A.K. Arof

Center for Ionics University of Malaya, Department of Physics, Faculty of Science, University of Malaya, Kuala Lumpur 50603, Malaysia

ARTICLE INFO

Article history:
Received 5 December 2016
Revised 26 May 2017
Accepted in revised form 5 June 2017
Available online 6 June 2017

Keywords:
SiO₂ nanoparticles
Anticorrosion coatings
Hydrophobic surface
EIS
FESEM

ABSTRACT

Hybrid polymeric based nanocomposite coating systems (NCs) were fabricated by solution intercalation method with the use of epoxy (E) and polydimethylsiloxane (PDMS) as the host hybrid polymeric matrix and different weight ratio of SiO₂ nanoparticles, ranging from 2 wt.% to 8 wt.%, as the reinforcing agents. The effects of introducing PDMS as a modifier to epoxy resin, as well as, the influence of embedding SiO₂ nanoparticles within the developed matrix were evaluated via utilizing X-ray diffraction (XRD), contact angle measurements (CA), field emission scanning electron microscope (FESEM), and electrochemical impedance spectroscopy (EIS). XRD and FESEM results revealed the good dispersion of the nanoparticles within the polymeric matrix and confirmed the efficiency of the solution intercalation method. CA findings confirmed the achievement of hydrophobic surface after modifying epoxy resin with PDMS with CA value at 96° for epoxy-PDMS coating system (ES 0). Also CA results indicated the ability of SiO₂ nanoparticles to participate in developing more hydrophobic surface as CA value up to 132° was achieved with utilizing 6 wt.% SiO₂ loading ratio. The results obtained from EIS studies revealed that the coating system with 2 wt.% had the best anticorrosion performance and have demonstrated an intact behavior over all the immersion period without any sign of coating damage or degradation.

© 2017 Elsevier B.V. All rights reserved.

1. Introduction

Degradation of material or corrosion had been quite an issue for industries. When surfaces are exposed to corrosive environment, degradation of materials occurs and the cost is at the expense of billions, both in capitals and lives [1]. X. Pei et al. have pointed out that corrosion phenomena significantly affect the lifespan, safety, and aesthetics of the infrastructure. That in turn leads to annual cost at approximately \$276 billion just in U.S as a direct cost of metallic corrosion. In addition, X. Pei et al. also reported that Canada spends about \$74 billion just to repair the reinforced concrete structure [2].

Organic coatings are one of the promising approaches in solving the issues. Furthermore, recent years had shown a tremendous effort in highlighting the performance of these coatings and that includes the organic coating system and polymeric hybrid coating system that combine the both the novelty of organic and inorganic functionalities [3–6].

Epoxy and PDMS are two different categories of polymer and both are used as coating systems for multipurpose including anti-corrosion [5,7,8]. Despite having remarkable resistance toward many elements, epoxy still fall short with its hydrophilic surface and weakness toward resistance to crack propagation [9–11]. This could lead to significantly

reduced barrier ability against water, oxygen and other corrosive elements making it a poor choice for anti-corrosion coating. PDMS on the other hand, has superhydrophobic surfaces with poor wettability with low surface energy. PDMS also possess large free volume that allows it to be used as element for many other applications [12–14].

While the former is considered to be organic and latter, inorganic, the combination of these two had proven to be a good anti-corrosion coating due to both properties combined together to form a superior coating. Ammar et al. had studied the effects of intercalation of PDMS with epoxy and revealed a significant increase of hydrophobicity of Epoxy-PDMS composite system compared to neat epoxy [8]. Rath et al. also discovered that PDMS-modified epoxy has lower surface energy with increases in contact angle measurement [15]. This shows that having both PDMS and epoxy together made a better anticorrosion coating due to having intercalation of PDMS into epoxy which lowers the surface energy and increase the hydrophobicity.

Silica or silicon dioxide, SiO₂ an inorganic nanoparticle, is often used as additives to enhance the properties of many organic base resins [16–18]. High mechanical strength, good thermal and chemical stability and high surface area make SiO₂ nanoparticles gain the trust as a useful tool to enhance the mechanical properties and reduce its thermal degradation at high temperature of the polymeric films [19,20]. Moreover, many researchers have confirmed the capability of SiO₂ nanoparticles in enhancing the barrier properties and the hydrophobicity of the coatings system by zigzagging the diffusion pathways against the

^{*} Corresponding author.
E-mail addresses: amreshata@siswa.um.edu.my (S. Ammar), rameshkas@um.edu.my (K. Ramesh).